

UCLA

UCLA Electronic Theses and Dissertations

Title

Understanding the Relationship between Osmotic Membrane Structure and Separation Performance

Permalink

<https://escholarship.org/uc/item/4x61s703>

Author

Wong, Mavis C.Y.

Publication Date

2014

Peer reviewed|Thesis/dissertation

UNIVERSITY OF CALIFORNIA

Los Angeles

Understanding the Relationship between
Osmotic Membrane Structure and Separation Performance

A dissertation submitted in partial satisfaction of the
requirements for the degree Doctor of Philosophy
in Civil Engineering

by

Mavis Ching Yan Wong

2014

ABSTRACT OF THE DISSERTATION

Understanding the Relationship between Osmotic Membrane Structure and Separation Performance

by

Mavis Ching Yan Wong

Doctor of Philosophy in Civil Engineering

University of California, Los Angeles, 2014

Professor Eric M.V. Hoek, Chair

Water scarcity, water-stress, and drought are becoming common terms to describe the world we live in. In order to augment the world's depleting fresh water supply, methods to treat non-traditional water sources to become potable water are being explored. Reverse osmosis is a very promising technology to desalinate seawater, brackish water and even waste water into fresh product water. Forward osmosis (FO) is a developing technology that is currently used to concentrate fruit juices and provide nutrient juices using impaired water sources. Furthermore, FO is also explored as a potential for low energy desalination. However, much research needs to be done to understand how to improve membrane performance, especially for FO applications.

The goal of this research was understand whether membranes with high hydrophilicity and large macrovoids will lower internal concentration polarization in FO membranes and increase water permeability and selectivity. Polyaniline (PANi) was used a model material due to

its hydrophilicity and tunable pore structure to develop this understanding between membrane structure and performance. First, a review of current membrane materials for RO and FO was provided, along with an overview of membrane formation techniques, and previous research on polyaniline used in membrane filtration. A computational fluid dynamics model study revealed that the base thickness of the membrane dictates the upper bound of a composite membrane. With the same polymer volume, distributing the polymer as an undulating film will always have higher permeability due to the creation of shorter diffusive path lengths. This research showed that the interplay between support membrane and thin film are vast. Then, phase-inverted PANi membranes along with membranes blended with polysulfone were coated with polyamide thin film by interfacial polymerization. Due to the hydrophilicity of PANi, it was found that more water was taken up than the amine during the immersion step, requiring changes in the amine concentration to increase diffusivity into the reaction zone. Through this study, it was found that the membrane structural parameter was not representative of the porous substructure, but rather of the mass transfer limitations of the membrane. As a result, FO membranes were made by phase inversion of pure PANi without thin film coating, and post-treated by wet-curing, acid and base to alter its performance and skin-layer morphology. By post-treating a membrane with camphor-sulfonic acid, enhanced performance was achieved due to denser skin layer and increased pore volume. This study provided an overview of the relationship between composite membrane structure and performance in finding that: 1) support membrane changes flux distribution, 2) thin film polymer distribution can change performance, 3) support membrane dictates thin film formation, and 4) phase inverted membrane skin layer dictates performance.

The dissertation of Mavis Ching Yan Wong is approved.

Richard B. Kaner

Shaily Mahendra

Gaurav Sant

Eric M.V. Hoek, Committee Chair

University of California, Los Angeles

2014

DEDICATION

I dedicate this dissertation to my family. For believing in me even when I had lost confidence in myself.

And to Noah, for understanding me when I thought no one would, for being my biggest supporter, and for being a part of my life.

TABLE OF CONTENTS

Section	Description	Page
	List of Figures	x
	List of Tables	xiv
	List of Abbreviations	xv
	Acknowledgements	xvi
	Vita	xviii
1	CHAPTER 1 – INTRODUCTION: Osmosis - Applications and its Limitations	1
1.1	Importance of Membrane Filtration	2
1.2	Osmosis and its Applications	4
1.3	Review of Current Commercial Membrane Materials for RO/FO	7
1.4	Phase Inversion of UF, RO and FO Membranes	8
1.4.1	Variations in Phase Inversion	14
1.5	Thin Film Coating of Phase-inverted Membranes to form Composite RO/FO Membranes	16
1.5.1	Solvent System Variations	17
1.5.2	Additives	19
1.5.3	Post-treatment Conditions	22
1.5.4	Monomer Structures	22
1.6	Mass Transport in Composite Membranes	27
1.6.1	Concentration Polarization in RO/FO Membranes	29
1.6.2	Relationship between Thin Film and Support Membrane	39

1.7	RO/FO Membrane Stability, Degradation, Fouling, and Scaling	41
1.8	Polyaniline and its Potential as a RO/FO Membrane Material	44
1.9	Summary	46
1.10	Research Hypothesis and Objectives	47
2	CHAPTER 2: Non-Uniformity of Thin Film and Support Membrane Morphology	49
	Introduction	50
2.1	Numerical Model	53
2.1.1	Geometry	53
2.1.2	Governing Equations	56
2.1.3	Scaling	57
2.2	Results and Discussion	59
2.2.1	Impact of Roughness on Permeability	59
2.2.2	Effect of Partition Coefficient on Permeability	62
2.2.3	Impact of Voids on Flux Distribution (location of hot spots)	64
2.3	Summary	72
3	CHAPTER 3: THIN FILM FORMATION CONDITIONS	74
	Introduction	75
3.1	Experimental	76
3.1.1	Materials	76
3.1.2	Support Membrane Formation	77
3.1.3	Thin Film Formation	77
3.1.4	Support Membrane Performance	78

3.1.5	RO Membrane Performance	79
3.1.6	FO Membrane Performance	80
3.2	Membrane Characterization	81
3.2.1	Support Membrane MPD Uptake	81
3.2.2	Support Membrane Microscopy	81
3.3	Results and Discussion	82
3.3.1	MPD Absorption Tests	82
3.3.2	Support Membrane Cross-Sectional Images	83
3.3.3	Performance of PANi/PSf Membranes	84
3.3.4	RO Performance of PA-PANi/PSf Composite Membranes	86
3.3.4.1	Variation of MPD Concentration	86
3.3.4.2	Variation of Organic Solvent	90
3.3.5	FO Performance of PA-PANi/PSf Composite Membranes	93
3.3.6	Stability of PA-PANi/PSf Composite Membranes in FO	96
3.3.7	Structure Parameter of FO Membranes on PANi/PSf Blended Support Membranes	97
3.4	Summary	99
4	CHAPTER 4: SUPPORT MEMBRANE CHARACTERISTICS	101
	Introduction	102
4.1	Experimental	103
4.1.1	Materials	103
4.1.2	Membrane Formation	103
4.1.3	Membrane Characterization	104

4.1.4	FO Membrane Performance	105
4.2	Results and Discussion	106
4.2.1	Casting Blade Height	106
4.2.2	Wet Curing PANi Membranes	108
4.2.3	pH Stability of the Membranes	109
4.2.4	Acid Dependence	113
4.2.5	Membrane Skin-Layer Characterization	116
4.2.6	Dopant Reversibility	119
4.3	Summary	122
5	CHAPTER 5: CONCLUSIONS AND FUTURE WORK	123
	Conclusions and Future Work	124
6	REFERENCES	129

List of Figures

Figure 1.1. Filtration processes and the relative sizes of materials it can separate.

Figure 1.2.1. Schematic showing the direction of water flow across a semi-permeable membrane in (a) Forward Osmosis and (b) Reverse Osmosis

Figure 1.2.2. Forward osmosis desalination using ammonium bicarbonate draw solution
(Adapted from Ref [1])

Figure 1.3. Cross sectional SEM images of the CTA membrane at (left) 250X and (right) 2500X magnification [2].

Figure 1.4.1. Schematic of phase inversion process

Figure 1.4.2. Cross-sectional image showing the asymmetric structure of the phase-inverted structure of a hand-cast polysulfone membrane

Figure 1.4.3. Ternary plot illustrating the composition paths of the phase inversion process
(Adapted from [3])

Figure 1.5. Schematic illustrating the formation of polyamide thin films by interfacial polymerization

Figure 1.5.2. (a) Conceptual illustration and (b) TEM cross-sectional image showing nanoparticles embedded in polyamide thin-film [42]

Figure 1.6.1. Schematic showing the concentration profile through a composite membrane illustrating the reduction in the osmotic pressure difference due to external concentration polarization

Figure 1.6.2. Schematic showing the concentration profile through an asymmetric membrane, illustrating the reduction in the osmotic pressure difference due to (a) concentrative ICP in PRO-mode and (b) dilutive ICP in FO-mode [4]

Figure 1.6.3. Schematic illustrating the geometry used to describe effective diffusion path length. a) side view b) top view of a unit cell (Adapted from [39, 61])

Figure 1.7. Reaction mechanism showing acetylation of cellulose followed by hydrolysis

Figure 1.8.1. Chemical structure of polyaniline in its three oxidation states

Figure 1.8.2. SEM images of membrane surface (left), full cross-section (middle) and skin layer cross-section (right) of PANi:PSf ratios of (a) 1:0, (b) 3:1 (c) 1:1, (d) 1:3, and (e) 0:1 [7].

Figure 2.1. Surface SEM (a) and cross-sectional TEM images (b/c/d) of polyamide RO membrane thin films

Figure 2.2. Schematic of geometry used in simulations for a) Out-of-phase and b) In-phase supported membranes

Figure 2.3. Schematic depicting the constant void and proportional void cases compared to the solid rough films without voids

Figure 2.4. Schematic of void volume changes on unsupported films for one wavelength

Figure 2.5. Illustration of unsupported films with same polymer volume distributed as a a) smooth flat film, b) rough periodically undulating film, c) random polymer globules

Figure 2.6. Permeability of unsupported film for solid, constant voids, proportional voids scenario plotted against roughness amplitude (Dotted lines indicate a partition coefficient, $K_{eq} = C_f/C_v = 0.01$)

Figure 2.7. Permeability of unsupported film for Case A, B, C plotted against Void Volume (Permeability Scaled against that of an equivalent film thickness. Dotted lines indicate a partition coefficient, $K_{eq} = C_f/C_v = 0.01$)

Figure 2.8. Phase Diagram indicating the scaled permeability as a function of flux variation for a) In-phase shown in open markers b) out-of-phase membranes shown in filled in markers (permeability scaled against that of an supported film with equivalent film polymer volume)

Figure 2.9. Flux variation values along with flux distribution plots for supported membranes solid film – a) in-phase b) out-of-phase

Figure 2.10. Flux variation values along with flux distribution plots for supported membranes with constant void a) in-phase b) out-of-phase

Figure 2.11. Flux variation values along with flux distribution plots for supported membranes with proportional void a) in-phase b) out-of-phase

Figure 2.12. Flux variation values and flux distribution plot for a segment of an in-phase supported membrane for a) Case A b) Case B c) Case C

Figure 2.13. Flux variation values and flux distribution plot for a segment of an out-of-phase supported membrane for a) Case A, b) Case B and c) Case C

Figure 3.1. Schematic of six-cell lab scale cross flow RO system [5]

Figure 3.2. Schematic of lab-scale FO system [5]

Figure 3.3. Water permeability and BSA rejection of un-coated PANi-PSf membranes

Figure 3.4. Water permeability and NaCl rejection of polyamide coated pure PANi support membrane with variation in a) immersion time b) concentration in aqueous MPD solution

Figure 3.5. Water permeability and NaCl rejection of polyamide coated PANi-PSf membranes using a) isopar b) hexane as the organic solvent

Figure 3.6. Water permeability and salt passage of FO TFC PANi-PSf support membranes using a) isopar b) hexane as the organic solvent.

Figure 3.7. Structural parameter of PANi-PSf TFC membranes using isopar and hexane as the organic solvent

Figure 4.1. Cross-sectional SEM images of PANi membranes cast on glass using a) 102 μm b) 152 μm blade height

Figure 4.2. Wet-cured phase-inverted PANi and CTA membranes tested in FO-mode

Figure 4.3. Water Permeability and Salt Passage of PANi and CTA after post-treatment with acid (HCl) at pH =1 and base (NaOH) at pH = 12 for 13 hours

Figure 4.4. Schematic depicting the effect of acid doping on pore connectivity in the skin layer of a PANi membrane (a) as-cast, (b) with acid dopant and (c) dedoped with water [9]

Figure 4.5. Phase-Inverted PANi membrane post treated with CSA and HCl in various pH for 1 hr

Figure 4.6. PANi-152 membrane FO water permeability and salt passage for a dopant cycle

Figure 4.7. FTIR spectra for PANi-152 post-treated membranes in a dopant cycle

List of Tables

Table 1.4. Summary of variations in phase inversion

Table 1.5.1. Physical properties of various organic solvents [41-43]

Table 1.5.2. Additives and their effects on polyamide TFC membranes

Table 1.5.4. Structures of monomers and resulting polymers formed by interfacial polymerization

Table 1.6. Studies using parameters K and/or S in characterization of osmotic membranes

Table 2.1. Summary of boundary conditions used in the simulations

Table 3.1. MPD absorption test results of pure and blended PANi and PSf unsupported membranes

Table 3.2. Cross-sectional SEM images of blended PANi/PSf membranes at 500X and 10,000X magnification

Table 3.3. Water permeability and salt passage for CTA and 1:3 PANi:PSf TFC membranes before and after immersion in NaOH (pH ~13.3) solution.

Table 4.1. Cross-sectional images of PANi-152 pre- and post- treated with 100mM HCl for 1hr

Table 4.2. Captive bubble water contact angle of PANi-152, PANi-102 and CTA before and after 100mM CSA and HCl post-treatments

Table 4.3. Surface FIB-SEM images of PANi-152 and PANi-102 pre- and post-treated

Table 4.4. Comparison of Water Permeability and Salt Passage of Post-treated PANi-152 in Short and Extended FO test

List of Abbreviations

4MP	4-Methylpiperidine	NF	Nanofiltration
AFM	Atomic force microscopy	NMP	<i>N</i> -methyl-2-pyrrolidone
ATR-FTIR	Attenuated total reflection Fourier transform infrared spectroscopy	PA	Polyamide
BSA	Bovine serum albumin	PANi	Polyaniline
CFD	Computational fluid dynamics	PEG	Polyethylene glycol
CP	Concentration polarization	PRO	Pressure retarded osmosis
CTA	Cellulose triacetate	PSf	Polysulfone
DMF	Dimethylformamide	PVP	Polyvinylpyrrolidone
DMSO	Dimethylsulfoxide	PVAm	Polyvinylamine
ECP	External concentration polarization	RO	Reverse osmosis
FIB	Focused ion beam	SEM	Scanning electron microscope
FO	Forward osmosis	SWRO	Seawater reverse osmosis
FV	Flux variation	TEA	Triethylamine
HMPA	Hexamethyl phosphoramidate	TEM	Transmission electron micrograph
ICP	Internal concentration polarization	TFC	Thin film composite
IPA	Isopropyl alcohol	TFN	Thin film nanocomposite
IPC	Isophthaloyl chloride	TMC	1,3,5-Benzenetricarbonyl trichloride or trimesoyl chloride
MF	Microfiltration	UF	Ultrafiltration
MPD	<i>m</i> -Phenylenediamine	XPS	X-ray photoelectron spectroscopy

ACKNOWLEDGEMENTS

I would like to first and foremost thank my adviser, Dr. Eric Hoek, for giving me the opportunity to work in his laboratory when I was an undergraduate student, and encouraging me to continue on as a graduate student. Through this experience, I have learned an extensive amount not only on membrane research and technology, but on project and time management, technical analysis and presentation skills, as well as general life skills that are incredibly valuable.

Without the support of current and former members of the NanoMeTeR group at UCLA, I know my graduate experience would have been much less rewarding. Words cannot describe my appreciation for the help they have given me towards my research, the insightful discussions we have shared, and the countless memories that will last a lifetime. Many, many thanks to not only my labmates, but to my friends: Dr. Jinwen Wang, Dr. Benjamin Feinberg, Dr. MaryTheresa Pendergast, Dr. Catalina Marambio Jones, Dukwoo Jun, Dr. Gregory Guillen, Dr. Gil Hurwitz, Brian McVerry and Dr. MaryLaura Lind. I would like to especially acknowledge Dr. Guy Ramon, who not only was a former post-doctoral researcher in the lab, but continued on to be a mentor in my research. He has spent many hours guiding me through difficult problems in my research and advising me through frustrating times in my graduate student life.

I would also like to acknowledge my friends for always supporting me and being there for me. Thank you to Kenji Sasaki, Nhon Luu, Zita Yu, Vanessa Thulsiraj and Jea (Jay) Cho. Thank you to my committee members for their support throughout my graduate studies, Professor Richard Kaner, Professor Shaily Mahendra and Professor Gaurav Sant. I greatly appreciate Professor Keith Stolzenbach for the advice he has given me over the years. Thank you also to the former and current students and staff in the Department of Civil and Environmental Engineering for all the help, guidance and reminders throughout the course of my degree.

Finally, I would like to acknowledge the funding sources for supporting my work throughout these years: The National Science Foundation (NSF) GK-12 Graduate Teaching Fellowship (SEE-LA Award no. 0742410) and UCLA Graduate Division Dissertation Year Fellowship.

VITA

- 2009 B.S., Chemical Engineering, Magna Cum Laude
University of California, Los Angeles
- 2009 – 2012 Teaching Assistant
Department of Civil and Environmental Engineering
University of California, Los Angeles
- 2010 Water Quality Intern
Advantageous Systems LLC.
Pasadena, CA
- 2011 M.S., Civil Engineering
University of California, Los Angeles
Thesis: “*Impacts of Feed and Draw Solution Properties on Osmotic Membrane Structural Parameter*”
- 2012 - 2013 Graduate Teaching Fellow
UCLA Science and Engineering of the Environment of Los Angeles
(SEE-LA) GK-12 Program
National Science Foundation

Publications and Presentations

1. Vilakati, G.D.; **Wong, M.C.Y.**; Mamba, B.B.; Hoek, E.M.V.; Relating Thin Film Composite Membrane Performance to Support Membrane Morphology Fabricated Using Lignin Additive., *J. Membr. Sci.*, (2014) DOI: 10.1016/j.memsci.2014.06.018.
2. McVerry, B.T.; **Wong, M.C.Y.**; Marsh, K.L.; Temple, J.A.; Marambio-Jones, C.; Hoek, E.M.V.; Kaner, R.B.; Scalable Antifouling Reverse Osmosis Membranes Utilizing Perfluorophenyl Azide Photochemistry., *Macro. Rapid. Commun.*, (2014) DOI: 10.1002/marc.201400226.
3. **Wong, M.C.Y.**; Ramon, G. and Hoek, E.M.V. “Transport through Composite Membranes, Part 3: Impacts of Thin Film and Support Membrane Morphology.” *North American Membrane Society*, Houston, TX, May 31 - June 4, 2014.
4. Wang, J.; Dlamini, D.S.; Mishra, A.K.; Pendergast, M.M.; **Wong, M.C.Y.**; Mamba, B.B.; Freger, V.I Verliefe, A.R.; Hoek, E.M.V.; A Critical Review of Transport through Osmotic Membranes., *J. Membr. Sci.*, 454 (2013) 516-537.

5. Thwala, J.M.; Li, M.; **Wong, M.C.Y.**; Tae, S.; Hoek, E.M.V.; Mamba, B. B.; Bacteria-Polymeric Membrane Interactions: Atomic Force Microscopy and XDLVO Predictions. *Lang.*, 29 (2013) 13773-13782.
6. Lin, C.; Héloïse, T-A.; **Wong, M.C.Y.**; Hoek, E.M.V.; Ober, C.K. Improved Antifouling Properties of Polymer Membranes Using ‘Layer-by-layer’ Mediated Method. *J. Matr. Chem. B.*, 1 (2013) 5651-5658.
7. **Wong, M.C.Y.** and Hoek, E.M.V. “Tunability of Polyaniline Phase-Inverted Membranes for Forward Osmosis Applications.” *North American Membrane Society*, Boise, ID, June 9-12, 2013.
8. Ramon, G.Z.; **Wong, M.C.Y.**; Hoek, E.M.V. Transport through composite membrane, part 1: Is there an optimal support membrane? *J. Membr. Sci.*, 415-416 (2012) 298-305.
9. **Wong, M.C.Y.**; Martinez, K.; Ramon, G.Z.; Hoek, E.M.V. Impacts of operating conditions and solution chemistry on osmotic structure and performance. *Desalin.*, 287 (2012) 340-349.
10. **Wong, M.C.Y.** and Hoek, E.M.V. “Understanding the relationship between osmotic membrane structure, chemistry, and performance.” *American Chemical Society*, Philadelphia, PA, August 19-23, 2012.
11. **Wong, M.C.Y.** and Hoek, E.M.V. “Polymeric Membranes Used in Water Treatment.” *American Chemical Society – Western Regional Meeting*, Pasadena, CA, November 9-11, 2011.

CHAPTER 1

INTRODUCTION

Osmosis – Applications and Limitations

1. Introduction

1.1. Importance of Membrane Filtration

One of the grand challenges of the 21st century set by the National Academy of Engineering is “providing access to clean water” [1]. One third of the world’s population lives in water-stressed conditions, and many in developing countries lack access to safe drinking water [2]. To exacerbate this situation, only 1% of the entire world’s water resources is accessible fresh water, as other fresh water sources are locked up in glaciers and groundwater inaccessible for human use [3]. Due to rapid population growth, investigations are being made in the production of potable water from non-traditional sources such as seawater, brackish water and even wastewater. Desalination, the process of removing salts and other minerals from saline water to produce fresh water, has been used to augment the world’s depleting fresh water sources. However, desalination by thermal processes, such as multi-effect or multi-stage flash distillation, has lower treatment capacity per plant, is relatively more energy intensive than membrane desalination and thus, unfeasible in developing countries and unsustainable in industrialized nations [4, 5].

Furthermore, compared to conventional drinking water treatment plants, advanced treatment plants utilizing membrane filtration has a much lower plant footprint, has stable product water quality, and is highly automated [6]. In conventional water treatment plants, raw source water is passed through a series of unit operations prior to being distributed for use. After screening the water for large objects, the water is dosed with a coagulant that destabilizes suspended solids so that they will nucleate and form larger particles during subsequent mixing in the flocculation basin [6]. The particles are then allowed to settle in the sedimentation tank before passed through a depth filter. Depth filters are beds of fibrous or granulated media that

catches suspended particles as the source water passes through. Unfortunately, as the treatment plant's only selective barrier, depth filters have an intrinsic downfall [7]. Specifically, depth filters have the lowest removal efficiency for particles around the size of a micrometer, which includes many bacteria. This drawback of depth filters was demonstrated in the cryptosporidium outbreak in Milwaukee in 1993 where over 400,000 people contracted the disease [6]. Thus, there was a push towards using membrane filters in water treatment, which provide absolute screens, rejecting particles larger than the pore sizes of the membrane. Microfiltration and ultrafiltration membranes can completely reject particles greater than the size of a micron, which includes any colloidal particles such as oil droplets, viruses, proteins, etc. Nanofiltration and reverse osmosis membranes can reject particles in the range of a 1/100 to 1/1000th of a micrometer, which includes materials such as aqueous salts, sugars, and amino acids. The different membrane filtration processes compared to particle filtration, the size of particles it can separate from water sources, and the required operating pressures are shown in Figure 1.1.

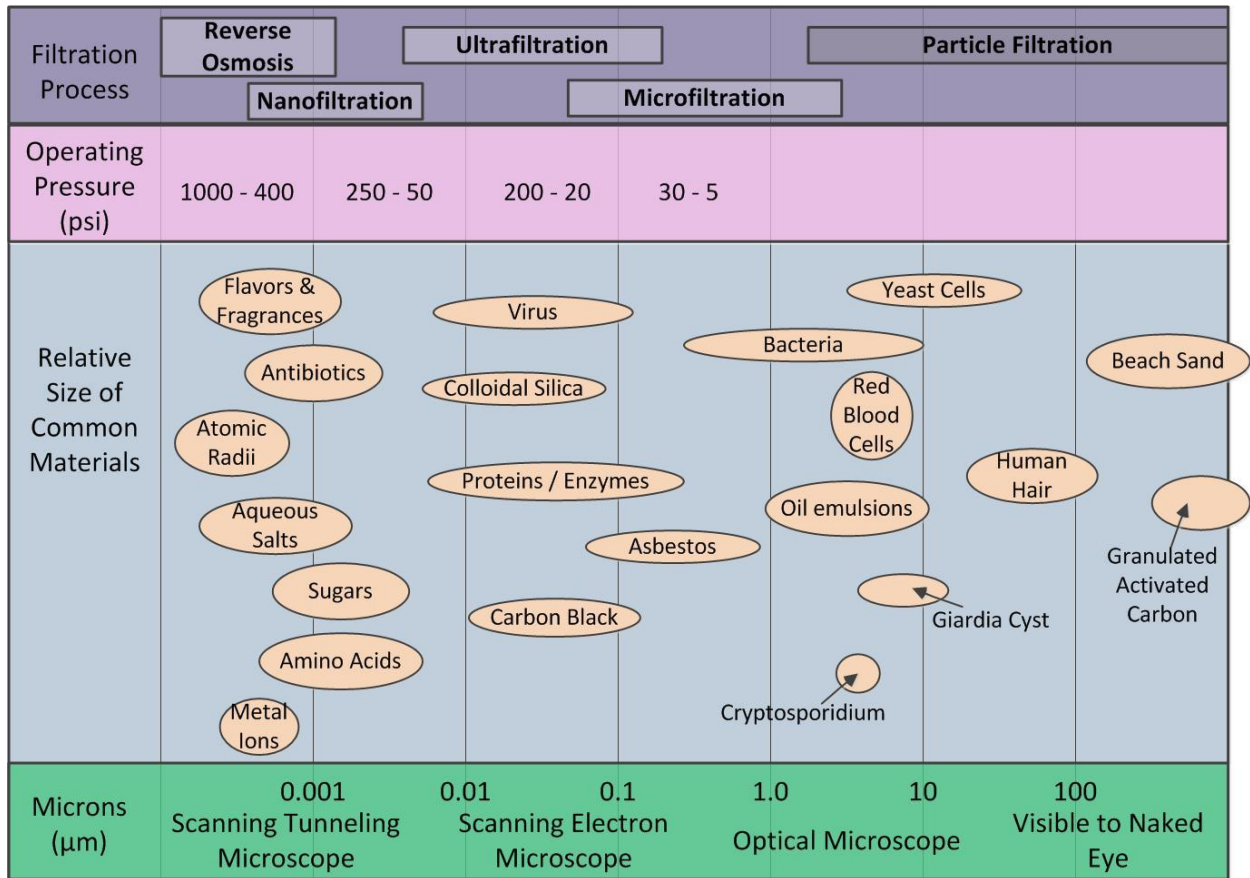


Figure 1.1. Filtration processes and the relative sizes of materials it can separate.

1.2. Osmosis and its Applications

Reverse osmosis (RO) is based on the concept of osmosis or forward osmosis (FO), which is the natural tendency for water to flow from a dilute source to concentrated source when separated by a semi-permeable membrane, i.e., a membrane that allows water to permeate but not solutes (Fig. 1.2.1a) [8]. The driving force for this process is the osmotic pressure difference ($\Delta\pi$) (or difference in the chemical potential of water) between the two solutions. RO is an engineered osmosis process in which application of a hydraulic pressure (ΔP) is sufficient to overcome the osmotic pressure difference causing water to permeate backwards through the semi-permeable membrane from the concentrated to the diluted solution (Fig. 1.2.1b). In the past

20 years, a number of factors (better RO membranes, pre-treatment technology, market forces, energy recovery devices, etc.) have made RO the most popular method of desalination [4, 5]. However, the large hydraulic pressure (800-1000 psi), and hence, energy requirement for RO, still limits this technology to developed and industrialized countries with low total dissolved solids waters.

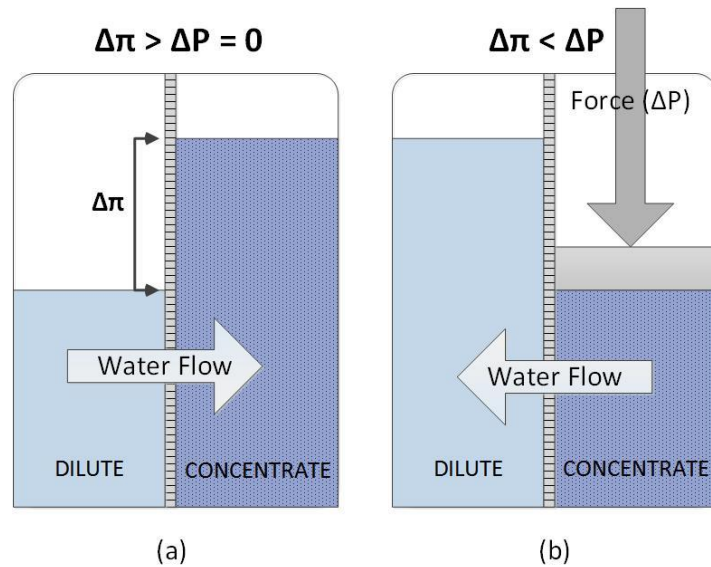


Figure 1.2.1. Schematic showing the direction of water flow across a semi-permeable membrane in (a) Forward Osmosis and (b) Reverse Osmosis

More recently, the engineered process of FO has been explored as an alternative to RO desalination, having the potential to reduce the energy demand for the process. For low energy desalination, water is drawn from the saline water source to a solution of higher solute concentration (draw solution) through a semi-permeable membrane [8]. The draw solution solute is then recovered and reused for the next batch of saline water. Various draw solutes have been proposed for this process, such as pH-sensitive solutes, thermolytic salts or magnetic particles

that can be recovered by shifting solution pH, heating the solution or using a magnetic, respectively [9-11]. One process that has attracted the most attention is by using a draw solution composed of dissolving ammonium bicarbonate, which evolves into ammonia and carbon dioxide gas when the solution is heated to 50°C. This heat is easily obtainable by coupling the process to an industrial plant that releases large amounts of waste heat [12, 13]. This process is depicted in Figure 1.2.2

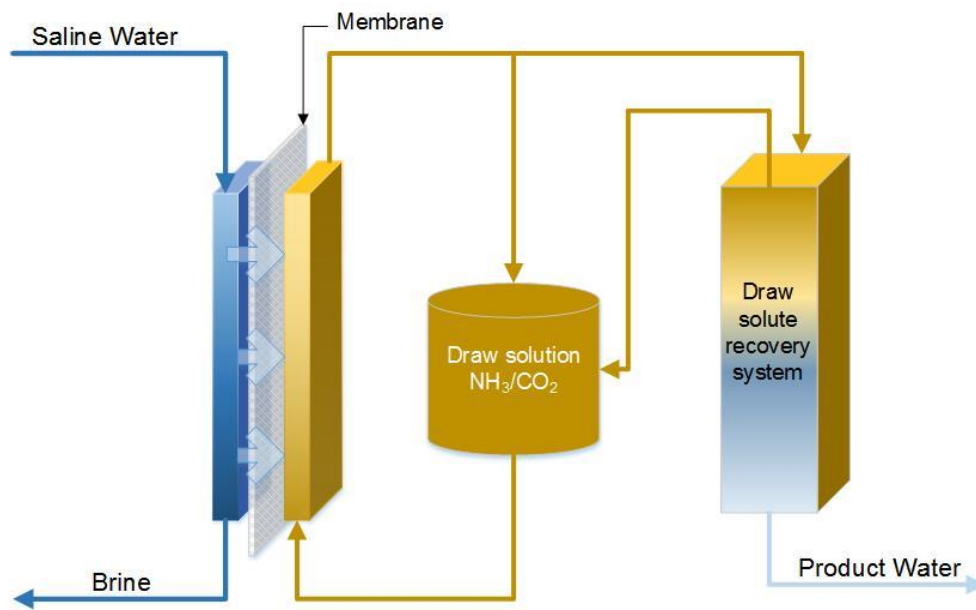


Figure 1.2.2. Forward osmosis desalination using ammonium bicarbonate draw solution (Adapted from Ref [13].)

In addition to using FO for desalination, there are also a variety of applications for which FO is currently used. One major application for FO is when the product is the concentrated stream instead of the dilute stream, such as in the concentration of fruit juices in which saline solutions are used to draw water from the juice [14, 15]. Another commercialized application is a disposable membrane bag which contains a concentrated nutrient powder (Hydration

Technologies Innovations, Albany, OR). The bag is intended to be placed in any available water source, even impaired water sources, and through osmosis, will be filled overnight to produce a nutrient drink that can be immediately consumed. The membrane bag is designed to inhibit growth of mold and bacteria [16]. This application is especially useful for hikers, astronauts, and people living in rural and undeveloped areas where water and nutrient sources are limited.

1.3. Review of Current Commercial Membrane Materials for RO/FO

The major hindrance in the development of FO low energy desalination is the membrane as the most commonly used material in commercial applications, made of cellulose acetate, has low chemical and thermal stability, and low water permeability, and thereby, is not suitable for the process [17]. The cellulose triacetate (CTA) membrane by Hydration Technologies Innovations (Albany, OR) is the most widely used FO membrane, and although manufacturing information is proprietary, cross-sectional scanning electron microscope (SEM) images of the membrane reveals an asymmetric membrane structure with an embedded screen support in the cellulosic material as shown in Figure 1.3. The images show a very dense polymer skin layer, followed by the woven fabric support, with relatively little polymer underneath the initial surface layer. By observation with the naked eye, the membrane is asymmetric with the skin layer surface being much smoother and lustrous than the other side. The CTA flat sheet membrane (OsMem™ CTA-ES, HTI, Albany, OR) is specified to be stable at a pH of 3-8 and a temperature of up to 71°C [18].

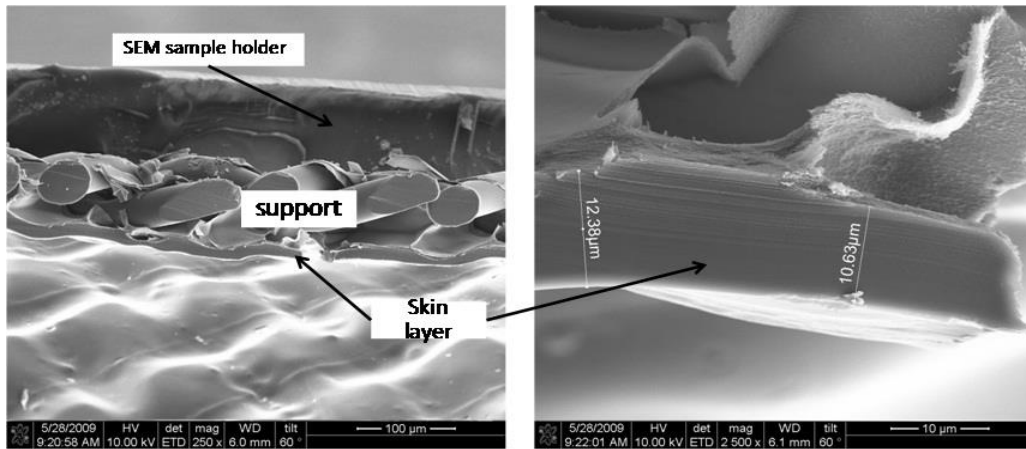


Figure 1.3. Cross sectional SEM images of the CTA membrane at (left) 250X and (right) 2500X magnification [19].

Typical modern RO membranes are thin film composite (TFC) membranes composed of three layers: 1) a top thin selective polymeric layer 2) a porous substructure, and 3) a bottom fabric for mechanical stability, providing the capability to withstand substantial hydraulic pressures needed for RO processes. The thin film is composed of polyamide formed by interfacial polymerization of an amine and an acid chloride, having a thickness ranging from 100-150 nm. The porous substructure is formed by phase inversion of polysulfone, polyethersulfone, polyacrylonitrile, depending on the application. Finally, the fabric is typically a polyester material with a thickness of 120-150 μm , although other nonwoven and woven fabrics have been used [20, 21]. Compared to asymmetric membranes, TFC membranes offer higher flux, and NaCl salt rejection, but low boron rejection, requiring post-treatment of the product water. The surface roughness of TFC membranes offer regions with higher propensity to foul, and due to the polyamide surface layer sensitivity, which degrades under contact with chlorine, a common disinfectant in treatment plants, need for pre-treatment is of another concern [22]. The

following sections will focus on how these membranes are made, followed by a discussion about their limitations.

1.4. Phase Inversion of UF, RO, and FO Membranes

The porous structure of the membrane is formed by a process called nonsolvent induced phase separation, or more commonly called phase inversion [23]. In this process (as shown in Figure 1.4), a casting solution consisting of a polymer dissolved in an organic solvent is spread on a fabric material such as polyester, and then immersed into a non-solvent coagulation bath. Due to the limited solubility of the polymer in the nonsolvent, and the miscibility of the solvent and nonsolvent, as the nonsolvent penetrates into the casting solution and solvent diffuses out, the polymer will precipitate into a film on top of the fabric material [7, 24]. The morphology of the membrane is dependent on the solvent-nonsolvent miscibility and the polymer-nonsolvent solubility [7], as will be discussed further in the next section.

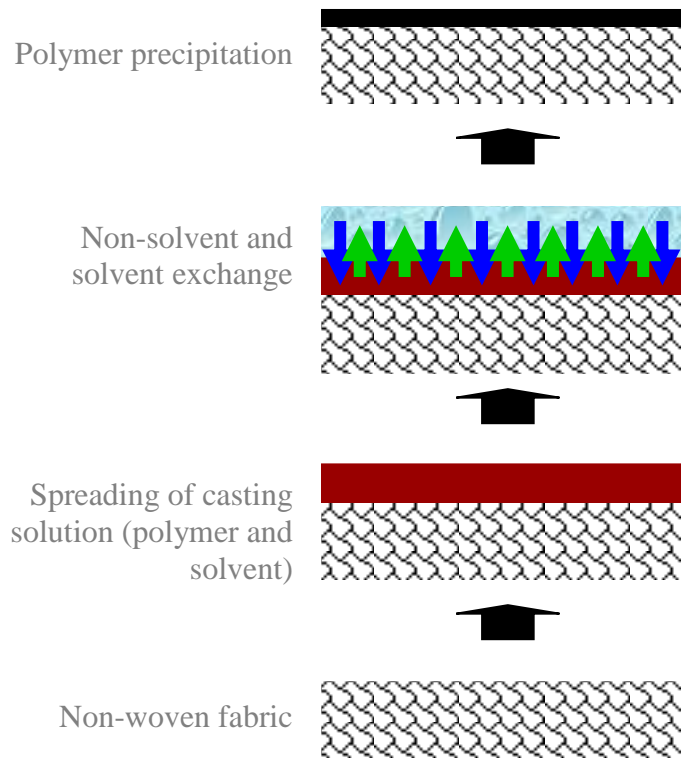


Figure 1.4.1. Schematic of phase inversion process.

As expected, once nonsolvent convectively enters the casting solution and precipitation of the polymer occurs, voids start to form. Figure 1.4.2 shows the typical asymmetric structure of a polysulfone membrane formed by phase-inversion. There is a dense skin layer with underlying dense finger-like pores that opens up to a more open, macrovoid-filled structure toward the bottom layer of the membrane.

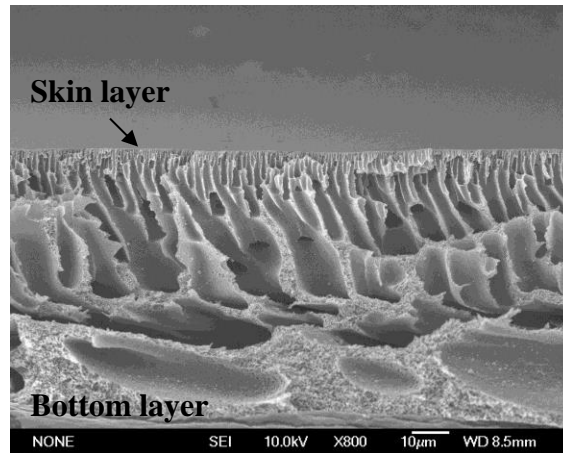


Figure 1.4.2. Cross-sectional image showing the asymmetric structure of the phase-inverted structure of a hand-cast polysulfone membrane

To better understand how solvent, nonsolvent and polymer interplay in determining the composition of the membrane, a ternary plot is typically used as shown in Figure 1.4.3. The miscibility gap (shaded in gray) represents the region where all components are completely miscible. The binodal curve is a liquid-liquid phase boundary that is usually determined experimentally by titration of nonsolvent into the casting solution until cloud point is reached [23]. Past the binodal curve is a two phase (white) region where the polymer solution will separate into a polymer rich and a polymer lean phase at equilibrium, which can be determined by drawing a tie-line parallel to the polymer-nonsolvent axis.

Following the yellow line in Figure 1.4.3, when the initial casting solution is spread on the fabric, it consists of polymer and solvent at a specific composition. Once it is immersed into the coagulation bath, it moves along the yellow line as the solvent-nonsolvent exchange occurs before reaching the precipitation point on the binodal curve. As demixing continues, the nonsolvent concentration overwhelms the volume of solvent in the film causing solidification to

occur. At this point, the equilibrium concentrations of the polymer rich and polymer lean phase are determined at the intersections of the tie-line with the binodal curve and solvent-nonsolvent axis, respectively. Once all the solvent has diffused from the film, the final membrane composition can be found on the polymer-nonsolvent axis. Instantaneous demixing would occur when the composition path from initial point to the precipitation point passes the binodal curve. However, if the composition profile does not pass the binodal curve before precipitation, then delayed demixing will occur. Instantaneous demixing of the solvent and nonsolvent has been found to form highly porous membranes, with high flux but low rejection while delayed demixing was found to form membranes with dense skin layer and sponge-like substructure with low flux and high rejection [23].

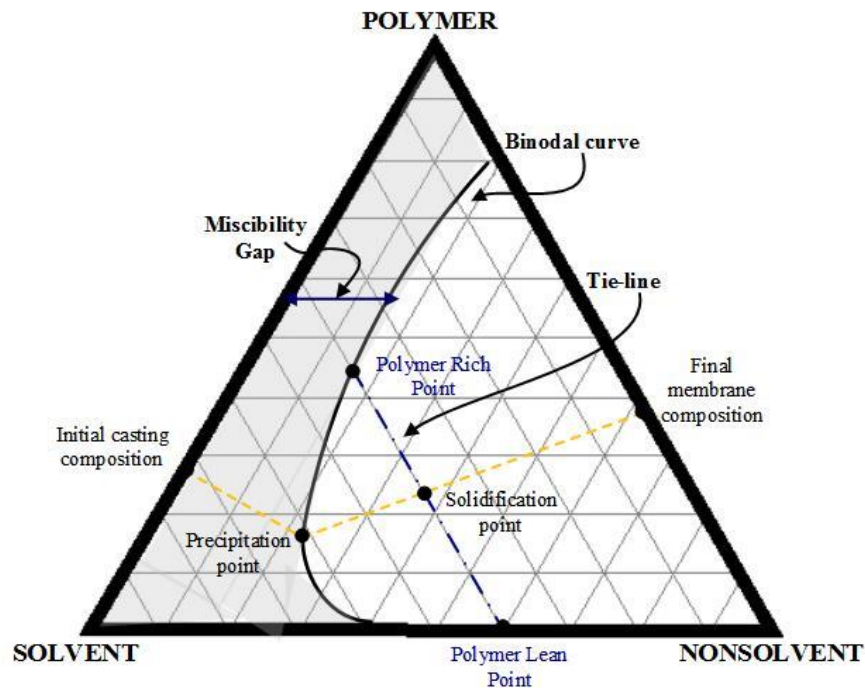


Figure 1.4.3. Ternary plot illustrating the composition paths of the phase inversion process
(Adapted from [25])

The process of phase inversion can be understood as a tradeoff between thermodynamic enhancement and kinetic hindrance. Sadrzadeh et al. argues that additives will enhance thermodynamic instability in the casting solution, which will move the binodal curve toward the polymer-solvent axis, to accelerate the coagulation process, forming more porous membranes [25]. By considering how the membrane skin layer thickness and the volume of solvent diffusing into the nonsolvent bath changes as a function of time, the authors derived a dimensionless parameter representing the kinetic hindrance effect, K ,

$$K = \frac{D_m}{\sqrt{D_{ns}}} \frac{M}{A\mu t_0^{0.5}} \quad (1)$$

where D_m is the effective diffusivity of solvent and additive in the nonsolvent, and D_{ns} is the diffusivity of the nonsolvent. M , A and μ are the mass, surface area and viscosity of the cast film, respectively, while t_0 is the experimental lag time for sensing organics in the nonsolvent bath [25]. K has a base value for an additive free film, which will decrease in the presence of an additive because D_m will decrease. This indicates greater hindrance as kinetics will be slower, which will result in denser membrane morphology. From their experimental work of adding various molecular weights of polyethylene glycol (PEG) and polyvinylpyrrolidone (PVP) into casting solutions of polyethersulfone, the researchers found that the binodal curves move closer to the polymer-solvent axis with higher concentrations and higher molecular weight of additive. Increasing the molecular weight of the additive also reduces the kinetic hindrance parameter. Thus, thermodynamic enhancement increases solvent-nonsolvent demixing, which favors the formation of a more porous structure, while kinetic hindrance delays demixing and tends to form relatively denser membranes.

1.4.1. Variations in Phase Inversion

As discussed in the previous section, additives in the casting solution can alter the morphology of a phase-inverted membrane drastically. Other variations can also be made throughout the process to change the morphology and performance of the membrane. Before exploring these possible variations, let's explore one of the first membranes formed by this process.

The first cellulose acetate membrane for RO was developed in the 1970's by Sidney Loeb together with Srinivasa Sourirajan. This type of membrane is now commonly referred to as the "Loeb-Sourirajan (L-S) Membrane" [26]. The L-S membrane is also formed by phase inversion in which the casting solution consists of cellulose acetate dissolved in a mixture of acetone, water and a small volume of magnesium perchlorate. It was found that the magnesium perchlorate acts as a "pore forming agent", increasing the permeability of the membrane. The casting was carried out at a low temperature (0 - 10°C) by having the coagulation bath composed of ice water. The resulting asymmetric membrane was then heated to 80°C to contract the membrane pore to increase its selectivity. The top skin layer had a thickness of 0.1 – 0.5µm, while the porous sublayer was 50-150 µm thick [27]. The L-S membrane had a pure water permeability of 5.48×10^{-13} m/s-Pa and a rejection of 99% using 40,000 ppm seawater, over 4 times more permeable and more selective than the available commercial cellulose acetate (Schleicher and Schuell GmbH, Dassel, Germany) membrane at that time [26].

Many variations can be made to the phase inversion process to tune the membrane morphology and affect the membrane performance, such as changes in polymer concentration, choice of polymer, solvent, nonsolvent and casting conditions. As previously discussed, it has been observed that instantaneous demixing will form a membrane with a porous, finger-like

substructure and a thin skin layer, which has low rejection but high flux. On the other hand, delayed demixing will form dense top layers with a sponge-like substructure, which forms membranes with high rejection and low flux [23]. Guillen et al. did a systematic study using polysulfone to probe how changes in solvents and nonsolvents affect resulting morphology. The researchers found that increasing polymer solution viscosity (increase polymer concentration, decreasing temperature, etc.) will hinder the extent of large void formation in the membrane. They postulated that the mechanism for void formation was the convective flow of nonsolvent through the polymer solution [28]. Table 1.4 briefly summarizes a few scenarios in which changes were made to fine tune the phase inversion process and the resulting membrane properties.

Table 1.4. Summary of variations in phase inversion

Change in Casting Condition	Resulting Change in Membrane Morphology
Polymer Concentration	<ul style="list-style-type: none"> An increase in polymer concentration will produce a membrane with low porosity even though instantaneous demixing occurs [23]
Polymer Type	<ul style="list-style-type: none"> Different polymers will offer various membrane properties, for example, polysulfone is easily processible and has good mechanical, thermal and chemical stability [29]. Polyethersulfone has higher glass transition temperature than polysulfone and is also widely used. [23]
Solvent	<ul style="list-style-type: none"> Higher the miscibility between the nonsolvent and solvent, higher likelihood of instantaneous demixing, to form more porous membrane Using Hansen solubility parameters, compatible solvents with the polymer can be estimated, for example acetone, dimethyl sulfoxide, dimethylformamide (DMF) should be compatible solvents with cellulose acetate, while DMF, <i>N</i>-methylpyrrolidone are commonly used for PSf
Additives	<ul style="list-style-type: none"> Polyethylene glycol (PEG) when added in the casting solution acts as a

pore forming agent when the molecular weight is greater than 200 Da. As the molecular weight of PEG increases, the number of pores increases, increasing the porosity of the membrane [23]

- Polyvinylpyrrolidone (PVP) is also added to increase the viscosity of the casting solution to prevent seepage into the fabric, which changes the morphology of the membrane by inducing macrovoids depending on the molecular weight used [23, 30]
-

1.5. Thin Film Coating of Phase-inverted Membranes to form Composite RO/FO Membranes

Phase-inverted membranes are generally used in ultrafiltration (UF) and microfiltration (MF) processes to reject bacteria and viruses, as they are not selective enough for RO/NF applications where rejection of salts and metal ions is the target. Thus, typical RO membranes consist of forming selective polymeric thin films on top of phase-inverted membranes to form a thin film composite (TFC) membrane. The synthesis of the selective thin film has been extensively studied, and the reaction conditions has been varied in many combinations in past research [31-38]. Aforementioned, a typical TFC RO membrane consists of aromatic polyamide (PA) thin film formed on top of a phase inverted structure, most commonly made of polysulfone (PSf), and a polyester (PET) fabric to provide mechanical strength to withstand significant RO operating pressures [39]. Since the PET fabric surface is too irregular and porous, it is unable to support a uniform thin film, therefore requiring a PSf layer to provide an integral microporous substructure between the PET and the thin film [20]. Polyamide thin films are formed by interfacial polymerization, in this process (shown in Figure 1.5), the phase-inverted support membrane is first immersed in an aqueous amine solution and then contacted with an organic acyl halide solution [32]. Due to the immiscibility of the two solvents, the reaction between the monomers occurs at the interface, forming a thin film about 100 – 150 nm thick. The TFC

membrane is then put through a curing step to increase crosslinking in the polyamide, and a series of rinses to remove remaining solvents and reactants from the membrane.

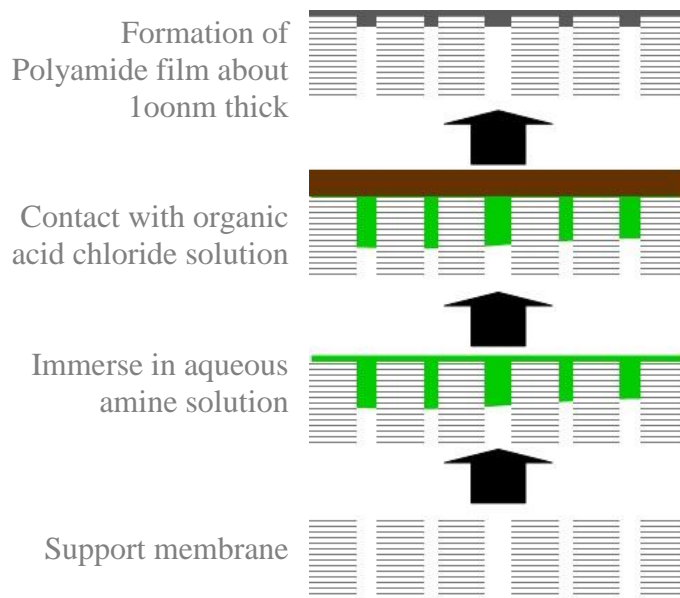


Figure 1.5. Schematic illustrating the formation of polyamide thin films by interfacial polymerization.

1.5.1. Solvent System Variations

In interfacial polymerization, reaction between the monomers occurs mainly in the organic phase due to the low solubility of acyl halides in water [29]. Thus, solutions are prepared using excess amine over acid chloride to provide a concentration driving force for the amine to diffuse into the organic phase [32]. For the common monomers used in polyamide membranes, *m*-Phenylenediamine (MPD) and 1,3,5-Benzenetricarbonyl trichloride (TMC), this ratio is approximately 20:1. Reduction of solvent surface tension will control amine solubility and thus, increase amine to acid chloride ratio in the reaction zone and the resulting degree of polymerization. Increasing water-organic miscibility may cause hydrolysis of acid chloride or de-protonation of amines, which reduces their reactivity and the extent of crosslinking. Ghosh et

al. determined that an organic solvent comprised of a mixture of isoparaffins under the trade name “Isopar™ G” (Gallade Chemical, Santa Ana, CA) is the most stable organic solvent with higher boiling and flash points compared to hexane, heptane and cyclohexane [32]. Isopar™ G will henceforth be referred to as isopar. The low boiling point of hexane and heptane led to near complete crosslinking since the temperature of the curing step post interfacial polymerization was sufficiently high enough to dehydrate the films. The authors found that more water permeable films are formed by increasing MPD diffusivity and reducing MPD solubility in the organic solvent, which also increases crosslinking. Table 1.5.1 summarizes the properties of a few commonly used organic solvents in interfacial polymerization. Some information for isopar is not available as the solvent is proprietary.

Table 1.5.1. Physical properties of various organic solvents [40-42]

Organic Solvent	Boiling Point (°C)	Specific Gravity	Vapor Pressure (mmHg at 20°C)	Surface tension (N/m)	Aqueous Solubility, S (mass % at 25°C)
Hexane	60.2	0.659	126.6	0.0185	0.00137
Heptane	90.0	0.679	36.4	0.0205	0.00024
n-Decane	174.0	0.730	1.5	0.0238	N/A*
Isopar	163.0	0.745	-	0.0230	-

*Not available at 25°C, at 0°C the aqueous solubility is 1.15×10^{-5} mass%

The boiling points of the solvents will dictate the curing temperature and times of the films after interfacial polymerization, which is used to cross-link the films in order to increase rejection. It is very likely that the increased heat will cause pore shrinkage in the support membrane. The

specific gravity will affect the depth of the reaction zone during the contact between the aqueous and the organic phase, the higher the specific gravity, the larger the reaction zone. The vapor pressure of the organic solvent introduces an extra step in the thin film formation: evaporation. The higher the vapor pressure, the more evaporation of the solvent will occur during the vertical holding step, and the cross-linking will occur more rapidly during the subsequent curing step without requiring further removal of the solvent. The surface tension is one indication of the ease of amine diffusion into the organic phase. The aqueous solubility is indicative of the miscibility between the aqueous and organic phase, which dictates the depth of the reaction zone. The relative diffusivity is defined as $D^* = \mu_{\text{water}}/\mu_{\text{solvent}}$, where μ is the viscosity of the medium [32]. The higher the relative diffusivity, the easier it is for water to penetrate into the organic solvent, creating a deeper reaction zone.

Since diffusivity is a function of temperature, the higher the temperature means the higher the average kinetic energy of the solute to move through the medium. Thus, variation of the temperature of the aqueous and organic phases is important in altering the monomer diffusion rate in their respective medium. Thus, increasing the aqueous solution temperature will better facilitate the diffusion into the support membrane, increasing the concentration within the material. Elevation of the organic solution temperature will help the TMC to diffuse towards the interfacial reaction zone, while increasing the aqueous solution temperature will aid the diamine in diffusion into the support membrane and subsequently into the reaction zone.

1.5.2. Additives

Various additives in the organic or aqueous phases have also been found to influence membrane performance as presented in Table 1.5.2. There has not been extensive research done on the mechanistic reasoning between changes to membrane performance and the additives

included in the solvent system. However, in a study by Kim et al., positron annihilation lifetime spectroscopy (PALS) was performed on MPD-TMC TFC membranes with different concentrations of DMSO added to the aqueous phase [43]. The authors found that besides measurable effects of higher degree of cross-linking, surface roughness, and increase in permeability with increasing DMSO concentration; there were also structural changes within the thin film. The number and size of network pores, defined as spaces between cross-linked polyamide chains, were found to increase with increasing DMSO concentration, which helps to explain the increase in water flux. However, while the number of aggregate pores, the spaces between polyamide networks, was also found to increase, its size inevitably decreased with the addition of DMSO.

Table 1.5.2. Additives and their effects on polyamide TFC membranes

Additives	Examples	Effects on Membranes
Miscibility enhancers	Isopropyl alcohol (IPA), Dimethylsulfoxide (DMSO), Acetone, Hexamethyl phosphoramide (HMPA)	Higher flux, rougher surface [32, 43, 44]
Improves amine absorption	Camphor sulfonic acid (CSA)	Increases water permeability [32]
Acid scavenger	Triethylamine (TEA) or acylation catalysts (ex. phosphate-containing compounds)	Increases permeability without observable loss of rejection [32]
Crosslinking inhibitor	<i>N,N</i> -Dimethylformamide (DMF)	Increases permeability [32]

To further improve water flux and selectivity of RO membranes, there have been recent investigations on using ceramic materials in membranes, in particular, nanoparticles. A conceptual illustration is shown in Figure 1.5.2 (a). Jeong et al. synthesized thin-film nanocomposite (TFN) membranes by embedding zeolite nanoparticles (NaA-type) into the polyamide thin-film which is shown in the transmission electron micrograph (TEM) in Figure 1.5.2 (b) [45]. The authors found that the nanoparticles enhance the permeability of TFC membranes while maintaining similar selectivity as the nanoparticles provided preferential flow paths for water due to their extreme hydrophilic pores. Furthermore, the hydrophilicity and charge densities can be tuned by varying the Si/Al ratio of the zeolites. As different zeolites have different pore sizes, the TFN membranes can then be tuned to reject specific foulants, with a target water flux.

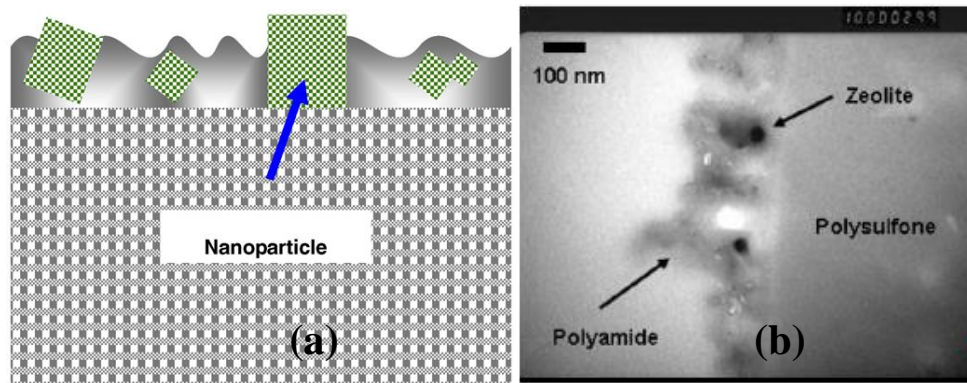


Figure 1.5.2. (a) Conceptual illustration and (b) TEM cross-sectional image showing nanoparticles embedded in polyamide thin-film [45]

Titanium oxide (TiO_2) has also been embedded in polyamide thin films by dip-coating the thin film after the surface has been functionalized with carboxylate groups. The resulting membrane showed excellent anti-fouling properties, due to enhanced hydrophilicity, when tested

with a feed solution containing *Escherichia coli* (*E.coli*) while maintaining permeability and selectivity [20, 44].

1.5.3. Post-treatment Conditions

The thin film is post-treated to increase cross linking and remove residual solvents and monomers. One series of post-treatment conditions in the synthesis of seawater RO (SWRO) membranes from Toray Industries (Poway, CA) includes curing the composite membrane in a hot water bath of 90°C, immersing it in sodium hypochlorite aqueous solution, and followed by a rinse of sodium bisulfite solution [46]. It is believed that the role of the hypochlorite is to slightly degrade the polyamide layer and release residual amine monomers, and the bisulfite solution is to dechlorinate the membrane so that additional degradation of the thin film does not occur [39]. Heat curing removes residual organic solvent and promotes additional crosslinking through dehydration of the monomers, which tends to increase water flux and salt rejection. Optimal curing temperature depends on the properties of the solvents, especially its boiling points. It is found that as the curing temperature approaches the boiling point of the organic solvent, water permeability and salt rejection increases while hydrophilicity decreases, indicating that there is evaporation of the residual solvent and increase in crosslinking of the film. However, further increase in curing temperature and time decreases the porosity of the film and consequently reduces the water flux [32].

1.5.4. Monomer Structures

There has been extensive research on using different monomers to tune the membrane permeability and selectivity. Some amine and acyl chloride structures and the resulting

polyamide are presented in Table 1.5.4 following an extensive discussion of the properties of each polyamide below.

Cadotte formed the first non-cellulosic composite membrane by interfacial polymerization with comparable flux and monovalent salt rejection in the 1970s. Upon further research, Cadotte found that the best perme-selective membrane can be formed using monomeric aromatic amines and aromatic acyl halides containing at least three carbonyl halide groups [20]. The resulting polyamide formed by interfacial polymerization of TMC and MPD forms the basis of current commercial RO membrane FT-30 by DOW FilmTec® [47]. The resulting polyamide has a “ridge and valley” morphology, which increases the propensity for the membrane to biofoul [48]. The selectivity can be tailored by curing the membrane to increase crosslinking, although pores in PSf membranes have been found to shrink at temperatures above 50°C.

A combination of aromatic triamines and diamines in the aqueous phase and aromatic tricarbonyl chlorides and dicarbonyl chlorides in the organic phase results in a membrane with slightly lower flux but similar salt rejection compared to the polyamide thin film formed with TMC and MPD. The lower water flux may be due to a less hydrophilic surface compared to the polyamide of TMC and MPD because of less nascent carboxylic groups after the reaction.

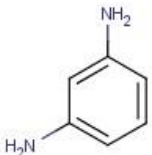
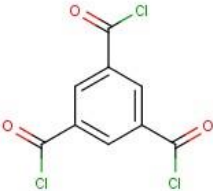
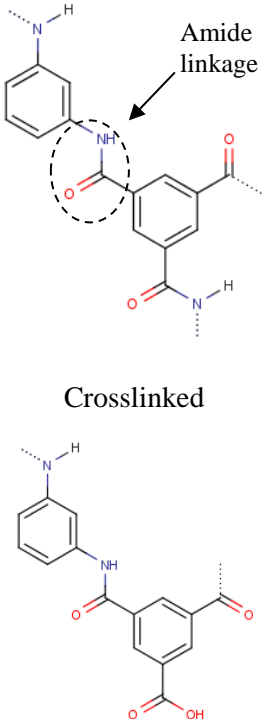
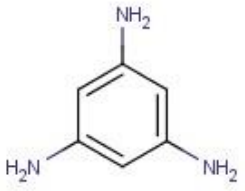
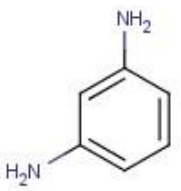
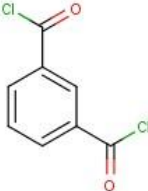
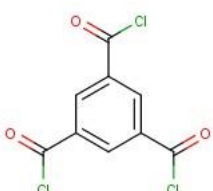
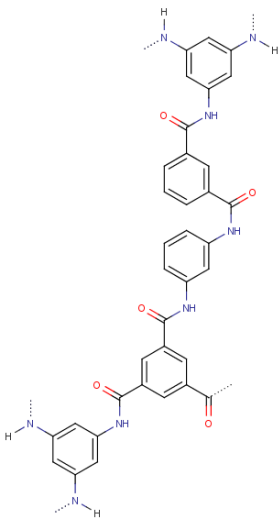
Using piperazine produces smoother, more water permeable, but less selective membranes compared to fully aromatic monomers possibly due to lower degrees of crosslinking and more flexible polymer chains [33, 49]. The smoothness of the membrane helps reduce the propensity of the membrane to biofoul [48]. Furthermore, piperazine-amides have reduced amidic hydrogen available, reducing the amides susceptibility to degradation by chlorine [20]. Polypiperazine-amide membranes can achieve excellent rejection of divalent ions due to Donnan effects, and are most suitable for NF applications.

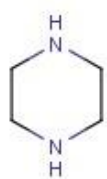
Reaction of MPD with aliphatic cyclohexane-1,3,5-tricarbonyl chloride resulted in a aralkyl polyamide thin film with better water flux but slightly lower salt rejection than fully aromatic polyamides. This may be attributed to less rigid polymer chains in the polyamide allowing for water molecules to more easily diffuse through the film.

To improve flux and rejection, MPD was reacted with 1-isocyanato-3,5-benzenedicarbonyl chloride. The resulting TFC membrane showed better resistance to fouling due to its reduced surface charge from reduced number of carboxylic groups, and higher tolerance to chlorine due to stronger polyamide-urea bonds.

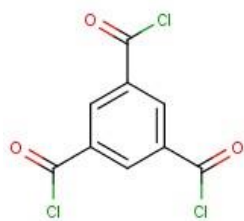
Yu et al. prepared NF membranes by interfacial polymerization of polyvinylamine (PVAm) with isophthaloyl chloride (IPC) on polysulfone UF membranes [50]. The advantage of using polyvinylamine is the ability to control the amount of amine units and amide units in the resulting polyamide by changing the formation conditions of the amine polymer. This allows tunable degree of crosslinking and surface potential in the resulting polymer. Due to the unfavorable partition coefficient of the polymeric amine in the organic phase, the acyl chloride needs to enter the aqueous phase. This reduces the reaction zone, producing a thinner and smoother film compared to polyamide formed from monomeric amines and acyl halides. The authors found that as the concentration of PVAm increases, the water flux and selectivity of the membrane also increases. The authors believe that this is because increased PVAm concentration increases the rate of polymerization, and the resulting thin film acts as a barrier to diffusion of IPC, creating a thinner and more permeable thin film. Furthermore, the increased PVAm concentration increases the $-RH_3N^+$ groups on the thin film under the testing conditions, increasing the hydrophilicity of the membrane and the salt rejection.

Table 1.5.4. Structures of monomers and resulting polymers formed by interfacial polymerization

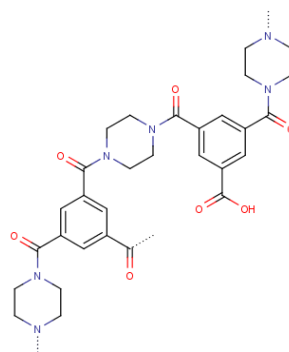
Amine	Acyl Chloride	Resulting Polymer
 <p>1,3-Benzenediamine or <i>m</i>-Phenylenediamine (MPD)</p>	 <p>1,3,5- Benzenetricarbonyl chloride or Trimesoyl chloride (TMC)</p>	 <p>Amide linkage</p> <p>Crosslinked</p> <p>Linear</p>
 <p>1,3,5-Benzene triamine</p>  <p>MPD</p>	 <p>Isophthaloyl chloride (IPC)</p>  <p>TMC</p>	



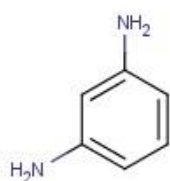
Piperazine



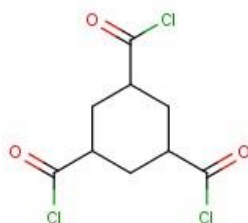
TMC



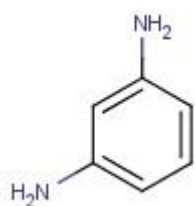
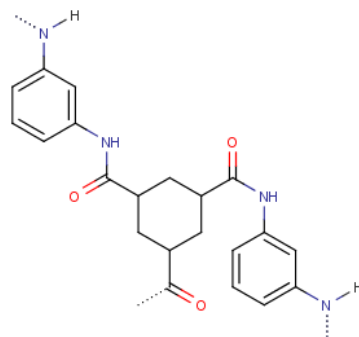
Polypiperazine-amide



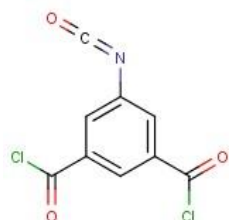
MPD



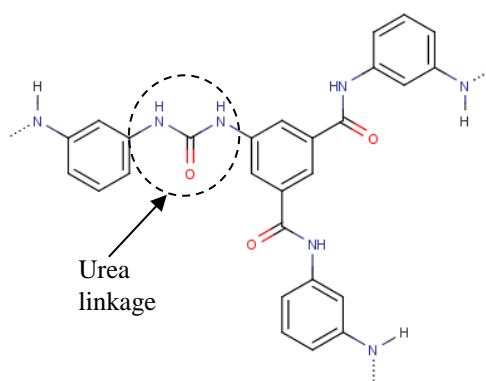
Cyclohexane-1,3,5-tricarbonyl chloride

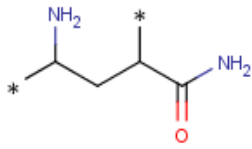


MPD

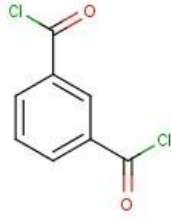


1-Isocyanato-3,5-benzenedicarbonyl chloride

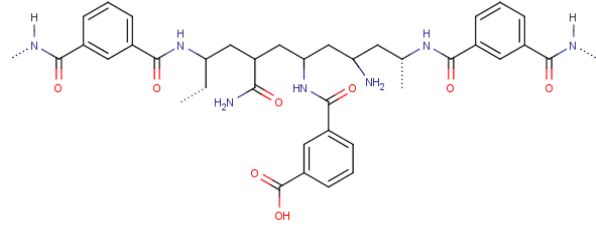




Polyvinylamine (PVAm)



IPC



1.6. Mass Transport in Composite Membranes

Both RO and FO membrane transport can be described by the solution-diffusion model. In this model, the permeants are assumed to dissolve in the membrane material and diffuse through the membrane due to a concentration gradient across the membrane [51]. This diffusion is best described by Fick's law of diffusion,

$$J_i = -D_i \frac{dc_i}{dx} \quad (2)$$

where J_i is the flux of a constituent (water or solute) through the membrane, D_i is the diffusion coefficient of the constituent in the membrane and dc_i/dx is the concentration gradient across the membrane. Concentration is related to the chemical potential of a solute in the membrane, assuming that the fluids on either side of the membrane are in equilibrium, and that the pressure throughout the membrane remains constant. From this, an equation for water flux, J_w , through the membrane is described by

$$J_w = \frac{D_w K_w V_w}{\Delta x R T} (\Delta P - \Delta \pi) = A (\Delta P - \Delta \pi) \quad (3)$$

where D_w , K_w , V_w , Δx , R , T is the water diffusion coefficient at the membrane, water-membrane partition coefficient, molar volume of water at the membrane, thickness of the membrane, the universal gas constant and absolute temperature, respectively [52]. These coefficients can be

grouped into a parameter called the intrinsic membrane pure water permeability, A . ΔP is the applied hydraulic pressure and $\Delta\pi$ is the osmotic pressure difference in the feed and permeate solutions, which must be overcome before any permeation through the membrane occurs in RO applications [51, 53].

The salt flux, J_s , through the membrane is described by

$$J_s = \frac{D_s K_s}{\Delta x} \Delta C = B(C_m - C_p) \quad (4)$$

where D_s and K_s is the solute diffusion coefficient in the membrane and the solute-membrane partition coefficient in the membrane, respectively, which can be grouped into another parameter called the intrinsic salt permeability, B . ΔC is the solute concentration difference between the concentrated (C_m) and the dilute or permeate (C_p) solutions on either side of the membrane [52]. Observed rejection, R_o is calculated by relating the bulk solution concentration, C_b to permeate solute concentration.

$$R_o = 1 - \frac{C_p}{C_b} \quad (5)$$

Typical seawater RO membranes have at least a flux of 15-20 gfd (gal/ft²/day) and 99.5-99.8% NaCl salt rejection when operated at a pressure of 800 psi at a temperature of 25°C for desalinating 35,000 ppm seawater [54]. The Dow Chemical Company (Midland, MI) has a line of TFC membranes called FILMTEC™ used in a variety of applications including desalination, water purification and waste water treatment. The FILMTEC™ brackish water membrane (BW30) when operated at 150 psi and 25°C, is reported to achieve 18 gfd and 99.4% rejection of both NaCl and CaCl₂ [55]. For the FILMTEC™ loose nanofiltration membrane (NF270), at 50 psi, 25°C and 18 gfd, 80% NaCl rejection, 50% CaCl₂ rejection and 99.3% MgSO₄ rejection can be achieved [55]. The HTI OsMem™ CTA-ES FO membrane is claimed to have a water flux of

4.5 gfd and a salt rejection of 99.4%, when tested with tap feed water and 1M NaCl draw solution at 25°C in FO-mode operation [18].

1.6.1. Concentration Polarization in RO/FO Membranes

The membrane structure and operating conditions in both RO and FO processes cause a buildup of solutes either on the membrane surface or within the membrane substructure, decreasing the driving force for water permeation. In reverse osmosis, a hydrodynamic boundary layer is believed to exist near the surface of the membrane that limits mass transfer. Convective transport is hindered by the membrane where only transport by diffusion allows water and salt to pass through the membrane. Thus, a buildup of salt at the membrane surface occurs, increasing the concentration of salt at the membrane surface compared to the feed solution concentration. This phenomenon is called external concentration polarization (ECP), causes the osmotic pressure difference ($\Delta\pi_{\text{eff}}$) across the membrane to be higher than the bulk ($\Delta\pi_{\text{bulk}}$), requiring a higher hydraulic pressure for permeation through the membrane (depicted in Figure 1.6.1). Furthermore, for high salinity waters, if ECP is significant the concentration of salt in feed may exceed its solubility limit and cause scaling on the membrane surface, thereby requiring even higher applied hydraulic pressure or chemical cleaning of the membrane for water permeation. Fortunately, the effects of ECP can be reduced by controlling the cross-flow across the surface of the membrane to increase mass transfer and decrease the thickness of the boundary layer [52].

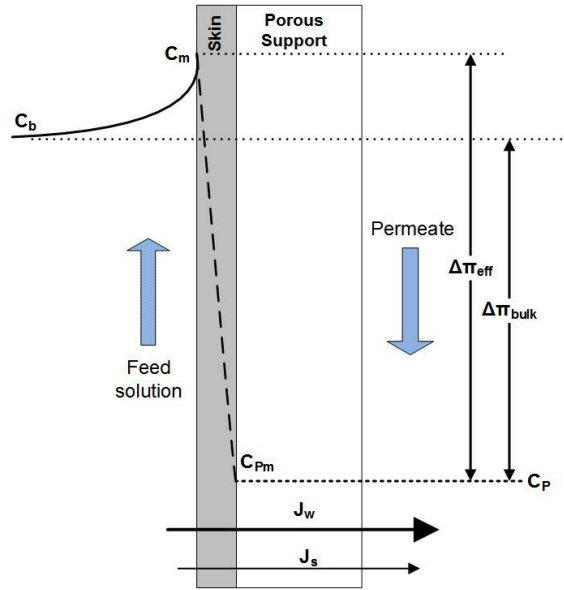


Figure 1.6.1. Schematic showing the concentration profile through a composite membrane illustrating the reduction in the osmotic pressure difference due to external concentration polarization.

As the concentration at the membrane surface cannot be directly measured, bulk solution concentrations can be related to the membrane concentration by knowing the hydrodynamic conditions. The concentrative concentration polarization modulus, CP is defined as:

$$CP = \frac{c_m - c_p}{c_b - c_p} \cong \frac{c_m}{c_b} = \exp\left(\frac{J_w}{k}\right) \quad (6)$$

where k is the mass transfer coefficient that is typically determined by correlations relating dimensionless numbers that accounts for fluid properties, flow properties, and channel geometries. For example,

- 1) For channels without spacers [56]

Under Laminar flow ($Re < 2000$)

$$Sh = 1.85 \times \left(ReSc \frac{d_H}{L}\right)^{\frac{1}{3}} = \frac{k d_H}{D} \quad (7)$$

Under turbulent flow ($Re > 2000$)

$$Sh = 0.04Re^{3/4}Sc^{1/3} = \frac{kd_H}{D} \quad (8)$$

2) For channels with spacer [57]

$$Sh = 0.46(ReSc)^{0.36} = \frac{kd_H}{D} \quad (9)$$

where Sh is the dimensionless group called the Sherwood number, Re is the Reynolds number

given by $Re = \frac{u_0 d_H \rho}{\mu}$, Sc is the Schmidt number given by $Sc = \frac{\mu}{\rho D}$, d_H is the hydraulic diameter

calculated by $d_H = 2WH/(W+H)$, where W is the width of the channel and H is the height of the channel, u_0 is the crossflow velocity, μ is the dynamic viscosity of the solution, ρ is the density of the solution and D is the diffusion coefficient of the solute in water. Many correlations have been developed for various geometries and have been summarized in a review paper by Wang et al. [52].

Using this information, the real rejection, R_r can be related to the observed rejection, R_o (Eqn. 4) and the intrinsic salt permeability, parameters that are commonly used to compare membrane performance, in the following manner,

$$R_r = \frac{c_m - c_p}{c_m} = 1 - \frac{c_p}{c_m} \quad (10)$$

$$R_o = 1 - (1 - R_r) \exp\left(\frac{J_w}{k}\right) = \frac{J_w}{J_w + B \exp\left(\frac{J_w}{k}\right)} \quad (11)$$

Currently, TFC membranes are used for both RO and FO applications. Although TFC membranes have a much higher chemical and thermal stability than cellulosic membranes, the mechanical stability of the membrane as needed in RO applications actually hinders mass

transfer and thus, water flux in FO, which operates under minimal hydraulic pressures (less than 5 psi). As mentioned in Section 1.4, the porous substructure, typically composed of polysulfone, formed by phase inversion, has dense finger-like pores at the surface followed by large macrovoids underneath [24]. In RO operation, the macrovoids allow for low hydraulic resistance, but in FO, the voids create stagnant zones limiting transport to diffusion. Therefore, in addition to ECP at the membrane surface, the unstirred boundary layer created by the porous substructure creates another prominent mass transfer limitation called internal concentration polarization (ICP). When the skin layer of the membrane faces the draw solution (PRO-mode), concentrative ICP occurs due to the solute from the feed side concentrating in the porous substructure as shown in Figure 1.6.2 (a). When the skin layer of the membrane faces the feed solution (FO-mode), dilutive ICP occurs as the draw solution concentration being diminished by the incoming water flux across the membrane as shown in Figure 1.6.2 (b). In either case, there is a substantial reduction in the effective osmotic pressure difference, which is the driving force for water flux in FO [58].

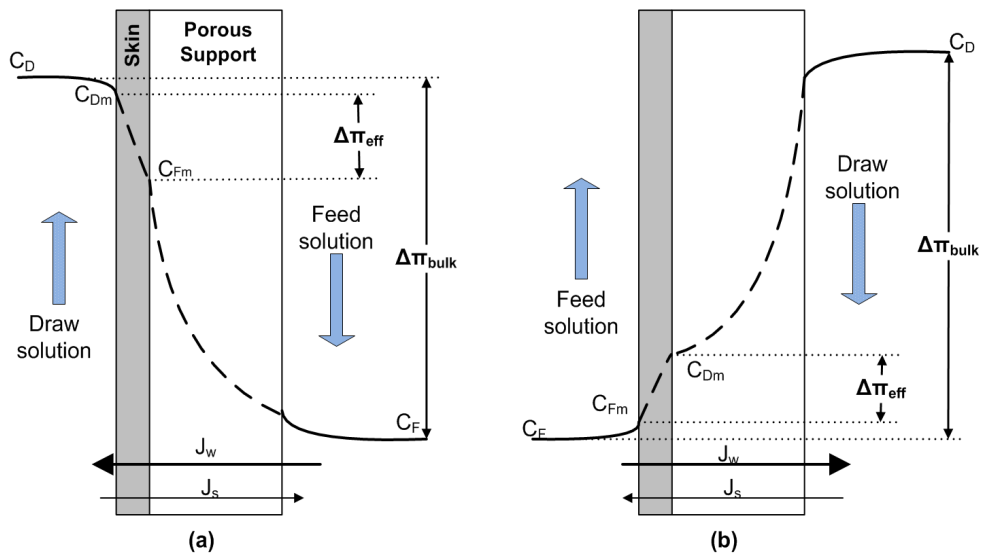


Figure 1.6.2. Schematic showing the concentration profile through an asymmetric membrane, illustrating the reduction in the osmotic pressure difference due to (a) concentrative ICP in PRO-mode and (b) dilutive ICP in FO-mode [59].

The extent of ICP has been investigated using a parameter called resistance to solute diffusion by the porous substructure, K , which depends on the orientation of the membrane. For the skin layer facing the draw and using Milli-Q water as the feed solution ($\pi_F = 0$) [53, 60],

$$K = \left(\frac{1}{J_w}\right) \ln \left(\frac{B+A\pi_D-J_w}{B+A\pi_F}\right) \quad (12)$$

And, when the skin layer faces the feed,

$$K = \left(\frac{1}{J_w}\right) \ln \left(\frac{B+A\pi_D}{B+J_w+A\pi_F}\right) \quad (13)$$

where π_D and π_F is the osmotic pressure of the draw solution and feed solution, respectively. The concentration is related to osmotic pressure using the Gibbs' equation [54].

$$\pi = -\frac{RT}{V_w} \ln x_w \quad (14)$$

where x_w is the molar fraction of water in the solution. To characterize the porous support, it is necessary to uncouple the solute resistance from the solution diffusivity by defining a membrane structural parameter or factor, S , as

$$S = KD = \frac{t_{\text{sup}} \tau}{\varepsilon} \quad (15)$$

where t_{sup} , τ and ε are the support membrane thickness, tortuosity and porosity, respectively [61]. The structural parameter, with units of length, can be thought of as the average distance a solute has to travel from the bulk solution, through the porous support, in order to reach the membrane active layer. According to Eq. (15), the lowest hindrance to diffusion, or the lowest amount of ICP, is achieved when the FO porous support is thin, non-tortuous, and very porous, which indicates that the best support is no support at all, although that is not realistic. FO supports should also be able to withstand necessary backwash in operation. Bui et al. formed TFC membranes using electrospun polysulfone-polyethersulfone nanofiber support layers, which exhibited at least two times higher water flux and 100 times lower salt flux than a commercial FO membrane. The authors rationalized the improved performance is due to higher porosity and lower tortuosity of the support, which decreased ICP [19]. According to a recent study by Widjojo et al., the most permeable and selective FO membranes were formed from coating 50% sulphonated polyethersulfone UF membrane supported a thin selective polyamide film [17]. The membrane had a spongy morphology, but had the highest flux and lowest salt passage, using DI water as the feed and 2M NaCl as the draw solution, compared to that reported in the literature. Thus, the authors concluded that the hydrophilicity of the support membrane is more important than the morphology in affecting water permeability [17]. This points out an interesting fact that the structural parameter does not account for membrane chemistry, which may significantly impact membrane performance.

Table 1.6, which is by no means comprehensive, describes various references that have used either parameter K or S in characterization of osmotic membranes. However, the membrane structural parameter is experimentally determined using water and salt permeability coefficients determined by RO experiments. It is expected that the permeability coefficients under RO

conditions (hydraulic pressures of over 400 psi) do not accurately reflect the permeability coefficients of the much thinner and structurally weaker FO membranes that operate under low pressure (FO, PRO) conditions. This issue has been recently addressed by Tiraferri et al. in which water and salt permeability coefficients along with the structural parameters are determined solely by a series of FO experiments [62]. Furthermore, the structural parameter does not account for certain characteristics of the support such as hydrophilicity, solute-membrane interaction, and pore geometry, which can have mechanistic effects on water transport. This was briefly explored by Wong et al. when the structural parameter of the HTI-CTA membrane was found to change with change in solution chemistries and flow conditions [59]. The authors concluded that as the draw solution ionic strength increased, the increase in structural parameter was possibly due to the de-swelling in the polymer matrix.

Table 1.6. Studies using parameters K and/or S in characterization of osmotic membranes

Year	Journal	Title	Authors	Brief Description	Ref.
1981	JMS	Membranes for power generation by pressure-retarded osmosis	K.L. Lee, R.W. Baker and H.K. Lonsdale	Evaluating PRO performance of membranes using FO and RO data - model (incorporating K) predicts concentration polarization within porous substrate lowers water flux under PRO conditions	[27]
1997	JMS	Effect of porous support fabric on osmosis through a Loeb-Sourirajan type asymmetric membrane	S. Loeb et al.	Using commercially available asymmetric L-S membranes to evaluate the resistance to solute diffusion of the support fabric using K	[9]
1998	Desal	Energy production at the Dead Sea by pressure-retarded osmosis: challenge or chimera	S. Loeb	Evaluation of feasibility PRO plants at the Dead Sea. K introduced in terms of thickness of fibers in hollow fiber membranes.	[30]
1998	JMS	A study of the direct osmotic concentration of tomato juice in tubular membrane – module configuration. I. The effect of certain basic process parameters on the process performance	K.B. Petrotos, P. Quantick, and H. Petropakis	Concentration of tomato juice using FO using different draw solutions. Resistance to mass transfer was evaluated using parameter K .	[31]
2006	JMS	Influence of concentrative and dilutive internal concentrative polarization on flux behavior in forward osmosis	J. R. McCutcheon and M. Elimelech	Experimental determination of solute's resistance to diffusion and its effect in PRO and FO performance - flux reduction by ECP and ICP	[32]
2007	JMS	Salinity-gradient power: Evaluation of pressure-retarded osmosis and reverse electrodialysis	J. W. Post et al.	Comparison of power density by PRO and RED - parameter K shows that development of PRO must focus on optimization of porous support	[33]
2008	Desal	Membrane processes in energy supply for an osmotic power plant	K. Gerstandt et al.	Improving PRO membranes for power generation - exploring TFC and asymmetric CA membranes	[34]
2009	JMS	Power generation with pressure retarded osmosis: An experimental and	A. Achilli , T. Y. Cath, and A. E. Childress	Development of a predictive PRO model with experimental results to verify model. K used to evaluate the membrane change at	[35]

		theoretical investigation		various solution concentrations.	
2010	EST	High Performance Thin-Film Composite Forward Osmosis	N.Y.Yip et al.	TFC membranes formed using PSf, tested with ammonium bicarbonate draw solution without degradation	[26]
2010	Desal	Characteristics and potential applications of a novel forward osmosis hollow fiber membrane	S. Chou et al.	Interfacial polymerization on the inner surface of a polyethersulfone hollow fiber membrane	[36]
2010	JMS	Well-constructed cellulose acetate membranes for forward osmosis: Minimized internal concentration polarization with an ultra-thin selective layer	S. Zhang et al.	Using FESEM and PAS to determine the double dense-layer structure of phase inversion CA FO membrane	[37]
2010	JMS	Selection of inorganic-based draw solutions for forward osmosis applications	A. Achilli , T. Y. Cath, and A. E. Childress	Protocol for selection of optimal draw solutions for FO applications - evaluated for water flux and reverse salt diffusion	[38]
2010	EST	Reverse Draw Solute Permeation in Forward Osmosis: Modeling and Experiments	W. A. Phillip , J. S. Yong and M. Elimelech	Membrane structural parameter to predict reverse solute flux, independent of draw solute concentration and membrane structure	[28]
2010	JMS	Characterization of novel forward osmosis hollow fiber membranes	R. Wang et al.	Hollow fiber FO TFC membranes characterized using K and S to show that substrates are highly porous with narrow pore size distribution.	[39]
2011	JMS	Relating performance of thin-film composite forward osmosis membranes to support layer formation and structure	A.Tiraferri et al.	Systematic study of TFC membranes formed by interfacial polymerization using PSf, different casting conditions, casting blade heights etc.	[20]
2011	Adv Mat	Nano Gives the Answer: Breaking the Bottleneck of Internal Concentration Polarization with a Nanofiber Composite Forward Osmosis Membrane for a High Water Production Rate	X. Song, Z. Liu, and D. Sun	Low structural parameter obtained from interfacially polymerized polyamide TFC nanofiber PES Supported membranes compared to TFC and HTI membranes	[40]

2011	JMS	Effect of substrate structure on the performance of thin-film composite forward osmosis hollow fiber membranes	L. Shi et al.	Hollow fiber TFC FO membranes - It was found that substrates with <300 kDa MWCO was preferred for good semipermeable skin	[41]
2011	JMS	Determination of a constant membrane structure parameter in forward osmosis processes	M. Park et al.	Numerical models to simulate FO processes to find consistent S values. Inconsistent S values due to the assumption that ratio of concentrations is proportional to the ratio of osmotic pressures.	[42]
2011	EST	Boric Acid Permeation in Forward Osmosis Membrane Processes: Modeling, Experiments, and Implications	X. Jin et al.	Predicting boron flux and other containments rejection in FO operation	[43]
2011	JMS	Synthesis and characterization of flat-sheet thin film composite forward osmosis membranes	J. Wei et al.	Flat sheet TFC polyamide FO membranes on PSf supports -low solute reverse diffusion, high water flux	[11]
2012	AIChE J	Developing thin-film-composite forward osmosis membranes on the PES/SPSf substrate through interfacial polymerization	K. Y. Wang, T-S Chung, and G. Amy	PPD/TMC monomers used for interfacial polymerization on PES/SPSf substrate with enhanced hydrophilicity in PRO mode	[44]
2012	EST	Superhydrophilic Thin-Film Composite Forward Osmosis Membranes for Organic Fouling Control: Fouling Behavior and Antifouling Mechanisms	A. Tiraferri et al.	No change in S by modifying TFC membranes with superhydrophilic surfaces - performance of fouling and antifouling experiments to test alginate and BSA fouling	[45]
2012	Desal	Standard Methodology for Evaluating Membrane Performance in Osmotically Driven Membrane Processes	T.Y. Cath et al.	Round robin testing of two commercial membranes in seven independent laboratories - to develop standard methodology for testing osmotically driven membrane processes	[46]
2013	JMS	Synthesis and characterization of thin film nanocomposite forward osmosis membrane with	D. Emadzadeh et al.	Formation of thin film nanocomposite FO membranes by incorporating different loadings of titanium dioxide nanoparticles into polysulfone substrate. Changes in flux	[47]

		hydrophilic nanocomposite support to reduce internal concentration polarization		was attributed to changes in parameter in K and S.
2013	JMS	Synthesis of novel thin film nanocomposite (TFN) forward osmosis membranes using functionalized multi-walled carbon nanotubes	M. Amini, M. Jahanshahi and A. Rahimpour	Thin film nanocomposite FO membranes were synthesized using amine functionalized multi-walled carbon nanotubes as the additive in the 1,3-phenylenediamine solution. S was used to characterize membrane structure. [48]

1.6.2. Relationship between Thin Film and Support Membrane

Concentration polarization occurs due to the formation of an “unstirred boundary layer” that causes solute buildup in the support layer of a composite membrane. By coupling the support membrane to the thin film, the permeability of the composite membrane changes significantly. As illustrated by Figure 1.6.3a, if the solute enters the membrane on top of the support matrix, instead of the solute having to diffuse through the thin film thickness, δ , to reach the bulk, it now has to diffuse through a longer “effective” diffusion path length, δ_{eff} . By using a very simplified model of a unit cell, as shown in Figure 1.6.3b, the porosity of the support membrane is defined as,

$$\varepsilon = \frac{\pi}{4} \left(\frac{R_1}{R_2} \right)^2 \quad (16)$$

By approximating the effective diffusion path length as the sum of the shortest and longest path length, to be proportional to the porosity and solidosity (i.e. $1-\varepsilon$) of the support, respectively, Ramon et al. derived the following expression for δ_{eff} [63],

$$\delta_{eff} = \varepsilon\delta + (1 - \varepsilon) \left(\delta + \sqrt{\frac{\pi R_1^2}{\varepsilon} - R_1} \right) \quad (17)$$

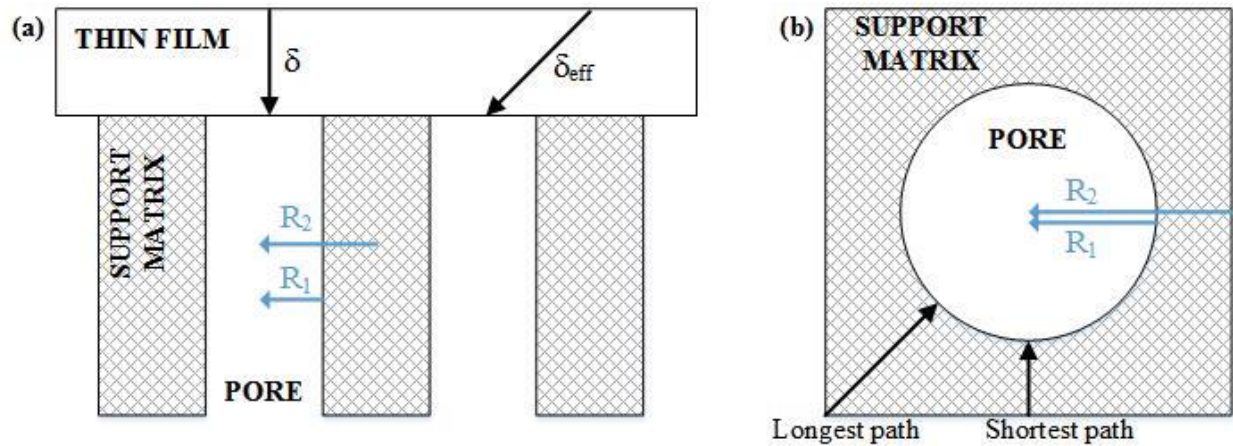


Figure 1.6.3. Schematic illustrating the geometry used to describe effective diffusion path length. a) side view b) top view of a unit cell (Adapted from [38, 63])

Using this analytical expression along with basic transport equations described in previous sections, the authors were able to relate permeability to porosity using commercial RO and NF membrane parameters. The authors found that to maximize rejection, supports with relatively low porosity and large pores should be used to maximize flux, while supports with high porosity and small pores are needed to maximize rejection. Furthermore, more permeable thin films are more greatly influenced by changes in the support membrane pore structure. When roughness is added to the thin film, the flux distribution changes depending on whether the pores are aligned with the roughness or the valleys of the film. Thus, “hotspots” or areas of high flux are created, indicating short effective diffusion path lengths. These hotspots are expected to have higher propensity for scaling and fouling due to higher external concentration polarization at these regions [64].

1.7. RO/FO Membrane Stability, Degradation, Fouling, and Scaling

Due to operational conditions, membrane properties, feed solution properties, TFC membranes face some drawbacks in industrial applications. This includes membrane stability, degradation, and propensity to fouling and scaling. During RO applications, TFC membranes are subject to high hydraulic pressures (800-1000 psi), which causes irreversible fouling, or compaction of the membranes. This compaction causes an increase in the hydraulic resistance of the membrane, and hence, reduces the water flux by up to 20% [38]. Pendergast et al. found that embedding zeolite nanoparticles in the polysulfone support of RO membranes helped the TFC membrane resist compaction due to enhanced mechanical stability [38].

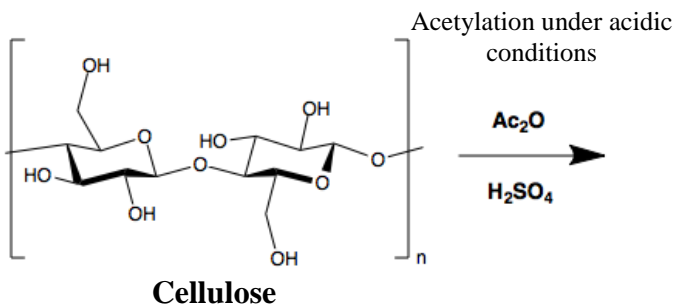
Bacteria can also colonize on the surface of the membrane and form a biofilm, which is difficult to remove by hydraulic means. To make matters worse, the polyamide (PA) thin film is subject to oxidative degradation by chlorine, and thus, chlorine disinfectants must be removed prior or dosed after membrane filtration, exacerbating the formation of biofilms and increasing the cost of pretreatment [39, 65]. The degradation of PA thin films by chlorine has been studied extensively [66-68]. It has been postulated that reversible chlorination occurs whereby the amide nitrogen is chlorinated, followed by a gradual irreversible Orton rearrangement where the chlorine attacks the aromatic ring causing the polyamide to undergo scission and form degradation products [69]. Research has been done to improve antifouling properties the PA thin film, including adding surface coatings, grafting polymers or embedding nanoparticles in the thin film. Many studies have focused on grafting polymers onto the polyamide surface to improve antifouling properties of the thin film, but also to impart increased hydrophilicity as it is believed that biofouling is higher due to hydrophobic interactions between the foulant and the membrane surface [70-73]. McVerry et al. utilized perfluorophenyl azide photochemistry to add

polyethylene glycol moieties of different molecular weight onto the polyamide thin film in order to increase the hydrophilicity of the membrane surface. The authors found that as the PEG molecular weight increased, the apparent contact angle decreased, indicating increased wettability of the membrane, and also decreased surface coverage of *E.coli* [74]. Kwak et al. embedded TiO₂ self-assembled nanoparticles in PA TFC RO membranes and found that the photocatalytic bactericidal effects of TiO₂ on *E. coli* were significantly higher than a membrane without nanoparticles and UV irradiation, even though the membranes had similar water flux and salt rejection data [75].

Depending on the source water and the type of pretreatment used in a treatment plant, colloidal fouling may also occur on the membrane surface. Furthermore, as product water is forced through the membrane, the remaining brine concentrates over the length of the module, causing some salts to exceed its solubility limit and scale on the surface of the membrane. Due to the high applied pressure in RO filtration, any suspended particles in the feed water will be convectively driven towards the surface of the membrane, resulting in an accumulation of colloidal material. A study by Vrijenhoek et al. of various aromatic polyamide RO/NF membranes found that colloidal fouling correlated well with membrane surface roughness, that is, more fouling was observed with rougher membranes [76]. The authors also found that particles tended to accumulate at the valleys of the PA film, causing “valley clogging”, which causes severe flux decline. These results were further explained by a computation fluid dynamics modeling (CFD) of TFC membranes by Ramon et al., which showed that when the support pores were aligned with the valleys of the thin film, regions of high flux or “hotspots” were formed that could be areas of high fouling propensity [63].

Thus, biofouling, scaling and colloidal deposition will increase the hydraulic resistance for permeation through the membrane, but are considered “reversible” fouling on membrane surfaces as the foulants can be removed, to some extent, by hydraulic means. This includes increasing crossflow rates, chemical washing, and backwashing.

Cellulosic membranes are also prone to the above drawbacks for TFC membranes, but are presumably less severe due to less surface roughness compared to TFC membranes. In addition, cellulose is a polysaccharide that is a major component of plant cell walls, which can act as a food source for many micro-organisms, increasing the propensity for biofouling and degradation. Lastly, cellulose acetate will hydrolyze over time, replacing the acetate group with a hydroxyl group. This hydrolysis is a minimum at a pH of 4-6, which limits the application of cellulosic membranes [39]. Although cellulose triacetate is more chemically and thermally stable than cellulose diacetate, it has lower resistance to compaction and is still susceptible to hydrolysis under acidic and alkaline conditions [20]. Studies have found that these cellulose triacetate films will hydrolyze under humid conditions, releasing acetic acid, which catalyzes further degradation [77-79]. Hence, this degradation process is commonly called the “vinegar syndrome”. The reaction scheme showing the acetylation of cellulose to form cellulose triacetate and the subsequent hydrolysis is shown in Figure 1.7.



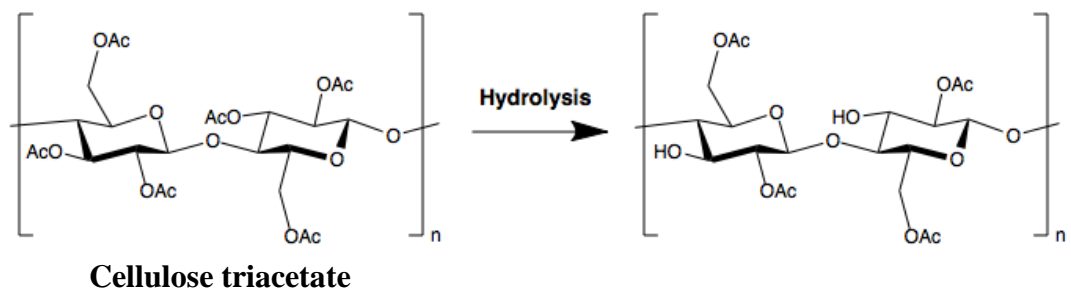


Figure 1.7. Reaction mechanism showing acetylation of cellulose followed by hydrolysis

1.8. Polyaniline and its Potential as a RO/FO Membrane Material

Polyaniline (PANi) is best known as a conducting polymer with three oxidation states. It is commonly used in a variety of applications including, antistatic coatings, electromagnetic shielding, flexible electrodes, gas separation membranes and chemical sensors [80-82]. It has also recently gained attention as an attractive material for membranes in water treatment due to its hydrophilicity [7, 83]. PANi is commonly formed by chemical oxidative polymerization of aniline. Typical procedure for PANi synthesis has been described elsewhere [57, 81]. In brief, aniline is dissolved in an acidic aqueous solution and combined with an oxidant, commonly containing peroxydisulfate anion. The anilinium cations participate in polymer chain growth until all the oxidant is consumed forming the emeraldine form of PANi. Guillen et al. further purifies the PANi by filtering the polymer through a microfiltration membrane, washing the polymer with NaOH, water and methanol prior to drying the polymer at 50°C [57].

PANi occurs in three oxidation states as shown in Figure 1.8.1. Leucoemeraldine, PANi's fully oxidized form, appears to be white and is not electrically conducting. Pernigraniline is the fully reduced form, while the emeraldine form, often referred to as emeraldine base is half

oxidized, and can be doped with acid, so that the imine nitrogens are protonated forming the conductive form of PANi, called the emeraldine salt [84].

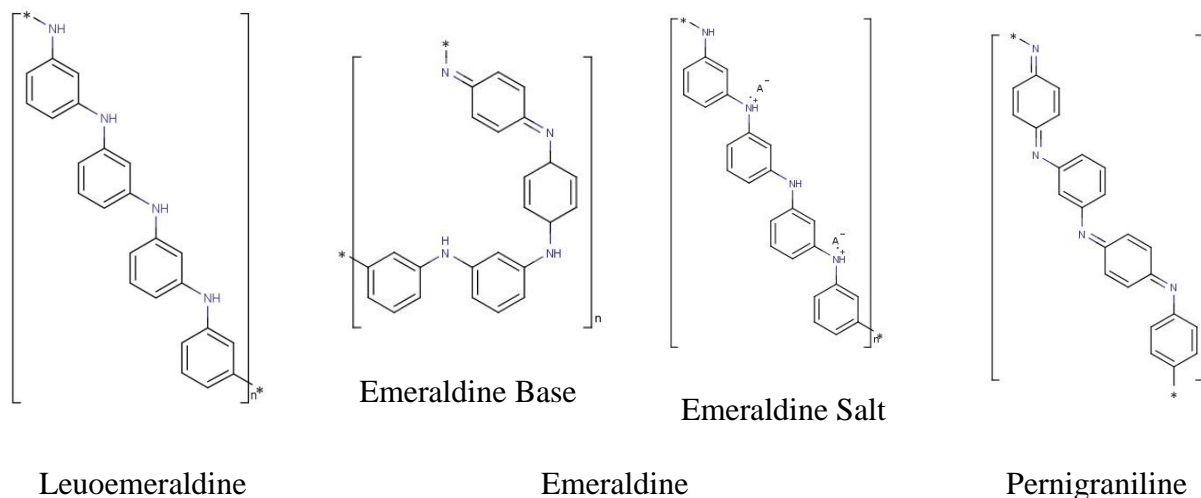


Figure 1.8.1. Chemical structure of polyaniline in its three oxidation states.

In gas separation, Mattes et al. formed conjugated emeraldine PANi films for separating gas pairs. The authors found that by subjecting the films through a doping and undoping treatment cycle, specifically washing the films with HClO₄ followed by NH₄OH and then again by HClO₄, resulted in significant separation factors. The authors postulated that the dopant occupied “free-volume” of the film [85]. In water treatment applications, Guillen et al. formed PANi UF membranes by phase-inversion with the procedure described above in Section 1.4. The authors formed UF membranes using blends of PANi and PSf in the ratios 1:0, 3:1, 1:1, 1:3 and 0:1 PANi to PSf, where a 3:1 ratio means the membrane casting solution contains 75% PANi and 25% PSf. They found that the pure PANi membrane had a pure water permeability an order of magnitude greater than a pure PSf membrane, although slightly lower rejection of silica particles. The membrane macrovoid structure also changed depending on the blend of the membrane as

shown in Figure 1.8.2. Pure PANi and pure PSf have the most macrovoids of all the blends, while the 1:1 PANi:PSf has the most spongy morphology [7].

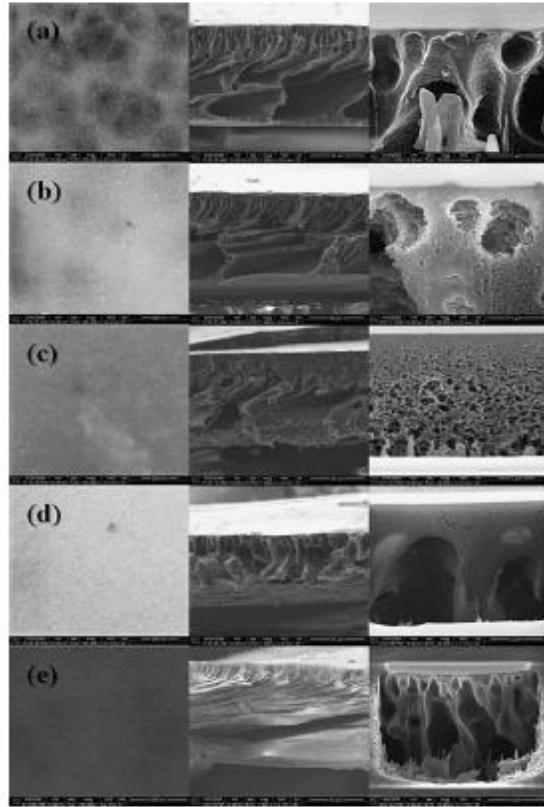


Figure 1.8.2. SEM images of membrane surface (left), full cross-section (middle) and skin layer cross-section (right) of PANi:PSf ratios of (a) 1:0, (b) 3:1 (c) 1:1, (d) 1:3, and (e) 0:1 [7].

1.9. Summary

The previous sections provide an overview of phase inversion and interfacial polymerization, and the membrane materials used in forward osmosis and reverse osmosis applications. Both membrane formation techniques can be altered by changing the solvent system, using additives, or post-treating the membranes, to induce properties such as increased hydrophilicity, permeability or anti-fouling functionalities. As phase-inverted membranes do not provide high enough selectivity for osmotic applications, polymeric thin-films are formed on the

surface via interfacial polymerization, forming thin film composite (TFC) membranes. External concentration polarization occurs due to a buildup of solute at the surface of the membrane, which decreases the driving force across the membrane surface, and requires higher hydraulic pressure for water permeation. In forward osmosis, when water permeation is driven by an osmotic pressure difference across the membrane, the composite membrane structure causes yet another mass transfer limitation called internal concentration polarization. This is caused by the unstirred boundary layer that the porous substructure creates, which decreases the effective driving force across the membrane. The support layer also interplays with the thin film by changing the flux distribution throughout the membrane, which creates hotspots or regions of higher fouling and scaling propensity. Current membrane materials for reverse osmosis has properties such as negative surface charge and high surface roughness that provide the ideal grounds to initial biofilm formation, against which traditional methods of cleaning such as back washing and chemical cleanings are not efficient. Furthermore, chlorine, a common disinfectant, degrades polyamide reverse osmosis membranes, thereby requiring a pre-treatment process to remove residual chlorine before the water is fed through the membrane modules. The only commercially available forward osmosis membrane material has limited chemical and thermal stability, limiting its use in applications such as low energy desalination. Polyaniline is being explored as a membrane material for filtration applications due to its hydrophilicity and tunable pore structure.

1.10. Research Hypothesis and Objectives

The above chapter reviews the basis of the techniques and background covered in this dissertation. As research has already been done on using polyaniline as a membrane material for filtration purposes, it will be extended in its use for osmotic applications and used in

understanding membrane structure and its role in determining membrane performance. From the review the limiting factor in high performing forward osmosis membranes is due to mass transfer limitations. Therefore, it is hypothesized that a membrane material with high hydrophilicity and large macrovoids will lower internal concentration polarization to provide high water permeability and low salt passage in forward osmosis applications. The high hydrophilicity combined with large macrovoids will allow higher mass transfer in the porous substructure.

The first objective is to develop a computation fluid dynamics structure-performance model for a composite membrane structure, in order to better understand how thin film interplays with the support membrane to affect overall composite membrane performance. This modeling effort will give insight as to how thin film and support membrane generate various flux distributions, and the different contributions of each. The second objective is to further understand the relationship between structure-performance relationships of osmotic membranes by forming a thin film on polyaniline. The purpose of this objective is to learn how the use of a hydrophilic support will alter thin film formation compared to relatively hydrophobic supports, and its consequence on the performance of the composite membrane. The third objective is to use polyaniline as a model membrane material to determine the potential as a forward osmosis membrane, and in doing so, understand how varying phase inversion formation parameters affect membrane performance. In this objective, methods to increase the water permeability and selectivity of the membrane to commercial standards will be sought, while characterizing the pore morphology and stability of the membrane.

CHAPTER 2

Non-Uniformity of Thin Film and Support Membrane Morphology

2. INTRODUCTION

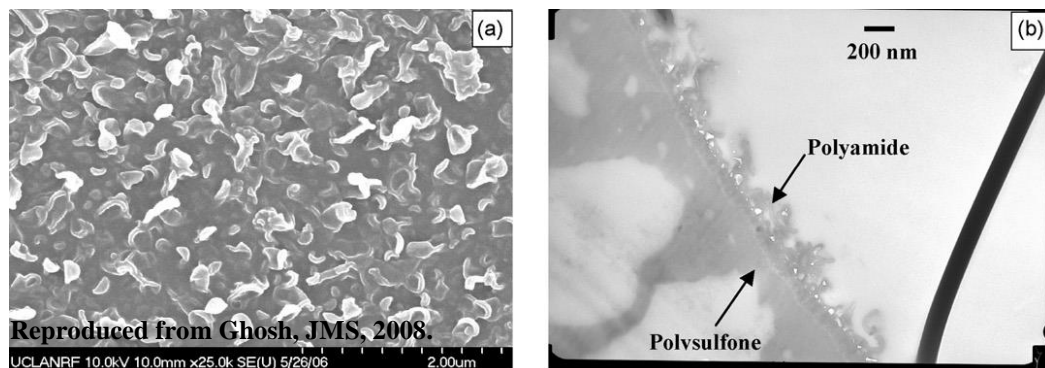
Most commercial reverse osmosis (RO) and nanofiltration (NF) membranes are comprised of an ultra-thin polyamide film formed over a microporous “ultrafiltration-like” support membrane (typically polysulfone or polyethersulfone cast over a polyester or polypropylene non-woven fabric). However, transport through these composite structures has not received much attention in the open literature. In particular, to address the basic questions of how the support membrane and the morphology of the typically rugose RO polyamide films, compared to the smooth NF films, impact transport through the composite membrane, and its implications on membrane fouling propensity. When comparing colloidal fouling behavior of smooth cellulose acetate RO membranes to that of rougher thin film composite membrane, Elimelech et al., found that flux decreased sharply for the TFC membrane, while only slowly for the cellulose acetate membrane [86]. Vrijenhoek et al., found experimentally that colloidal particles tend to deposit more on rough membranes than on smooth membranes, especially at “valleys” causing valley clogging, contributing to flux decline [76].

In our first theoretical study employing numerical analysis of diffusion through composite membrane structures [63], we found local “hot spots” of high flux (2-9 times the surface area average flux) occurring over support membrane pores; such hot spots could serve to initiate or enhance NF/RO membrane fouling and scaling phenomena. In a second study, we extended the model to consider thin film roughness [64]. Results illustrated how hot spots may be dampened by aligning roughness features directly over support membrane pores, increasing support membrane porosity, and increasing solute permeability through the microporous regions of the support membrane (i.e., the “solid” phase, not the skin layer pores). It was further shown

that there is a trade-off between dampening flux hot spots and maintaining high-permeability, suggesting that high flux composite membranes may be inherently fouling-prone.

Recent innovations in microscopy and higher resolutions in imagery have allowed improved characterization of thin film composite membranes, which revealed the detailed morphology of RO and NF membrane structures. Figure 2.1, comprises of a few images extracted from recent journal articles, highlighting the features and rough morphology of the thin film of RO membranes. SEM surface images of RO membranes reveal structures that have been referred to as “ridge and valley”, “leafy protrusions” or “carpet-like” morphology typical of fully aromatic polyamide films. A few studies have attempted to explain how this structure is formed, including Ghosh et al., who suggested that the support membrane characteristics play an important role in determining the permeability of the composite membrane. The researchers suggested that more porous and hydrophilic support membranes produced thinner, less rough, and less permeable thin films due to higher uptake of aqueous amine solution during the interfacial polymerization process compared to hydrophobic supports, as supported by experimental data [36]. A modeling study by Freger and Srebnik concluded that most acid chlorides and amines have fully developed concentration profiles after 20s with a tail extending into the organic phase, which is used to explain the rough morphology observed for RO membranes [87]. Furthermore, characterization and modeling efforts of various RO and NF membranes have suggested that the thin-film is inhomogeneous in composition and structural distribution. Using Rutherford Back-scattering (RBS), Mi et al. found that most polyamide films have incomplete crosslinking from the presence of unreacted carboxyl groups from the acid chloride monomers, causing an electrical charge gradient along the film [88]. Coronell et al. further elucidated this heterogeneity by using RBS, X-ray photoelectron spectroscopy (XPS) and

Atomic force microscopy (AFM) to find that there was a higher content of carboxylic groups and a lower concentration of nitrogen in the surface away from the support layer in the thin film of commercial RO and NF membranes, supporting the fact of depth heterogeneity [89]. Upon closer inspection of the TEM cross-sectional images, the films do not look entirely uniform in composition, with regions of dense polymer film and regions of open voids, which may even be fluid filled under testing conditions (see Fig 2.1c). A few research groups have observed this structure in RO thin films, with a dense basal region near the support layer, overlaid with “fluffy” polymer leafs that have voids underneath [90, 91]. This shows that roughness measurements captured by AFM and other techniques will not account for the void space underneath the polymeric mass as reported by some researchers. Kurihara et al. found using a TEM that the “protuberances” were “cave-like”, having the polyamide layers creating empty pockets (see Fig 2.1d). They suggested that this supports the claim that water permeability increased with surface area, which increased with the amount of protuberances available [92]. Kim et al. have found that by adding dimethyl sulfoxide into the aqueous phase during interfacial polymerization can not only produce rougher thin film composite membranes with higher flux, but also increases the network pores in the cross-linked polyamide thin film as confirmed by positron annihilation lifetime spectroscopy [43].



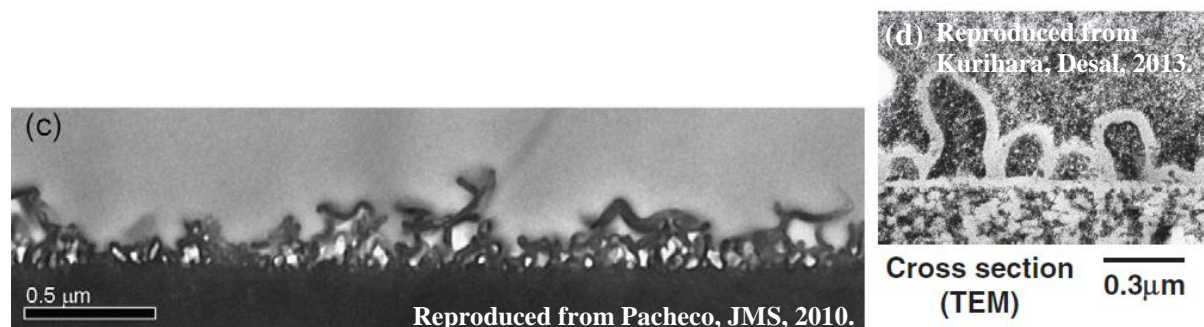


Figure 2.1. Surface SEM (a) and cross-sectional TEM images (b/c/d) of polyamide RO membrane thin films.

In this chapter, we build further on our prior efforts and consider heterogeneous films, in which the presence of fluid-filled cavities creates hollow, lobe-like coating films, as aforementioned for certain commercial RO membranes [91, 92]. The introduction of hollow domains between the coating film and support membrane raises interesting questions with respect to possible transport mechanisms through composite NF/RO membranes. In the previous study, we found that by increasing the roughness of the film without decreasing the base film thickness, the permeability of the membrane will decrease. We further investigate whether changing the distribution of the same amount of polymer around a void can impact the decrease in permeability and influence its flux distribution.

2.1. Numerical Model

2.1.1. Geometry

Here a sinusoidal wave was used to simulate the rough morphology of a polyamide thin film as was used in companion papers [63, 64]. Voids were introduced into the film to simulate inhomogeneity and to try best represent that which has been observed in TEM images. Support pores located directly underneath a valley is defined to be “in-phase” with roughness, whereas

pores aligned with a roughness feature is defined to be “out-of-phase”, and simulations without the support are referred to as “unsupported” as shown in Figure 2.2.

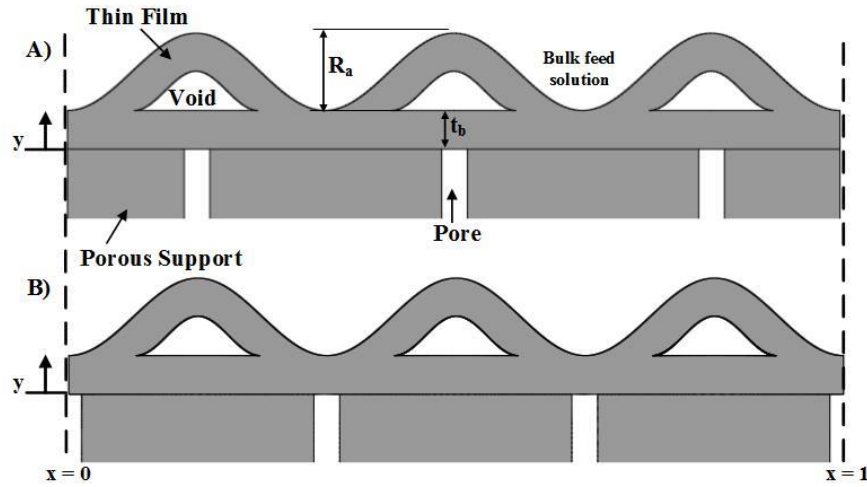


Figure 2.2. Schematic of geometry used in simulations for a) Out-of-phase and b) In-phase supported membranes

Simulations were plotted against a roughness factor or scaled roughness amplitude (R_f), which is defined as the roughness amplitude (R_a) scaled by the base film thickness, or R_a/t_b . As a basis of comparison, a solid rough film case was included in which the roughness was increased proportionally to the base thin film thickness. This case is used to represent when more material is involved in the reaction and more film is formed as a result. In the first set of simulations as shown in Figure 2.3, we defined a “constant void” case by introducing a sinusoid void with a height half the base film thickness into the thin film. For these simulations, the roughness amplitude of the thin film was increased while keeping the void height and area constant. For the “proportional void” set of simulations, the voids were increased proportionally with the roughness amplitude such that the film mass (or area) was kept constant.

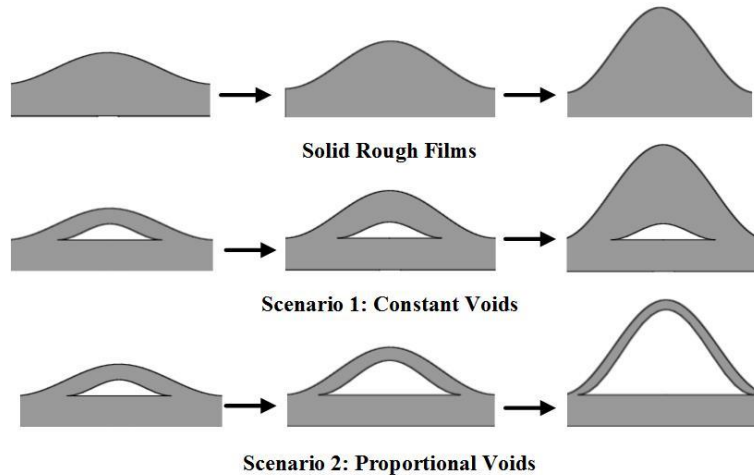


Figure 2.3. Schematic depicting the constant void and proportional void cases compared to the solid rough films without voids

In the second set of simulations, we wanted to probe the degree in which the thickness of the top film and base film above and below the void contributes to changes in permeability. Referring to Figure 2.4 as a guide, Case A describes the increase of the void volume by extending the base of the void, thereby decreasing the effective thickness of the base film. In Case B, the void volume was increased by adding volume to the curvature of the void sinusoid to decrease the top film thickness. In Case C, the void volume was increased by decreasing both the top film thickness and the base film thickness. In these simulations, the roughness amplitude was kept constant (at $R_f = 2$) and hence the surface area was also kept constant. In reality, films may be a combination of these scenarios, but for clarity and conciseness of analysis, simulations were kept separate.

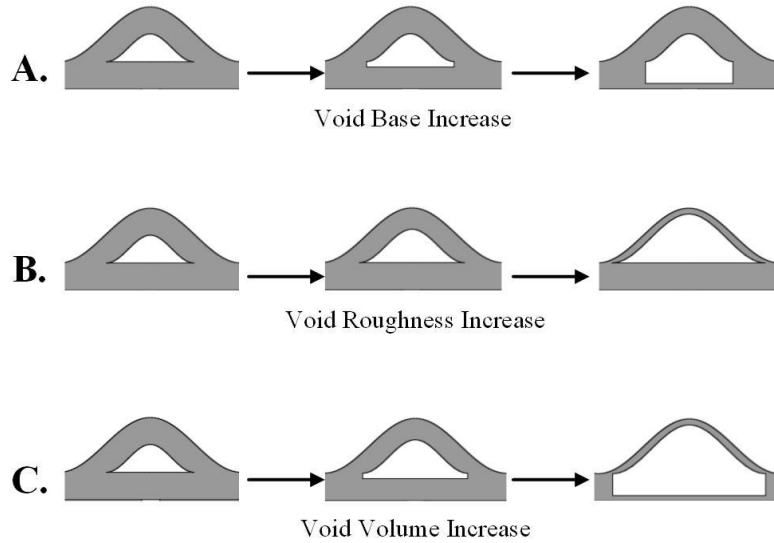


Figure 2.4. Schematic of void volume changes on unsupported films for one wavelength

2.1.2. Governing Equations

The numerical model follows the ones used in the companion papers [63, 64], which are governed by Fick's laws of diffusion. The boundary conditions applied are the same as the previous paper in which a scaled potential of unity is applied at the boundary between the film and bulk feed solution, a potential of zero is applied at the interface between the film and support pore to simulate a complete sink, and continuity is applied at the boundaries between the solid phases, and between the film and voids. Finally, the symmetry condition is used in the simulation where applicable. The diffusivity in the voids is set to be 100 times that in the film to represent a region of higher diffusivity, while the support diffusivity is 1×10^{-20} times that in the film to represent an impermeable support. The effect of support permeability was previously explored by Ramon et al [63]. In Section 2.2.2, a partition coefficient is introduced into the simulation, to determine the effect of concentration distribution between the film and voids on water flux across the membrane, this condition and all others used are summarized in Table 2.1.

Table 2.1. Summary of boundary conditions used in the simulations

Boundary	Condition**	Description
$x = 0, x = 1$	$\frac{\partial C}{\partial x} = 0$	Symmetry
Film/Bulk interface	$C = 1$	Unity potential
Film/Pore Interface, Support/Pore Interface	$C = 0$	Zero potential
Film/Support Interface	$D_f \frac{\partial C_f}{\partial y} = D_s \frac{\partial C_s}{\partial y}$	Continuity
Film/Void Interface	$D_f \frac{\partial C_f}{\partial y} = D_v \frac{\partial C_v}{\partial y}$	Continuity
Film/Void Interface	$K_{eq} = \frac{C_f}{C_v}$	Partitioning

**C is the scaled concentration, x and y are the scaled horizontal and vertical coordinates as labeled in Figure 2.2.

2.1.3. Scaling



Figure	Simulation Permeability	Permeability scaled by Unsupported base film	Permeability scaled by Membrane with Equivalent Polymer Volume
A	5.927	1	1

B	11.29	0.56	1.90
C	12.82	N/A	2.16

Figure 2.5. Illustration of unsupported films with same polymer volume distributed as a a) smooth flat film, b) rough periodically undulating film, c) random polymer globules

In this chapter, the permeability of the membranes, depending on the geometry, will be scaled in two different ways. The first is scaling the permeability with that of an unsupported base film. This means that the permeability of the membrane for each case will inevitably decrease compared to the base film as more polymer is added to increase roughness. Furthermore, for some simulations, the base film thickness changes along the distance of the membrane, and thus determining which base film to scale against is of concern. The second method of scaling is to scale the permeability against that of a membrane with the same amount of polymer distributed as a smooth flat film. The purpose is to demonstrate that the permeability of a membrane can significantly change depending on how the same amount of polymer is distributed. To illustrate this concept, Figure 2.5 shows three simulations of unsupported membranes with the same amount of polymer distributed in various ways with a table underneath showing the permeabilities scaled in the ways previously described. As expected, each film has a different permeability but without basis of comparison, it is difficult to determine which membrane has a higher permeability. When scaled against an unsupported base film, the permeability of Fig 2.5a) is scaled against itself as the base film is the smooth flat film. However, for Fig 2.5b) the scaled permeability is much lower as the base film is much thinner (therefore, has much higher permeability) than the entire membrane thickness. For Fig 2.5c), no base film can be determined since the base film thickness changes along the distance of the membrane. When the

permeability is scaled against that of a membrane with equivalent polymer volume distributed as a smooth flat film, the undulating film has a higher permeability than the smooth flat film as the valleys provide shorter paths of diffusion. The randomly distributed film has a higher permeability compared to that of the undulating film, due to the higher number of effective diffusion path lengths provided by the random distribution of polymer. As this illustrates, this scaling method provides a way to determine how distribution of polymer in different geometries affect the permeability.

When studying flux distributions, a parameter called the flux variation is defined, which is the peak scaled flux subtracted by the lowest scaled flux. This parameter is used to determine how the various “hotspots” in flux affects permeability, which in turn has implications in membrane scaling, fouling and defect formation.

2.2. Results and Discussion

2.2.1. Impact of Roughness on Permeability

For the simulations modeled in this paper, the solute first diffuses from the bulk on the feed side through a polymeric film, and possibly through a void of much higher diffusivity, then through another base film prior to reaching the bulk on the permeate side of the membrane. From Figure 2.6a, when scaled against a smooth unsupported film, the permeability of an unsupported solid rough film decreases due to increased diffusion path length as the roughness or polymer volume increases. This also indicates that although rougher membrane leads to higher surface area or contact area between the bulk feed solution and the membrane, the permeability still decreases. However, by adding a small void in the polymer film (Fig 2.3 Constant Void Case), the permeability of the membrane increases only slightly compared to the solid film case. This is because the shortest diffusion path length remains the valleys of the undulating film, and adding

the small void in the film does not significantly change this. From the solid film and constant void case, the permeability of the film increases as roughness increases because any polymer added on top of the base film only decreases the permeability of the membrane. In other words, the base film sets the upper bound in membrane performance.

In the proportional case scenario, after the initial decrease in permeability due to the addition of polymer for roughness, the polymer volume is then kept constant. This means the void volume increases proportionally to the increase in polymer volume (or roughness). The resultant permeability increases slightly as roughness increases because the top film thickness is spread over a larger surface area, which effectively becomes thinner. Thus, the top film thickness can decrease the permeability even when the base thickness is kept constant. This will be discussed further in the next scenarios.

When scaled against the permeability of a smooth membrane with equivalent polymer volume, the permeability of the solid and constant films trend similarly, which increase with increasing roughness. This means that two membranes of same polymer volume, one distributed as an undulating film will always have higher permeability than a smooth membrane with same base film thickness. By creating a rough undulating film, the valleys provide shorter diffusion path lengths than a solid smooth film. Although the flux distribution is no longer uniform, which will be discussed in a later section, the ridge and valley morphology creates a channeling effect that is not provided by a smooth solid film of equivalent polymer volume. As expected for the proportional case, the permeability trends as when the permeability is scaled by the permeability of the unsupported base film. This is because regardless of the roughness, the membranes are scaled by the permeability of membrane with the same polymer volume.

Figure 2.7 shows the permeability for Case A, B and C as a function of void volume when scaled against membrane of equivalent polymer volume. The reason that this scaling is used for these scenarios is because the base film thickness changes as the void volume changes. For Case A, when the void volume increases by decreasing the base film of the thin film region, the permeability increases as the void volume increases. At high void volumes, the base film becomes so thin that the shortest path length for diffusion is through the thin film on top of the void space, through the void, to reach the bulk on the other side of the membrane. With the resistance of the base film reduced to almost zero, the permeability of the membrane surpasses that of a smooth film of same polymer volume. These results highlight the importance of the base film in determining the permeability of the membrane.

For Case B, the void volume increases by decreasing the top film thickness of the thin film. The permeability decreases as the void volume increases. This indicates that the base film thickness has more effect in dictating the diffusion path length and thereby the permeability the overall membrane. This confirms that the base film sets the upper bound to membrane permeability.

For Case C, the void volume increases by decreasing both the top film and base film thickness of the thin film. The permeability changes minimally as the void volume increases. This is because Case C is a combination of Case A and Case B, where a decrease in base film thickness allows for higher permeability, while increase in void volume decreases the polymer volume and the permeability of the smooth unsupported solid film of which it is scaled against.

2.2.2. Effect of Partition Coefficient on Permeability

The partition coefficient is defined as the ratio of the equilibrium solute concentration in the film to that in the void, which is expected to be bounded by 0 and 1. The dotted lines in Figures 2.6 and 2.7 represent imparting a partition coefficient of 0.01 on the transport. Figure 2.6 shows that the permeability of the membrane does not change significantly as the partition coefficient decreases for the constant void scenario while increases slightly for the proportional void scenario, with increasing scaled roughness amplitude. This indicates that as more solute is able to partition in and out of the void, the permeability of the membrane increases only when the base film thickness is low. This is because the base film acts as a final resistance to diffusion before reaching the bulk, regardless of how fast diffusion was prior to reaching it. This is better illustrated in Figure 2.7, where the roughness in all cases remains the same, and only the void volume changes. In Case A, decreasing the partition coefficient significantly increases the permeability at higher void volumes due to decrease in base film thickness. Contrary, for Case B, no significant change is observed when the partition coefficient is decreased due to the base film thickness kept constant in the simulation. Finally, for Case C, although the increase in void volume decreases the base film thickness, this is countered by the simultaneous decrease in overall polymer volume.

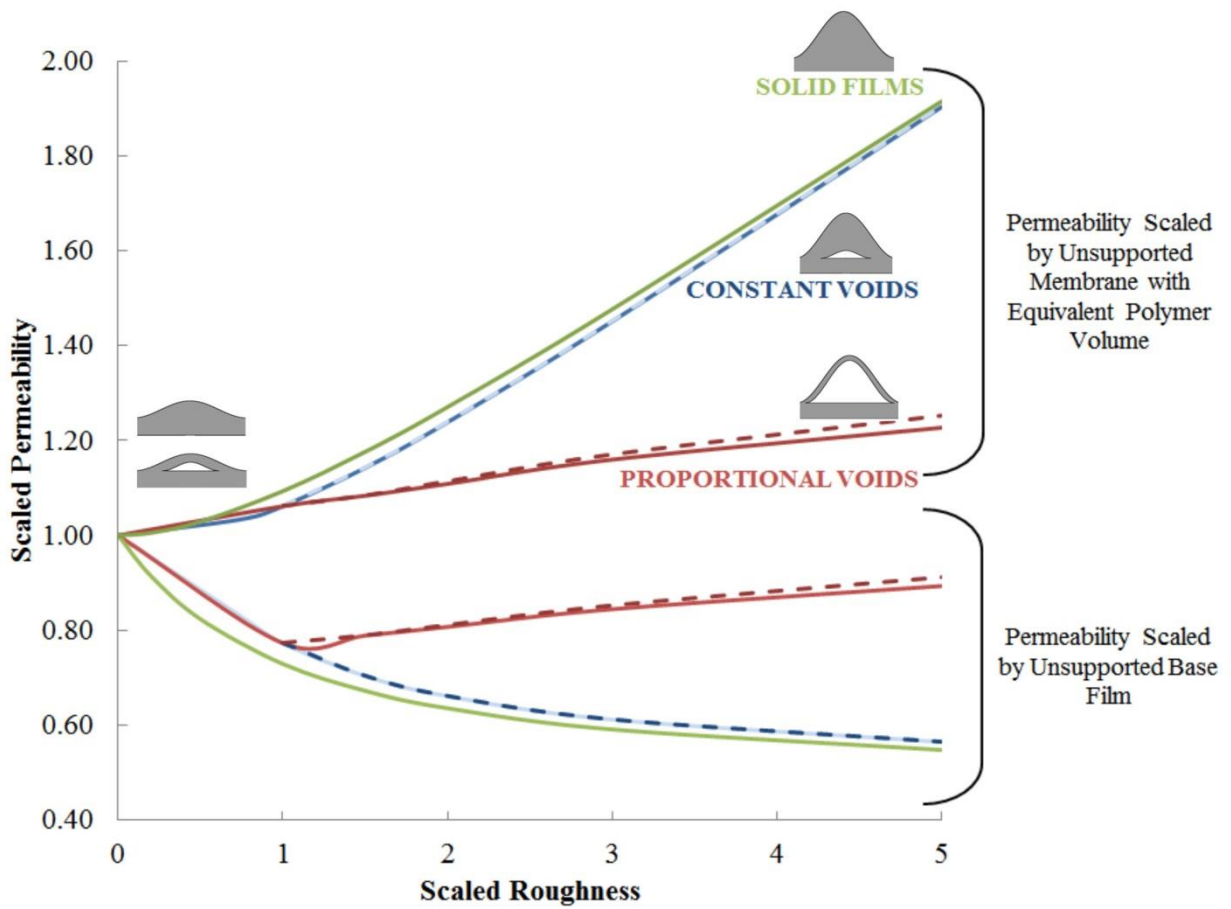


Figure 2.6. Permeability of unsupported film for solid, constant voids, proportional voids scenario plotted against roughness amplitude (Dotted lines indicate a partition coefficient, $K_{eq} = C_f/C_v = 0.01$)

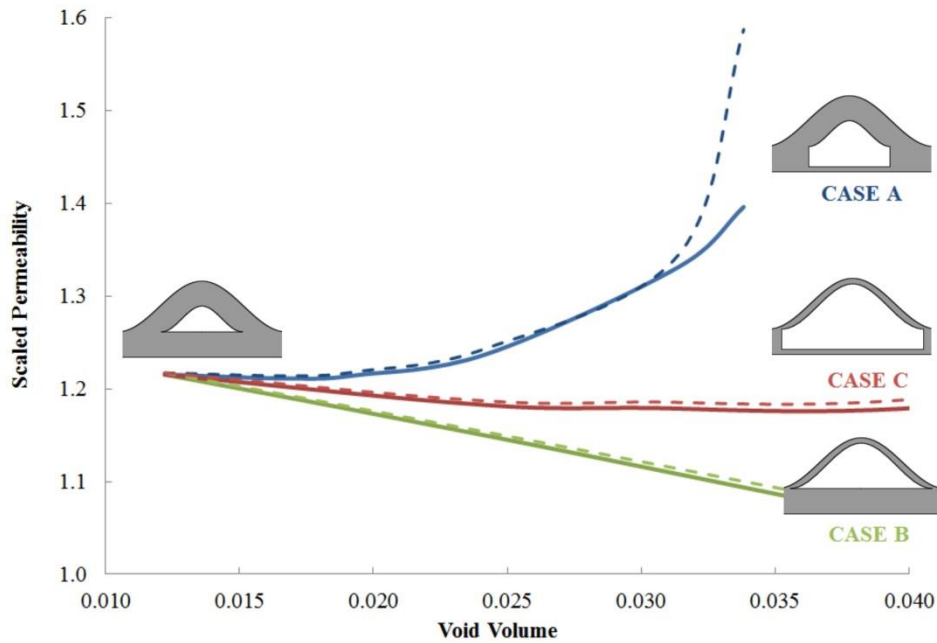


Figure 2.7. Permeability of unsupported film for Case A, B, C plotted against Void Volume (Permeability Scaled against that of an equivalent film thickness. Dotted lines indicate a partition coefficient, $K_{eq} = C_f/C_v = 0.01$)

2.2.3. Impact of Voids on Flux Distributions (location of hot spots)

To determine how the flux distribution along the membrane affects permeability, the permeability of supported membranes is plotted against the flux variation parameter, or the difference between the average maximum and minimum scaled flux values. The lower the flux variation (FV) parameter signifies the smaller the difference between the peak and the lowest flux. On the contrary, the higher the FV parameter means a large variation in flux along the membrane and in highlighting hotspots for fouling. As shown in Figure 2.8 for supported membranes, the in-phase cases have much larger flux variation compared to the out-of-phase cases, which means the flux distribution is dampened when the pores are not aligned with the

valleys of the roughness. This is because for in-phase cases, the shortest diffusion path lengths will always be on top of the valley of the support, creating areas of high flux, while leaving “dead volumes” of polymer that do not contribute to flux. On the other hand, for the out-of-phase scenarios, a funneling effect is created whereby the flux is better distributed around the polymer roughness to find the shortest diffusion path length to “funnel” into the pore. This implies that although similar permeability can be achieved for a particular membrane, less hotspots or regions prone to fouling, will be obtained if the thin film roughness is out-of-phase with the support. There is an exception, for Case A, where the base film is almost negligible, the flux distribution is low, but permeability is high due to short diffusion path length. This is reminiscent of the basis that motivated this research, the TEM image (Fig 2.1d) showing the thin films with voids of little or no base film.

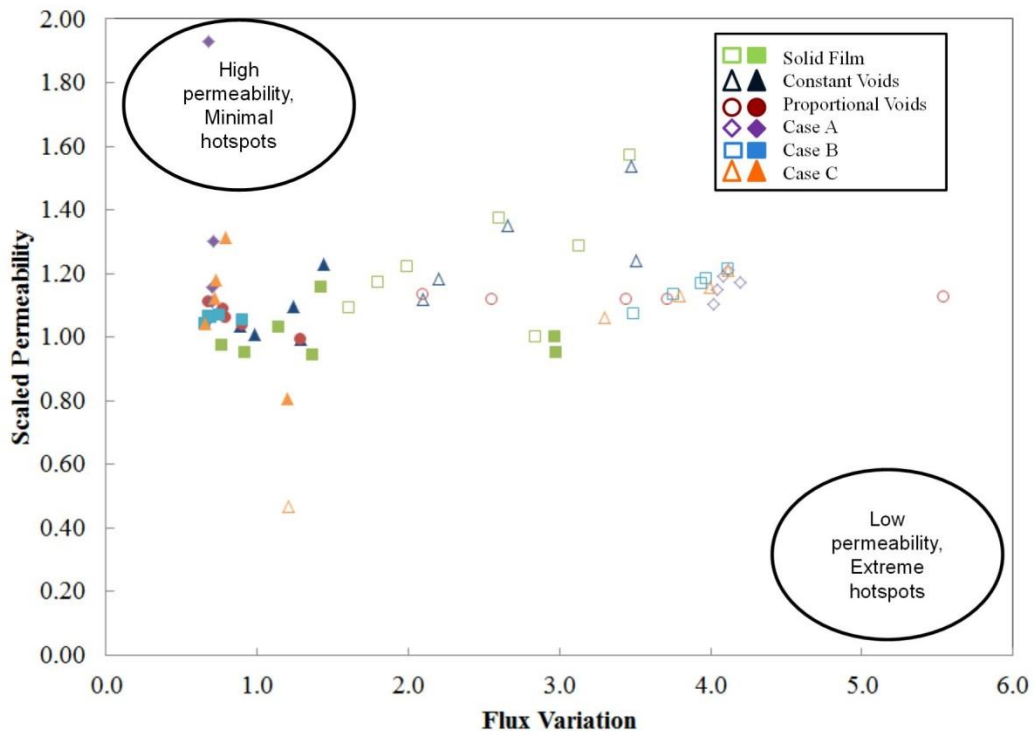


Figure 2.8. Phase Diagram indicating the scaled permeability as a function of flux variation for a) In-phase shown in open markers b) out-of-phase membranes shown in filled in markers (permeability scaled against that of an supported film with equivalent film polymer volume)

Figure 2.9 shows the flux distributions and the streamline plots of supported solid films, and beneath shows the flux variation (FV) and permeability (P) of the films. From Figure 2.9 a), when the thin film is not aligned with the support pores, the shortest diffusion path is through the thin film directly above the pore. When $R_f = 2$, the emergence of “dead polymer volume” occurs, which has little or no contribution to flux through the membrane. These regions are highlighted by the limited streamlines in the thin film, and become larger as the roughness increases. For the out-of-phase scenario (Fig 2.9b) where the pores are misaligned with the valleys of the thin film, no clear trend in flux variation and roughness is observed. For $R_f = 0.5$ and $R_f = 1$, the flux is highest at the pores, as that location provided the shortest diffusion path length compared to the valley that was directly on top of the support. However, compared to $R_f = 2$, the magnitude controlled streamlines show that the streamlines are almost equally distributed throughout the membrane, and the low FV value suggest similar diffusion path lengths as the valleys started to provide short diffusion path lengths compared to the pores. As the roughness increases further, the dead volumes also increase, contributing to higher FV values as the flux increases through the valleys instead of the peaks as it provides shorter diffusion path lengths to the pores. However, the out-of-phase scenarios have more dampened flux distributions and lower permeability than in-phase scenarios.

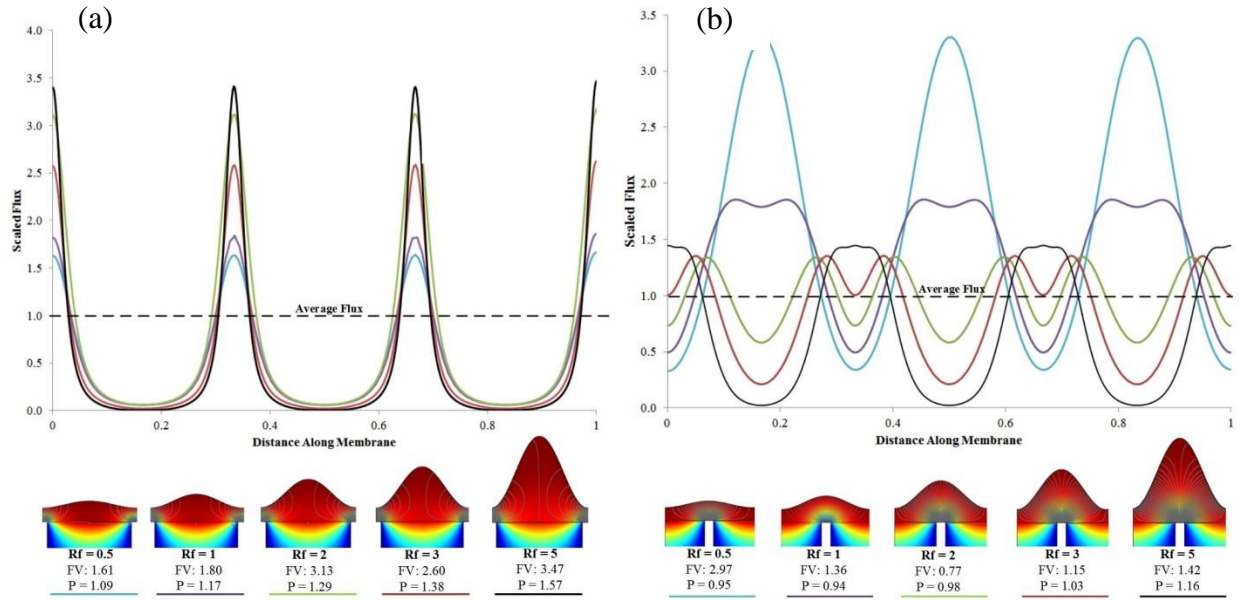


Figure 2.9. Flux variation values along with flux distribution plots for supported membranes solid film – a) in-phase b) out-of-phase

When voids of constant volume are added into the film, as shown in Figure 2.10, the flux distributions are similar to those observed in the solid film case. For the in-phase scenario (Fig 2.10a), the flux is directed towards the valley of the film directly above the pore for the shortest diffusion path length. This becomes even more clear when the roughness increases and more dead volume appears as the streamlines cut straight towards the pore. A similar effect is noticed for the out of phase case (Fig 2.10b) in which the void acts as a funnel for flux towards the support pore but does not improve the flux variation. The largest resistance or “the rate limiting step” to reach the pore remains diffusion through the base film, and thus since the base film thickness remains the same in both this case the solid film case, no drastic difference is expected. However, the flux variation parameters are slightly higher in all cases compared to the solid film case due to decreased resistance to permeation in the membrane, increasing all the diffusion

effects described in the solid film case. Thus, this shows that including a void of much higher diffusivity in the thin film does not improve the flux variation significantly nor change the flux distribution because the base film and support pore dictate the location of hotspots.

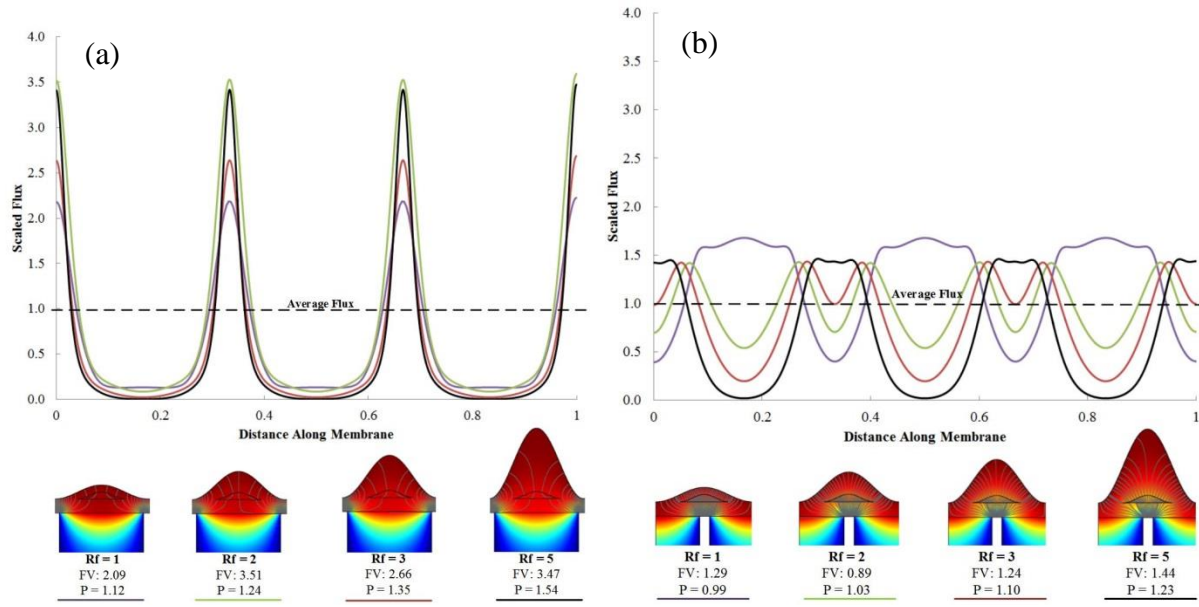


Figure 2.10. Flux variation values along with flux distribution plots for supported membranes with constant void a) in-phase b) out-of-phase

When voids are added proportionally to the roughness of the thin film as shown in Figure 2.11, similarly with the solid film and constant void scenarios, the flux distribution is dramatically damped when the membrane is out-of-phase. However, in the in-phase scenario (Fig 2.11a), the flux distribution increases dramatically as the roughness increases. This is because the same amount of polymer is being spread over a smaller surface area, decreasing the diffusion path length as roughness increases, and thus even though permeability increases for higher roughness, the flux variation parameter is large, signifying intense hotspots. On the contrary, as roughness

increases for the out-of-phase scenario, the flux distribution is dampened and the variability is lowered, due to equivalent path lengths for flux. This demonstrates that the support membrane alignment is crucial in not only determining the permeability, but also the flux variability of the membrane.

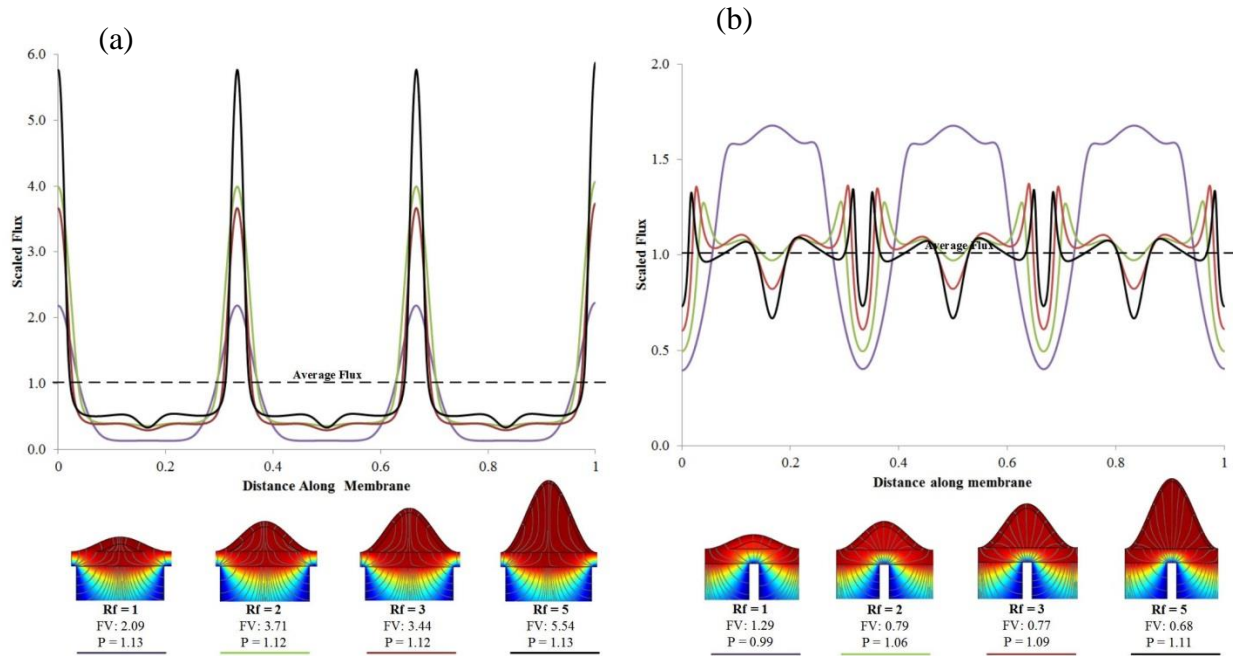


Figure 2.11. Flux variation values along with flux distribution plots for supported membranes with proportional void a) in-phase b) out-of-phase

When the void volumes are altered as shown in Figures 2.11 and 2.12, the flux variation is not as predictable as in the constant void scenarios. In the in-phase scenario, for Case A (Fig 2.12a), as the base film thickness decreases, the flux distribution remains constant with little change in the flux variation parameter. This indicates that the flux through the membrane is primarily through the valleys on top of the support pore, regardless of how low the base film thickness is at the void regions. Similarly, the same trend is observed for Case B (Fig 2.11b),

where although the top film thickness is gradually reduced by increase in void volume, the flux through the membrane remains through the valley of the thin film on top of the support pore, as this provides the shortest diffusion path length. For case C (Fig 2.12c), although the highest flux is on top of the support pores, as the void volume increases, the flux distribution dampens due to less polymer everywhere providing shorter diffusion path lengths throughout the membrane.

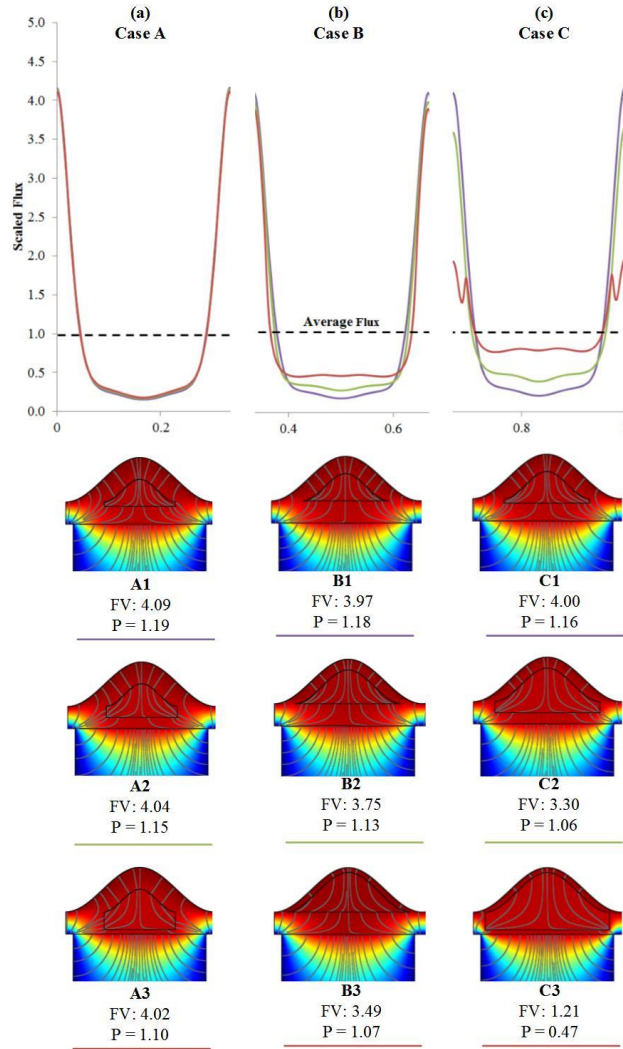


Figure 2.12. Flux variation values and flux distribution plot for a segment of an in-phase supported membrane for a) Case A b) Case B c) Case C

For the out-of-phase scenarios, the highest flux regions are no longer on top of the support pores as this is the roughest part of the thin film. The highest flux regions are inbetween the ridge and valley regions, since a short diffusion path length is provided to the support pore, aided by the void. Interestingly, the highest flux regions is not on top of the support more, because the solute has to diffusive through three regions, the top film, the void and the base film, whereas in the in-phase scenario, diffusion is only through the base film. The flux variation parameter changes insignificantly for Case A (Fig 2.13a), but increases for Case B as the void volume increase or the top film thickness decreases. Thus, even though the top film has little effect on changing the permeability of an out-of-phase membrane, it does change the flux distribution of the membrane. The thinner the top film, the higher the flux variation as shown in (Fig 2.13b), due to “short-cuts” to the support pore provided by the thin top film as discussed previously. When both the top and base film is decreased simultaneously or the entire void volume is increased in Case C (Fig 2.13c), the flux distribution is exacerbated as the diffusive path length is further shortened by the decrease in the amount of polymer in reaching the support pore.

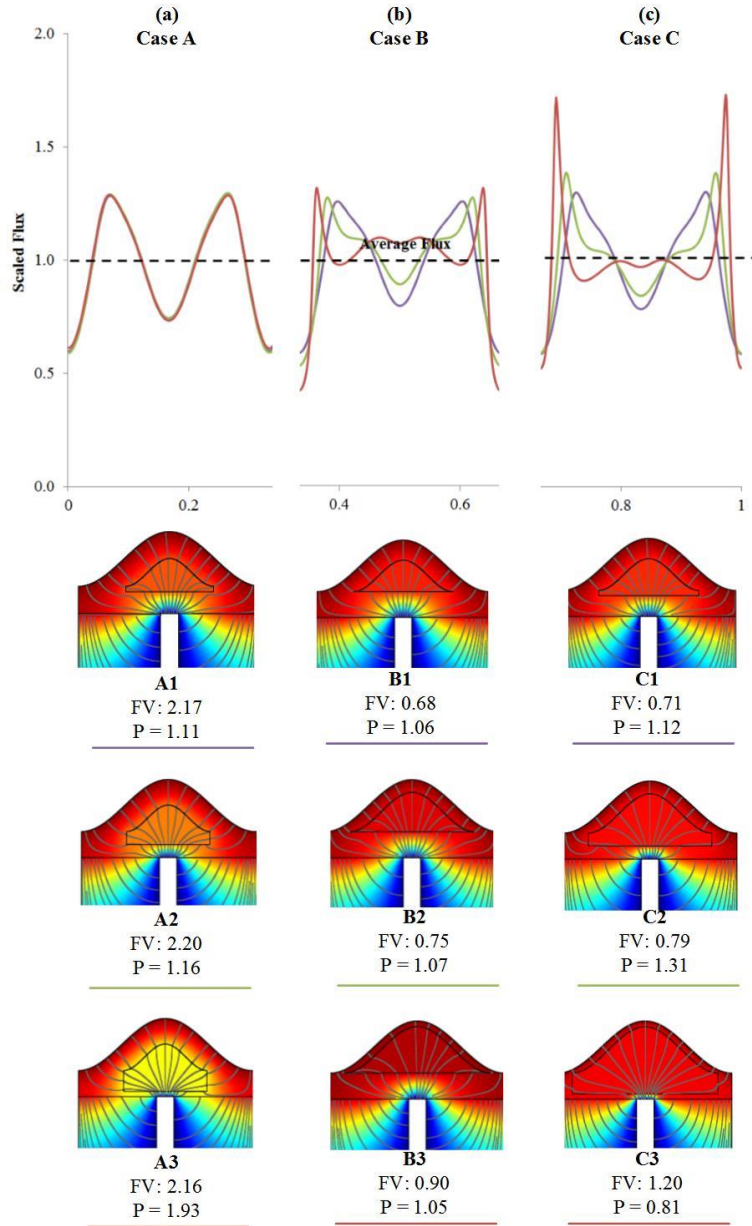


Figure 2.13. Flux variation values and flux distribution plot for a segment of an out-of-phase supported membrane for a) Case A, b) Case B and c) Case C

2.3. Summary

By introducing voids into the thin film, the effect of non-uniform thin films on the permeability of membranes was explored. The permeability of the membrane will only decrease if the base film thickness is kept constant, regardless of the morphology added on top, as the base

film determines the upper bound of membrane performance. However, using the same amount of polymer, if the membrane is formed into an undulating film, higher permeability is achieved due to the creation of shorter diffusion path lengths. The most effective method in increasing the permeability of a membrane is to decrease the base film thickness, which indicates that the surface area of the thin film has limited effect on membrane performance. However, when the membrane is out-of-phase with the support, the top film thickness changes the flux distribution, which has implications on “hotspots” for fouling in real world applications. Thus, by tuning the volume of the voids, the location of these hotspots can be tailored such that fouling can be localized to areas in which cleaning or surface modifications (i.e. grafting) would be easier.

CHAPTER 3

Thin Film Formation Conditions

3. INTRODUCTION

In this chapter, we experimentally extend the modeling efforts from the previous model by altering MPD-TMC thin film chemistry on blends of PANi-PSf porous support material to determine how it affects membrane performance. The reason why PANi was chosen as a support material was specifically for its hydrophilicity as described in Section 1.8. Ghosh et al. studied the influence of the support membrane pore structure and chemistry on the interfacial polymerization of MPD-TMC thin films by introducing polymer additives in the support membrane [36]. By introducing polyethylene glycol (PEG) and polyvinyl pyrrolidone (PVP) in the casting solution consisting of polysulfone dissolved in *N*-methyl-2-pyrrolidone (NMP), the hydrophilicity of the support membrane was increased. They found that the water permeability was lower for TFC membranes formed on top of the relatively hydrophilic support membranes. For the hydrophilic supports containing PEG, it is hypothesized that during the initial immersion step into the aqueous MPD solution, the MPD interacts with PEG through hydrogen bonding penetrating deeper into the pore of the support membrane. Thus, TMC must penetrate deeper into the pore to react, forming a polyamide thin film deeper in the pore, increasing the effective diffusion path length for water and salt, and thereby decreasing permeability. They conceptually described an eruption of MPD in the initial stages of polymerization, and how hydrophilic supports limit that eruption so that the resulting thin films are smoother, and formed deeper in the pore of the support membrane. On the other hand, for hydrophobic supports, there is less hindrance in the eruption of the MPD, causing the thin film to be formed more on the surface of the membrane, which is also rougher. They conclude that more, large, hydrophobic skin layer pores in a support membrane will produce more permeable and rough TFC membranes.

First, absorption tests will be conducted to determine whether the hydrophilicity of PANi affects absorption of MPD into the support membrane. Then, factors such as MPD concentration, immersion time and organic solvent of a traditional thin film recipe used for interfacial polymerization on a relatively hydrophobic polysulfone support will be reevaluated to alter its formation, and consequently, the overall membrane performance.

3.1. Experimental

3.1.1. Materials

The polymer solution used to form the support membrane consisted of polyaniline (PANi, 65 kDa, Santa Fe Science and Technologies, Santa Fe, CA) and polysulfone (PSf, 22 kDa, Sigma-Aldrich, St. Louis, MO), 4-Methylpiperidine (4MP, Sigma-Aldrich) and *N*-Methyl-2-pyrrolidone (NMP, Sigma-Aldrich). For thin film formation, the monomers 1,3-phenylenediamine (MPD, Sigma-Aldrich) dissolved in water and 1,3,5-Benzenetricarbonyltrichloride (TMC, Sigma-Aldrich) dissolved in Isopar™ G (Gallade Chemical, Santa Ana, CA) were used for interfacial polymerization. For the rinses after thin film formation, sodium bisulfite (NaHSO₃, Sigma-Aldrich) and sodium hypochlorite (NaOCl, 10-15%, Sigma-Aldrich) were used. To test the support membrane rejection, bovine serum albumin (BSA, Sigma-Aldrich) was used. In RO testing, the feed solution used to test salt rejection consisted of sodium chloride (NaCl, Sigma-Aldrich), and in FO testing, the draw solution consisted of sodium chloride while the feed solution was Milli-Q water. The cellulose-triacetate (CTA) membrane was provided by Hydration Technology Innovations (HTI, Albany, OR). All materials and solvents were used as received.

3.1.2. Support Membrane Formation

The membranes were formed by non-solvent induced phase inversion described in detail in Section 1.4. The polymer solution used to form the support membranes consisted of 12 wt% of polyaniline and polysulfone, in ratios of 1:0, 1:3, 1:1 and 1:3 dispersed in 6.5 wt% 4-methylpiperidine and 81.5wt% *N*-Methyl-2-pyrrolidone. 4MP was used in the polymer solutions as previous research showed that it prevented gelling of the PANi solutions by preventing hydrogen bonding between polymer chains [23, 93]. The prepared polymer solutions were stirred in air tight containers for at least three days prior to casting. Polyester fabric was taped onto a reinforced glass plate, using electrical tape to ensure the fabric was completely flat on the plate. A stainless steel casting blade (Microm II, Gardco, Pompano Beach, FL) set to 152 μm (using a film gauge) was used to spread the polymer solution uniformly onto the fabric. The glass plate was immediately immersed into a room temperature Milli-Q water bath to induce precipitation of the polymer. The membrane was left in the coagulation bath for at least 30 minutes before being transferred into plastic zip-lock bags filled with Milli-Q water and stored in 4°C until testing.

3.1.3. Thin Film Formation

In order to investigate the relationship between support membrane and thin film formation, interfacial polymerization parameters will be varied as described in the following sections. However, prior to any variation, a typical thin film formation procedure needs to first be described. This detailed procedure has been previously described by Lind et al. [37, 94]. Briefly, polyamide thin films will be formed on support membranes formed by phase inversion described in Section 3.1.2 in PANi:PSf ratios of 1:0, 1:3, 1:1 and 1:3. Pure PSf supports were not considered as the molecular weight of PSf is different than the pure PANi used in membrane preparation and different weight percentage will need to be used to prepare the casting solution

in order to achieve similar viscosity solutions. The membrane support is taped onto a glass plate, and then immersed into a dish filled with aqueous MPD solution (3.4 wt%) for 2 mins. Excess MPD solution is then removed using an air knife (model 110012SS-316, Exair, Cincinnati OH) operated at 15 psi moving over the membrane surface at a height of 0.5". Excess solution is wiped from the edges and the back of the glass plate to prevent polymerization at those locations. The plate is then immersed in a vertical container filled with TMC in Isopar™ G (0.15 wt%) solution for 1 min. The plate is removed from the organic solution, and supported vertically for 2 min to allow excess solution to run off and some of the organic solvent to evaporate. The membrane is then placed in a hot water bath of $90 \pm 5^\circ\text{C}$ for 2 mins, and subjected to post-treatment rinses of 200 ppm NaOCl in deionized water for 1 min followed by 2 g/L NaHSO₃ in deionized water for 30 s, and another hot water rinse for 2 mins. The membranes are stored in deionized water in light-proof containers at 4°C prior to testing.

3.1.4. Support Membrane Performance

Pure water flux and BSA rejection of the support membrane was measured in dead-end filtration cell (HP4760, Sterlitech, Kent, WA), with an effective membrane area of 12.57cm². The membrane was first compacted with deionized water at 20 psi before measuring the water flux and BSA rejection. The permeate flow rate was measured after it was stabilized (~2-3 hours). The water permeability was determined by calculating the water flux scaled by the applied pressure. BSA rejection was obtained by changing the feed solution in the chamber from deionized water to a solution of 1 g/L BSA with 50mmol/L NaCl. BSA concentration was evaluated using a UV-Vis spectrometer (absorption peak wavelength at 278.01 nm), while NaCl concentration was evaluated using a conductivity meter.

3.1.5. RO Membrane Performance

The TFC membrane's water and salt permeability was determined through RO experiments. The RO system employed was a cross-flow system consisting of six stainless steel cells operating under the same pressure and the same feed water (Fig. 3.1). Each cell has an effective membrane area of 19.5 cm² and a channel height of 2 mm. The feed solution was pressurized in the system by a diaphragm pump (Hydracell; Wanner Engineering, Minneapolis, MN) and a back-pressure regulator (KPB series, Swagelok, Long Beach, CA). The feed solution was kept at a constant temperature by heat exchanger coils, submerged in the feed tank, connected to a circulating water bath (NTE RTE7; Fisher Scientific, Pittsburgh, PA). Using Milli-Q water as the feed solution, the membranes were compacted for at least 12 hours at 225 psi before water permeability is measured. The water permeability was determined by using Milli-Q water as the feed solution, measuring the flow rate at increasing pressure increments of 50 psi, and determining the slope of a regression line from a water flux against pressure plot. The salt permeability was found by switching the feed solution to 2 g/L NaCl, collecting the permeate solution at 225 psi, and measuring the conductivity of the solution to determine salt rejection.

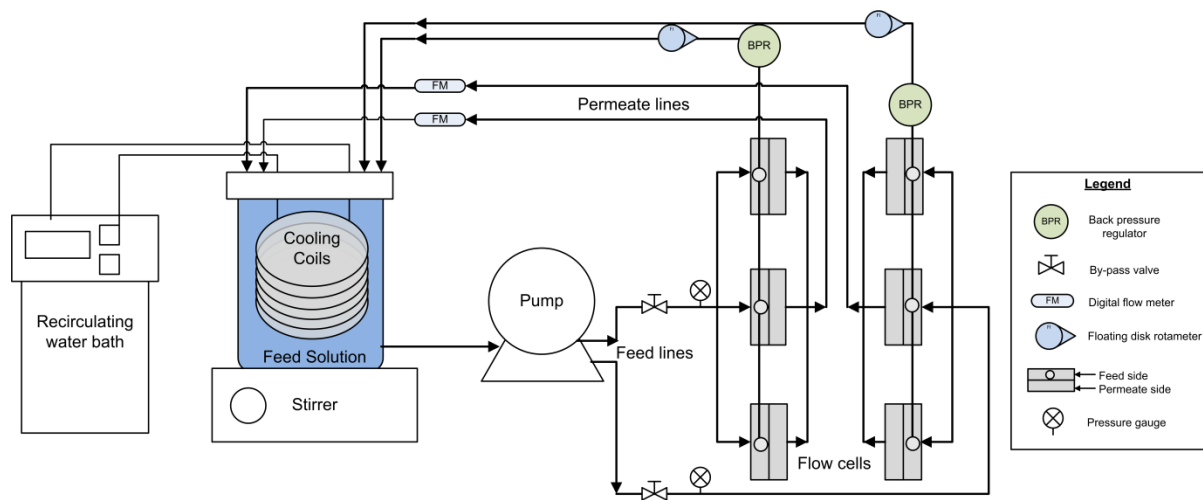


Figure 3.1. Schematic of six-cell lab scale cross flow RO system [59]

3.1.6. FO Membrane Performance

The FO experiments were conducted in our lab scale FO system (Figure 3.2) using a custom designed flow cell made of polycarbonate with transparent acrylic windows on both sides for viewing. The flow channels on both sides of the membrane are 2.54 cm wide, 7.62 cm long and 1 mm high. The draw solution flowed co-currently with the feed solution, controlled independently by gear pumps (MicroPump A, Cole Parmer, Barrington, IL), and measured by rotameters (Blue White Industries Ltd, Huntington Beach, CA). The draw solution was placed on a balance (PI-2002, Denver Instruments, Bohemia, NY) to record its mass every 30 seconds on a computer, from which the water flux was calculated. The conductivity of the feed solution was continuously monitored and recorded during the experiment with a calibrated conductivity probe (Cell constant: 10cm^{-1} , Accumet XL50, Fisher Scientific) immersed in the feed solution. Both the water flux and salt flux reached steady-state approximately 5 minutes into the experiment. The initial volume of both draw and feed solutions were one liter, and the experiment length of 30 minutes, during which less than 30 mL of water permeated through the membrane to the draw and less than 1 g of salt passed into the feed for all experiments conducted. Thus, within the duration of the experiment, dilution of the draw and concentration of the feed was safely assumed to be negligible.

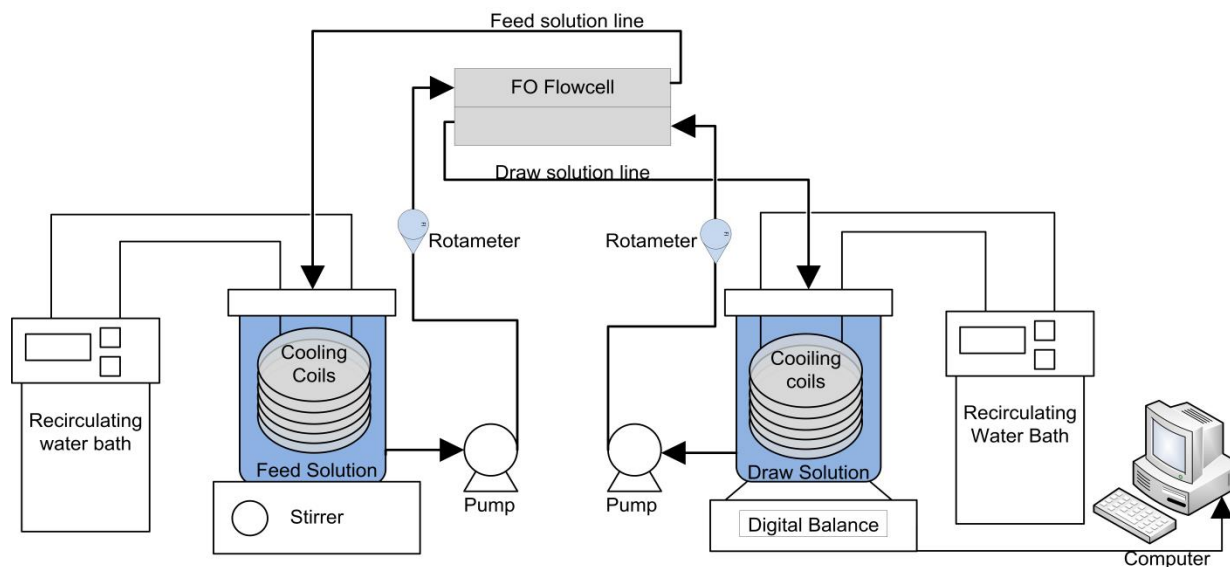


Figure 3.2. Schematic of lab-scale FO system [59]

3.2. Membrane Characterization

3.2.1. Support Membrane MPD Uptake

MPD absorption tests were used to determine the amount of MPD taken up by the membrane support. The support membranes were cut into circular pieces 5/8" in diameter using a membrane punch out. The pieces were then weighed before immersion in 15 mL of aqueous 1.5 wt% MPD solution for 10 mins. Samples of the solution were taken before and after immersion and diluted 250 times. The concentration of MPD was measured using an UV-vis spectrophotometer (Lambda 20, Perkin Elmer) at a wavelength of 289.13 nm, where MPD was found to have an absorption peak [95].

3.2.2 Support Membrane Microscopy

Cross-sectional images of the membranes were obtained by a scanning electron microscope (SEM, JEOL JSM-6700F, Tokyo, Japan) operated at an accelerating current of 10 kV and an emission current of 10 μ A. The samples were cast without fabric and freeze-fractured

using liquid nitrogen at (approximately 77 K) to obtain a clean edge for imaging prior to placing on a vertical SEM holder. Prior to imaging, the samples were first coated with gold by a sputtering system (Hummer 9.2, Anatech Ltd., Denver, Virginia) at a plasma current of 15 mA for 1 min, for an approximate gold thickness of 4 nm.

3.3. Results and Discussion

3.3.1. MPD Absorption Tests

In order to understand how the amount of PANi in the support membrane affects the uptake of MPD and water and the subsequent thin film formation compared to PSf support membranes, MPD absorption tests (described in Section 3.2.1) were conducted. This will determine whether the MPD-TMC chemistry used for polyamide thin-film formation on pure PSf support membranes is suitable for support membranes containing PANi. Table 3.1 shows the results after these absorption tests for various blends of unsupported PANi membranes.

Table 3.1. MPD absorption test results of pure and blended PANi and PSf unsupported membranes

Unsupported Membrane (PANi:PSf Ratio)	Membrane Mass Change (g)	Percent Change of MPD in solution (%)	$\frac{\text{mass}_{\text{MPD}}}{\text{mass}_{\text{membrane}}}$ (g/g)	$\frac{\text{mass}_{\text{water}}}{\text{mass}_{\text{membrane}}}$ (g/g)
1:0	0.032 ± 0.002	-0.64 ± 0.54	0.088 ± 0.076	1.86 ± 0.16
1:3	0.042 ± 0.003	-0.53 ± 0.15	0.057 ± 0.016	2.02 ± 0.17
1:9	0.035 ± 0.003	-1.29 ± 0.99	0.090 ± 0.066	1.80 ± 0.10
0:1	0.0002 ± 0.0000	-0.80 ± 0.18	0.109 ± 0.025	0.01 ± 0.00

According to the results, there is not a significant difference in the amount of MPD absorbed by the support membranes regardless of the composition. However, the major difference that significantly impacts the results is the change in membrane mass, which indicates that PSf uptakes much less water than support membranes containing PANi. On the other hand, supports with PANi uptake a lot of water, diluting the amount of MPD absorbed by the support. This indicates that although PANi increases the hydrophilicity of the support it may also hinder thin-film formation by diluting the amine concentration in the reaction zone. With this information, the typical recipe described in Section 3.1.3 used for pure PSf support membranes will be altered to account for this diminished amine concentration, including increasing MPD concentration, increasing aqueous amine immersion time and changing the organic solvent for TMC.

3.3.2. Support Membrane Cross-sectional Images

The blended support membranes cross-sectional images are shown in Table 3.2 at magnifications of 500X and 10,000X to show the full cross section as well as the skin layer of the membrane. The images show that as the PANi concentration in the membrane increases, the overall porosity also appears to increase. This becomes even more apparent when looking at the skin layer of the membrane when the morphology becomes denser as the concentration of PSf increases, changing from a more finger-like morphology (1:0) to a more sponge-like morphology (1:3). This may also explain why PSf has been commonly used for RO membranes, as its dense, consistent morphology provides a uniform surface for polyamide coating films, and has high resistance under high RO hydraulic pressures.

Table 3.2. Cross-sectional SEM images of blended PANi/PSf membranes at 500X and 10,000X magnification

Membrane (PANi: PSf Ratio)	Full Cross-Section (Mag: 500X)	Skin Layer (10,000X)
1:3		
1:1		
3:1		
1:0		

3.3.3. Performance of PANi/PSf Membranes

The performance of the PANi-PSf blended support membranes without polyamide coating were first determined in dead-end filtration tests. Figure 3.3 shows the water permeability and BSA rejection of pure PANi and PANi-PSf blended membranes. There is no

clear trend between PANi concentration in the membrane and water permeability which is inconsistent with past research done by Guillen et al., who found that as PANi concentration increases, water permeability increases as well [7]. There is a positive correlation between PANi concentration in the membrane with BSA rejection, which is also inconsistent with Guillen et al., who reported virtually no rejection of BSA for pure PANi membranes. The inconsistencies may be related to the difference in molecular weight of the PANi used in the experiments as the PANi used in these experiments were commercially purchased and is speculated to have a higher molecular weight (~65 kDa) than the PANi that was formed by chemical oxidative polymerization (~22 kDa) by Guillen et al. This increased molecular weight will cause chain entanglement and denser membranes, increasing the BSA rejection. Furthermore, due to this increased molecular weight, 4MP was used in the preparation of the membranes as a gel inhibitor, which may change the chemical structure of the membranes. The addition of a lower molecular weight PSf (~22 kDa), may loosen up the PANi chains and lower BSA rejection, and increase water permeability, as shown by increasing PANi:PSf ratios in the membrane.

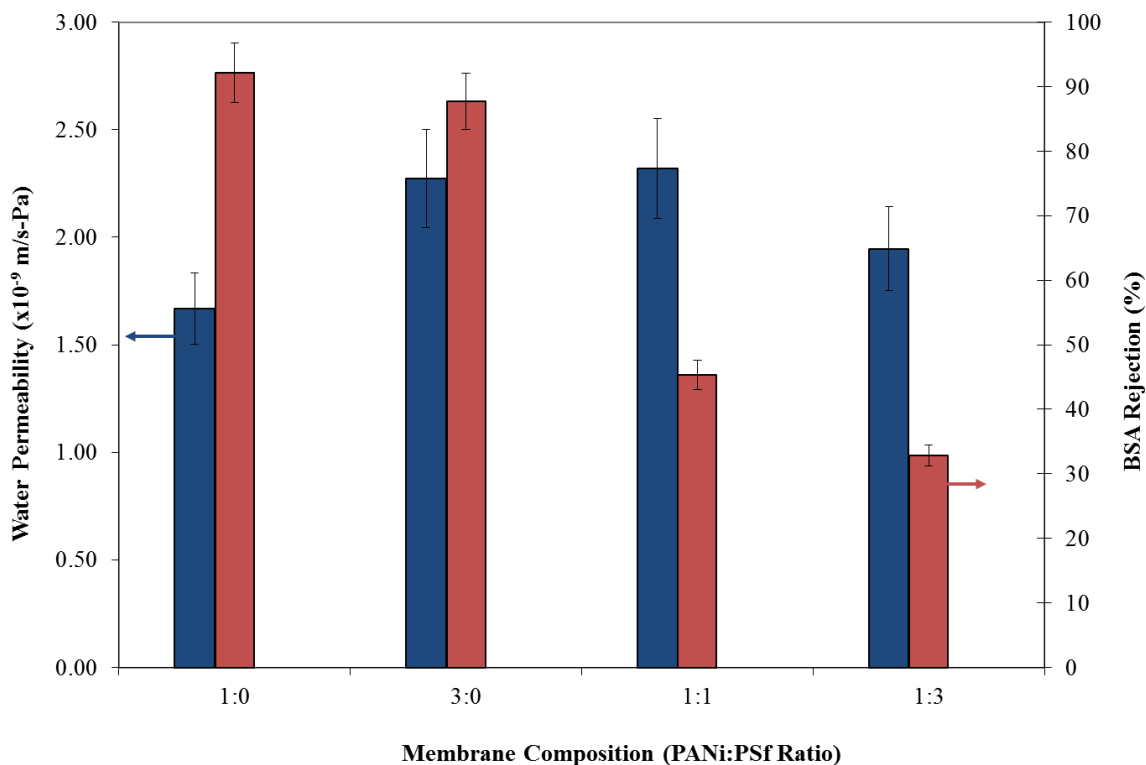


Figure 3.3. Water permeability and BSA rejection of un-coated PANi-PSf membranes

3.3.4. RO Performance of PA-PANi-PSf Composite Membranes

The PANi/PSf support membranes were then coated with polyamide thin films using the recipe described in Section 3.1.3. In the subsequent sections, the MPD concentration will be varied, and the organic solvent will be changed from isopar to hexane to determine how to improve thin film formation on a relatively more hydrophilic support than PSf.

3.3.4.1. Variation of MPD Concentration

The MPD:TMC ratio of 20:1 used in thin-film formation of a pure PSf membrane is used as the control membrane as the resulting TFC membranes have been well characterized and reproduced [32, 37]. As aforementioned, the ratio 20:1 is empirically chosen to promote amine diffusion into the organic phase due to the large concentration gradient. However, as shown in

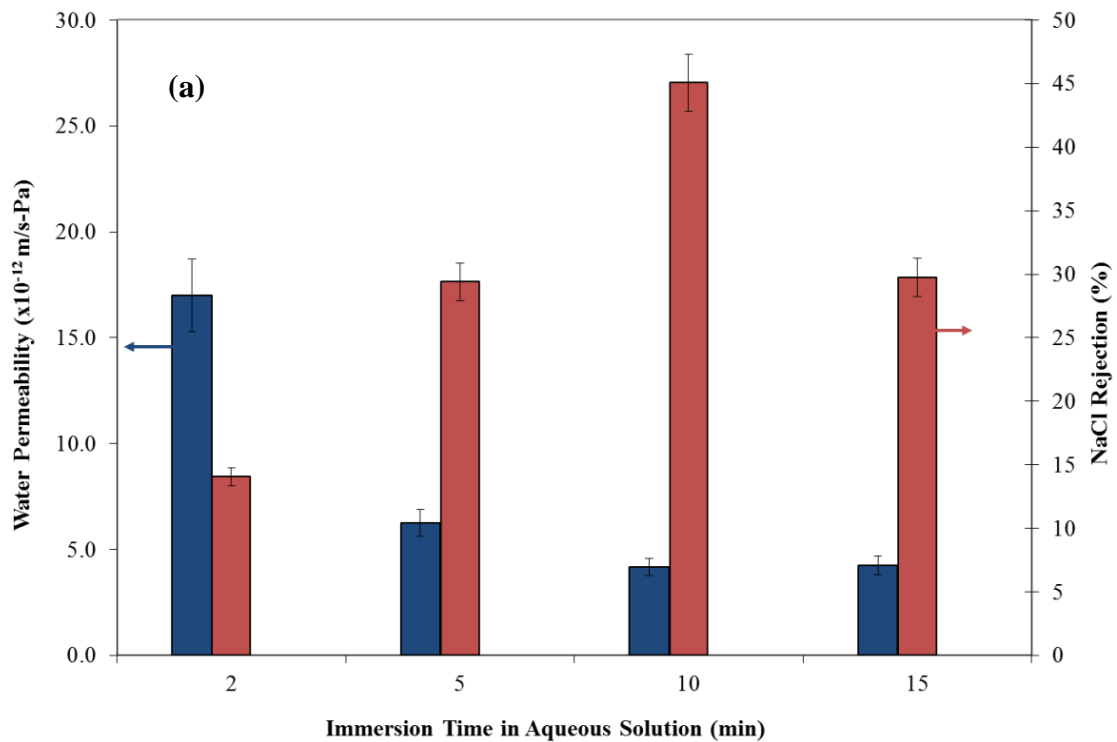
the MPD absorption data, PANi membranes appear to uptake more water than PSf membranes, so although the same amount of amine diffuses into the membranes, the amine concentration in PANi will be much less than in PSf. Therefore, altering the ratio of MPD:TMC by 1-2 times may not be enough to ensure a sufficient amine concentration in the PANi membrane. There will be two approaches taken to increase the concentration of MPD in PANi support membranes: 1) Increase the immersion time of the membrane in the aqueous solution, and 2) increase in MPD concentration in the aqueous solution. The reasoning behind these two approaches is simply based on Fick's law of diffusion as presented in Eqn (2).

An increase in MPD concentration in the aqueous solution will therefore increase the concentration gradient from the exterior to the interior of the membrane, while an increase in immersion time will also increase the concentration of MPD in the membrane as flux is time dependent. For all the blended support membranes studied, the MPD concentration will be changed from 3.4, 6.8, 13.6 to 27.2 wt% to increase the concentration gradient driving MPD into the membrane. The upper concentration limit is chosen to not exceed the solubility limit of MPD in water, which is 35 wt% (350 g/L) at 25°C [40]. In all the cases presented, the TMC concentration will be the control variable maintained at a concentration of 0.15 wt%. It is expected that the higher MPD concentration will form a more uniform thin film on the PANi support membrane as it will compensate for the significant water uptake. Furthermore, the concentration of MPD needed for a contiguous thin film to form will help determine whether it is practical to use MPD as the amine monomer. The support membrane immersion time will be altered from 2, 5, 10 to 15 minutes in the aqueous amine solution. The longer the immersion time, the more MPD is expected to diffuse into the support membrane. The 2 minutes immersion is from the original recipe described previously in Section 3.1.3 and used as a basis for comparison.

Both concentration and immersion time will help determine whether using MPD-TMC thin film recipe is practical for PANi support membranes. If either the MPD concentration is very high or the immersion time is long that is required to form a thin film, it may be uneconomical to use MPD as the diamine for polyamide thin film formation or PANi as a support.

Based on the MPD absorption tests results presented in Section 3.3.1, pure PANi membranes absorb a lot more water than pure PSf membranes, diluting the concentration of MPD in the membrane and subsequently, reducing the amount in the reaction zone for interfacial polymerization. In order to increase the MPD concentration in the PANi membrane, the immersion time in the aqueous solution and the MPD concentration in the aqueous solution were independently increased and the resulting cross-flow RO composite membrane performance is presented in Figure 3.4. As the immersion time in the MPD aqueous solution increased (Figure 3.4a), the water permeability decreased, while the NaCl rejection increased. This indicates that the immersion time does increase the MPD concentration in the reaction zone, forming a tighter film than the original recipe that was intended for pure PSf supports. However, compared to commercial RO membranes, the salt rejection is still low, indicating these supports may not be suitable for SWRO membranes (water permeability: $\sim 10^{-12}$ m/s-Pa, NaCl Rejection 99.9+%) [35]. On the other hand, when the concentration of MPD is increased in the aqueous solution (Figure 3.4b), the water permeability increases while the salt rejection decreases, indicating a looser thin film is being created. It seems as though the increase in immersion time and the increase in concentration of MPD in the aqueous solution results in contradictory results even though both variables were intended to increase the concentration of MPD in the support layer. However, based on the MPD absorption tests presented in Section 3.3.1, PANi membranes absorb a lot of water compared to MPD, thus an increase in immersion time would only increase the amount of

water absorbed in the membrane since the MPD concentration was kept constant. Furthermore, based on the previous discussion in Section 1.5.1, previous research found that an increase in the MPD solubility in the organic solvent was found to form more water permeable thin films [32]. However, if more water is in the reaction zone, the solubility of MPD would be decreased due to decreased partitioning into the organic and less water permeable thin films would form as observed (Fig 3.4a). As the MPD concentration is increased in the aqueous solution, more MPD is able to partition into the support membrane due to a concentration difference between the bulk and the support, which then partitions back out into the reaction zone during interfacial polymerization. This enhanced “flux” of MPD acts similar to increased diffusivity, which as discussed above, is observed to produce more water permeable films as confirmed by the results (Fig 3.4b).



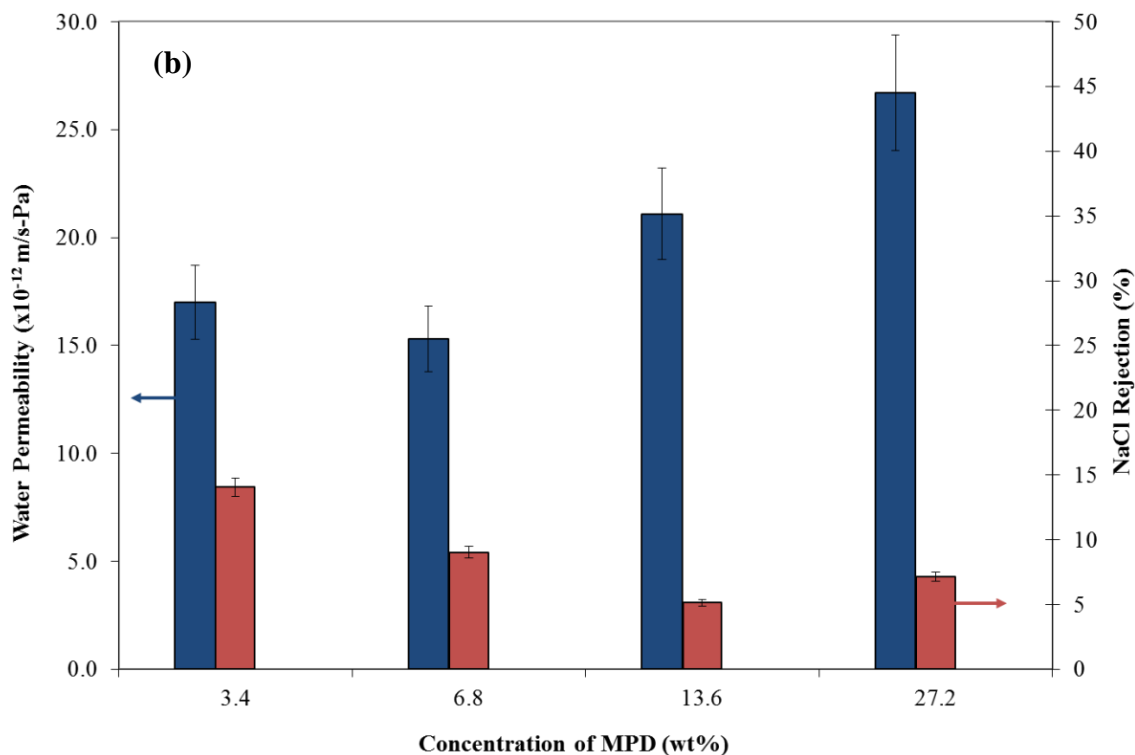


Figure 3.4. Water permeability and NaCl rejection of polyamide coated pure PANi support membrane with variation in a) immersion time b) concentration in aqueous MPD solution

3.3.4.2. Variation of Organic Solvent

As shown in the previous section, only increasing the concentration of MPD in the aqueous solution can enhance permeability of the membrane, while jeopardizing the selectivity. Thus, in this section, the organic solvent will be altered to determine whether changing the reaction zone depth will change the thin film performance since polymerization occurs predominantly in the organic phase due to limited solubility of the acyl halide in water. Support membranes with different PANi:PSf ratios were coated with a standard polyamide chemistry described in Section 3.1.3. The water permeability and NaCl rejection of the coated membranes using isopar as the organic solvent are presented in Figure 3.5a. The performance of the

membranes is much lower than that of commercial seawater RO membrane (water permeability: $\sim 10^{-12}$ m/s-Pa, NaCl Rejection 99.9+%), but the goal of these studies is to elucidate a relationship between support membrane and thin film chemistry, and not to make a better a membrane. One reason why no clear trend is observed in the performance may be because of the difference in molecular weights between PANi and PSf, and the use of the gel-inhibitor, 4MP, that is used based on the polymer concentration. Figure 3.5b shows that when hexane is used as the organic solvent, the water permeability decreases dramatically while the salt rejection increases compared to when isopar was used (note: scale bar). As discussed in Section 1.5.1, hexane has a lower surface tension and lower specific gravity compared to isopar, which indicates that MPD can diffuse faster into hexane than into isopar, which means that the reaction zone for polymerization using hexane is smaller. Thus, as increasing the PANi in the support membrane increases the amount of water absorbed into the polymer matrix, the MPD concentration will be diluted in the reaction zone, therefore, the faster diffusion rate of MPD into hexane and the smaller reaction zone will form less permeable films as observed in the performance results. Lastly, as the vapor pressure of hexane is higher than isopar, the TMC concentration will increase faster in the reaction zone for hexane due as it evaporates faster than isopar, which will also create a denser, less permeable film. This shows that using the same support membrane, slight changes in the thin-film chemistry can drastically change the composite RO membrane performance.

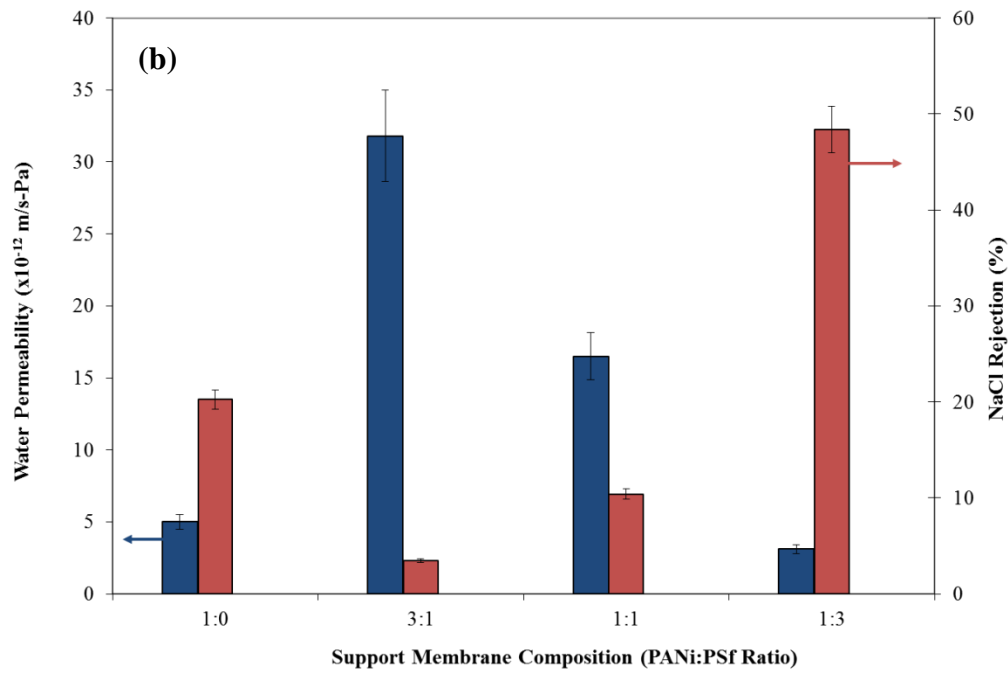
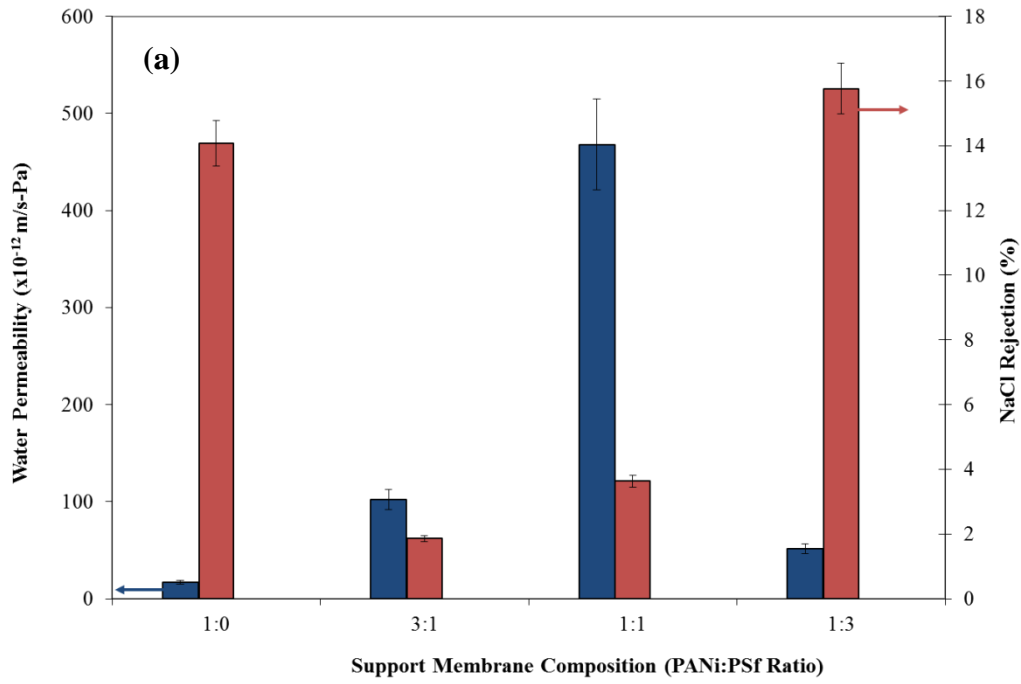
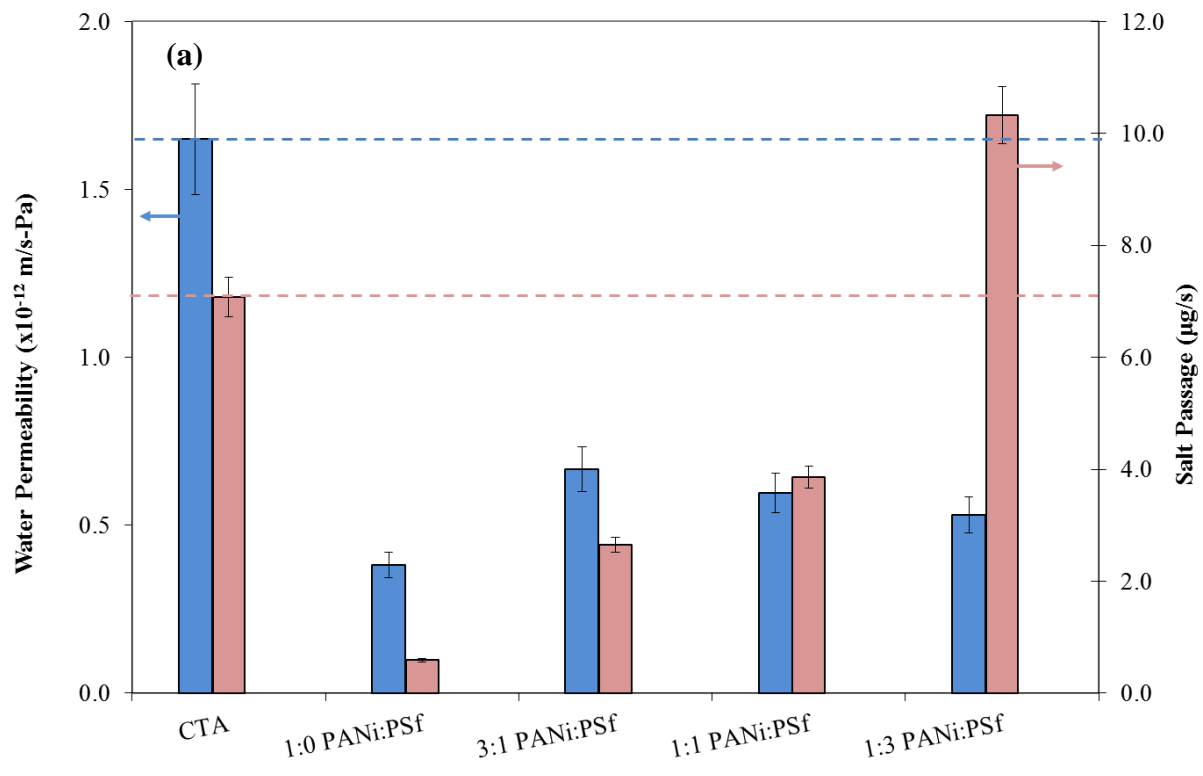


Figure 3.5. Water permeability and NaCl rejection of polyamide coated PANi-PSf membranes using a) isopar b) hexane as the organic solvent

3.3.5. FO Performance of PA-PANi/PSf Composite Membranes

The composite membranes were also tested in PRO-mode to determine how the change in driving force, from osmotic pressure to hydraulic pressure changes membrane performance. Thus, polyamide thin-films were interfacially formed on PANi-PSf blended support membranes of ratios 0:1 (pure PSf), 1:3, 1:1 and 1:0 (pure PANi) and tested in PRO-mode using 32 g/L NaCl as the draw solution and DI water as the feed. The water permeability and salt passage of the TFC membranes compared to commercial CTA membrane are shown in Figure 3.6. The studies are done to better understand the membrane structure and not intended to make a FO composite membrane using PANi-PSf blends as shown in Chapter 2 the polyamide coating is not necessary to form a FO membrane As the amount of PANi decreases, the TFC becomes more permeable to salt, but not to water, indicating that there may be some difference in charge distribution in the thin film due to the support chemistry. Figure 3.6b shows the FO performance of the TFC membranes when formed using hexane as an organic solvent. Hexane was chosen as the organic solvent because previous work [32] showed that it would form a more permeable and more selective TFC membrane. However, hexane has a low flash point (-10°C) making it unsafe for industrial membrane fabrication. The results show that the TFC membranes formed using hexane does not have significantly improved performance compared to that formed using isopar, which is unexpected based on the improved RO performance results presented in Section 3.3.4.



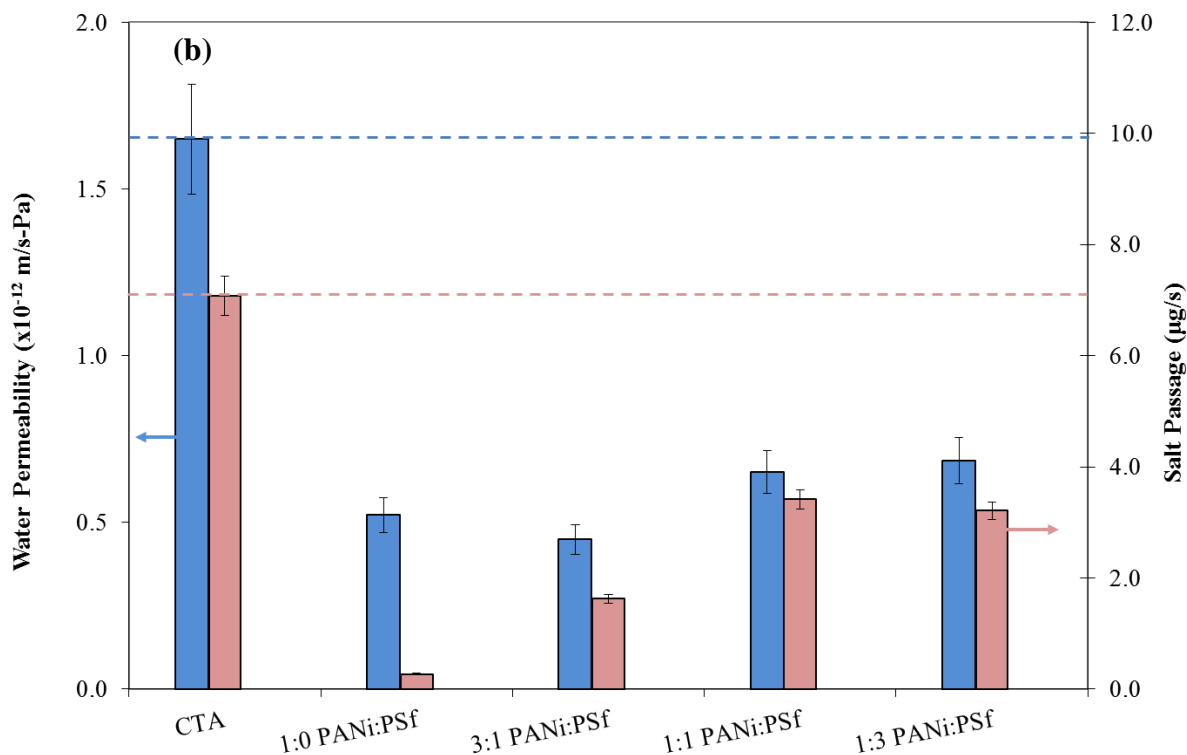


Figure 3.6. Water permeability and salt passage of FO TFC PANi-PSf support membranes using a) isopar b) hexane as the organic solvent.

To reiterate, as more water is taken up in the MPD immersion step by support membranes containing PANi, which dilutes the concentration of MPD reaching the reaction zone during interfacial polymerization, the use of hexane rather than isopar will increase the concentration of TMC reaching the reaction zone. This is because first, hexane is less viscous than isopar, allowing TMC to diffuse faster towards the interface of the reaction, and second, hexane has a much higher vapor pressure than isopar, evaporating faster from the surface of the membrane, and again concentrating the amount of TMC reaching the diluted MPD interface. Due to the lower boiling point than isopar, hexane should require a lower curing temperature, but to only

vary one parameter in this set of experiments, the curing temperature was set at 90°C. Hence, all these factors combined to create a much denser, less permeable thin film on top of the supports when hexane was used as the organic solvent than when isopar was used as was observed with the RO results. However, when these membranes were tested in FO experiments (PRO-mode), the density of the thin film did not seem to alter the performance significantly. This could be due to the low pressure application where no hydraulic pressure is applied on the membrane to cause compaction, and also indicating that the highest resistance to permeation in FO application for these membranes is not in the thin film. This will be further explored in subsequent section by calculating the structure factor.

3.3.6. Stability of PA-PANi/PSf Composite Membranes in FO

To justify using PANi blended supports to make FO membranes, it was important to show that the TFC membranes are more stable than CTA membranes. As aforementioned, the CTA is stable in a pH range 3-8, which limits its application in low energy desalination where the solutions are not necessarily in the neutral pH range, as in the ammonium bicarbonate draw solution (pH ~13). A CTA membrane and a 1:3 PANi-PSf TFC membrane were first tested in PRO-mode using DI water as the feed and 32 g/L NaCl as the draw solution. The membranes were then immersed in 0.2M NaOH (pH ~13.3) solution for approximately 66.25 hours before being re-tested in PRO-mode using the same feed and draw solutions. The water permeability and salt passage both prior to and after the NaOH treatment are shown in Table 3.3. The CTA membrane completely degraded after the NaOH treatment, being more permeable to salt and not providing a sufficient barrier for osmotic flux across the membrane. The basicity of the NaOH solution most likely hydrolyzed the acetate, disrupting the hydrogen bonding between CTA

chains by replacing the electron donating acetate group with an electron withdrawing hydroxyl group as described in Section 1.7. On the other hand, the TFC membranes using 1:3 PANi:PSf as the support maintained its permeability even after the prolonged NaOH treatment. This is because unsaturated bonds in PANi and PSf provide resonating electrons to mitigate the effect of electron withdrawing property of the hydroxyl group, thereby reducing the effect of disrupting hydrogen bonding between adjacent chains. This shows that the PANi:PSf blended TFC membranes are stable even at high pHs, making it a proponent for a wider variety of FO processes as compared to the CTA membrane.

Table 3.3. Water permeability and salt passage for CTA and 1:3 PANi:PSf TFC membranes before and after immersion in NaOH (pH ~13.3) solution.

Membrane	Before NaOH Treatment		After NaOH Treatment	
	Water Permeability, <i>A</i> (m/s-Pa)	Salt Passage (g/s)	Water Permeability, <i>A</i> (m/s-Pa)	Salt Passage (g/s)
CTA	2.23	6.84	N/A*	N/A
1:3 PANi:PSf TFC**	0.61	0.41	0.54**	0.40

*Degradation of membrane - no measurable water flux

**1:3 PANi:PSf blended support was cast on top of a less open nonwoven fabric, and the PANi-PSf polymer blends were dissolved using the wrist-shaking instead of by magnetic stirring

3.3.7. Structure Parameter of FO Membranes on PANi/PSf Blended Support Membranes

Based on the RO and FO performance data of TFC membranes formed using PANi-PSf blended support membranes, the structural parameter was calculated using Eqn (13) and (15)

from Section 1.6.1. The structural parameter is used to describe the effect of mass transfer due to enhanced concentration polarization in the unstirred boundary layer, that is, the porous support layer of a TFC membrane. In effect, the structural parameter gives an approximation of the effective diffusive path length that a solute must travel through from the porous support to reach the skin layer of the membrane. Figure 3.7 shows the structural parameter of the TFC membranes formed using PANi-PSf support membranes using both isopar and hexane as the organic solvent. As a comparison the structural parameter of the commercial CTA FO membrane is reported to have a structural parameter of about 350 μm when tested under the same conditions [59]. The results show that for the blended support membranes (1:3, 1:1 and 3:1), as the PANi concentration decreases, the structure factor increases. The hydrophilicity of the blended membranes decreases as the PANi concentration decreases, which increases the effect of concentration polarization as less water is able to permeate into the porous support. However, the effect of hydrophilicity and hydrophobicity is not included within the structural parameter calculations. By changing the thin film chemistry (i.e. organic solvent), the structural parameter changed dramatically for the blended membranes. However, the structural parameter should not have changed significantly, if at all, as it is defined to characterize the porous support and the thin film chemistry should not have altered the support membrane morphology. This issue has been discussed in previous research describing the drawbacks in using the structural parameter to characterize FO membranes [59, 62]. Using water and salt permeability coefficients obtained from pressurized RO experiments reflects poorly on the transport characteristics of FO membranes as membranes under RO conditions are compacted, changing the structure of the porous support, and possibly changing the interaction between the porous support and the thin film. Furthermore, the salt permeability defined in RO describes salt molecules travelling in the

same direction as water molecules, but in FO conditions, solute is travelling from the draw to the feed and from the feed to the draw, causing a coupling effect which is not accounted for in the structural parameter.

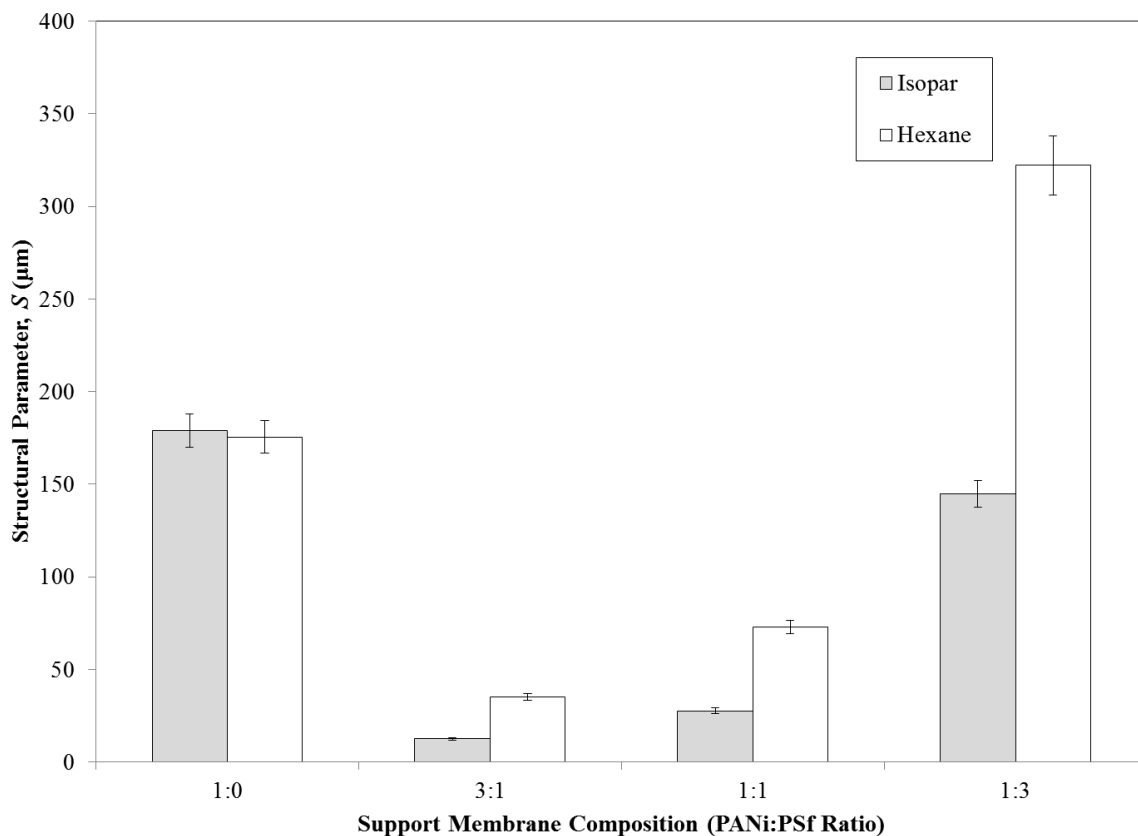


Figure 3.7. Structural parameter of PANi-PSf TFC membranes using isopar and hexane as the organic solvent

3.4 Summary

In this chapter, TFC membranes were made using pure PANi and PANi/PSf blended support membranes. It was found that increasing the immersion time in the aqueous MPD solution did not improve RO performance, while increasing MPD concentration in the aqueous solution did due to more MPD partitioning into the reaction zone instead of water as shown by

absorption tests. Using less dense, lower vapor pressure hexane as the organic solvent instead of isopar, the RO permeability is drastically reduced, indicating the formation of a denser, less permeable thin film. However, when the membranes were tested in FO-mode, the permeability was comparable regardless of the organic solvent used, and was lower compared to the commercial CTA membrane. Using RO and FO parameters, the structural parameter for the PANi/PSf TFC membranes were calculated and found to change with changes in the organic solvent used in the thin film formation. This implies that the organic solvent used greatly affects the morphology of porous substructure below, which is unlikely. These results indicate that the structural parameter calculated using RO parameters is erroneous due to compaction that occurs during RO operation, which changes the porosity, thickness and tortuosity of the substructure, and therefore, does not reflect the membrane under FO conditions. Furthermore, the structural parameter does not account for factors such as membrane chemistry, solution chemistry and hydrophilicity.

CHAPTER 4

Support Membrane Characteristics

4. INTRODUCTION

As shown in Section 3.3.5 of the previous chapter, forming thin films on PANi/PSf blended support membranes provided low permeability composite membranes regardless of the organic solvent used in interfacial polymerization. Thus, is forming thin film on phase inverted membranes the best method to form an FO membrane? Or does the phase-inverted support membrane offer high enough resistance to permeation? In this chapter, pure PANi FO membranes will be formed by non-solvent induced phase inversion as described in Section 1.4. As introduced in Chapter 1, PANi has recently gained attention as an attractive material for membranes in water treatment due to its hydrophilicity [7, 83]. Guillen et al. found that by blending different amounts of polysulfone (PSf) and PANi, membranes formed by non-solvent induced phase separation have drastically different water contact angles, pore morphologies, water permeabilities, silica and bovine serum album rejections [7].

As previously described, the search for commercially viable FO membranes continues as the thermal and chemical instability of cellulose triacetate (CTA) films has been known since before it was used in membranes. In the 1940s, CTA replaced flammable cellulose nitrate as a material for photographic film supports in the 1940s [78], however, studies have found that these cellulose triacetate films will hydrolyze under humid conditions, releasing acetic acid, which catalyzes further degradation [77-79]. In this chapter, we describe the use of PANi to form FO membranes by phase inversion, and compare its thermal and chemical stability as well as its FO performance to the commercial CTA membrane. Since phase-inverted membranes typically have low salt rejection, we use various post-treatments such as wet-curing and acid and caustic immersions to decrease the salt passage of the PANi membranes, while improving the water permeability.

4.1. Experimental

4.1.1. Materials

The polymer solution used to form the FO membranes consisted of polyaniline (PANi, 65kDa, Santa Fe Science and Technologies, Santa Fe, CA) dissolved in 4-methylpiperidine (4MP, Sigma-Aldrich, St. Louis, MO) and *N*-Methyl-2-pyrrolidone (NMP, Sigma-Aldrich). Solutions used in post-treatment of the membranes were hydrochloric acid (HCl 1N, Fisher Scientific, Hampton, NH), sodium hydroxide, (NaOH Pellets > 97%, Fisher) and camphor-10-sulfonic acid (CSA 98%, Sigma-Aldrich). In FO testing, the draw solution consisted of 32 g/L sodium chloride (NaCl, Sigma-Aldrich) and the feed solution was Milli-Q water. The cellulose-triacetate (CTA) membrane was provided by Hydration Technology Innovations (HTI, Albany, OR). All materials and solvents were used as received.

4.1.2. Membrane Formation

The procedure to form pure PANi membranes is similar to that of blended PANi/PSf membranes as described in the previous chapter. The polymer solution used to form the FO membranes consisted of 12wt% of polyaniline (PANi, 65kDa, Santa Fe Science and Technologies, Santa Fe, CA) dissolved in 6.5wt% 4-methylpiperidine (4MP, Sigma-Aldrich, St. Louis, MO) and 81.5wt% *N*-Methyl-2-pyrrolidone (NMP, Sigma-Aldrich). 4MP was used in the polymer solutions as previous research showed that it prevented gelling of the PANi solutions by preventing hydrogen bonding between polymer chains [32, 94]. This allows uniformly dispersed casting solutions to be prepared. The membranes were formed by non-solvent induced phase inversion that has been described in detail in Section 1.4. The prepared pure PANi solutions were stirred using a magnetic stirrer in air tight containers for at least three days prior to casting.

Polyester fabric was taped onto a reinforced glass plate, using electrical tape to ensure the fabric was completely flat on the plate. A stainless steel casting blade (Microm II, Gardco, Pompano Beach, FL) set to the desired height (using a film gauge) was used to spread the polymer solution uniformly onto the fabric. The glass plate was immediately immersed into a room temperature Milli-Q water bath to induce precipitation of the polymer. The membrane was left in the coagulation bath for at least 30 minutes before being transferred into plastic zip-lock bags filled with Milli-Q water and stored in 4°C until testing. For the post-treatments, the membranes were soaked in solutions of 0.1 M or 0.001 M HCl, 0.1 M NaOH, 0.1 M CSA or water baths of 35, 50, 75, or 100°C for duration of 2 min, 1 hr or 13 hr, depending on the experiment.

4.1.3. Membrane Characterization

Water contact angle on the membranes were measured using a goniometer (DSA, 10, KRÜSS GmbH, Hamburg, Germany) by a captive bubble technique. Captive bubble was chosen over sessile drop technique due to the hydrophilic nature of polyaniline membranes. Twelve measurements were obtained, the highest and lowest measurements were discarded and the average of the remaining ten measurements was taken to represent that water contact angle.

Membrane thicknesses were visually characterized from cross-sectional scanning electron microscope (SEM) images using ‘Image J’ software (Version 1.45r, downloaded at: <http://rsb.info.nih.gov/ij/>). PANi membranes were cast on glass without fabric and freeze-fractured in liquid nitrogen to obtain the clean cross-sections for imaging. All membrane surfaces were coated with gold to prevent electron charging with a sputtering system (Hummer 9.2, Anatech Ltd., Denver, Virginia) at a plasma current of 15 mA for 1 min, for an approximate thickness of 4 nm. Images were taken at a magnification of 500 X, accelerating voltage of 10 kV

and emission current of 10 μA , using a JEOL SEM (JSM-6700F FE-SEM, Peabody, MA). At least ten thickness measurements were obtained from three membrane samples to ensure the values were representative of the entire membrane. All these values are presented as average values plus or minus a standard deviation, and are best approximations based on the SEM images obtained.

Scanning electron micrographs were also taken while simultaneously exposing gold-sputter coated membrane surfaces to a focused ion beam using a FIB-SEM (Nova 600 NanoLab DualBeam™-SEM/FIB, FEI Company, Hillsboro, OR). The focused ion beam removes surface material by bombarding the surface with gallium ions. The images were taken at a magnification of 50 000 X with the ion beam operating at an emission current of 10 pA and an accelerating voltage of 10 kV.

Attenuated total reflection Fourier transform infrared spectroscopy (ATR-FTIR, JASCO FT/IR-6300 with ATR PRO450-S ZnSe crystal) was done at a resolution of 4 cm^{-1} on the membrane samples after being dried in vacuum.

4.1.4. FO Membrane Performance

The FO system used to test the membranes has been previously described in Section 3.1.6. The phase inverted membranes were tested in FO-mode with the skin-layer facing the draw solution. The draw solution consisted of 32 g/L of NaCl, and the feed was DI water flowing co-currently. The membranes casted at two different blade heights were compared to CTA in terms of water permeability and salt passage.

4.2 Results and Discussion

4.2.1. Casting Blade Height

The PANi membranes cast by phase inversion has a top skin layer of finger-like pores that opens up to a more porous substructure of macrovoids as shown in Figure 4.1. From here on, the membrane cast at 102 μm and the membrane at 152 μm will be referred to as PANi-102 and PANi-152, respectively. PANi-102 (Fig 4.1a) has a thickness of about 40 μm , which is approximately half as thick as PANi-152 (Fig 4.1b) that is about 84 μm thick. This means that the casting blade height is not indicative of the thickness of the resulting membrane after phase inversion, and the relationship between casting height and membrane thickness is not linear. The cross-sectional SEM images shown in Figure 4.1 are of membranes cast on glass plates without the fabric support, which may not be representative of the thicknesses cast on fabric since polymer solution seepage can occur in that scenario. However, since the solutions and fabric of the two membranes at different casting blade heights are the same, it is safe to assume that the polymer solution seeping into the fabric, and diffusing out into the coagulation bath is similar and the relative differences in membrane thickness can be compared.

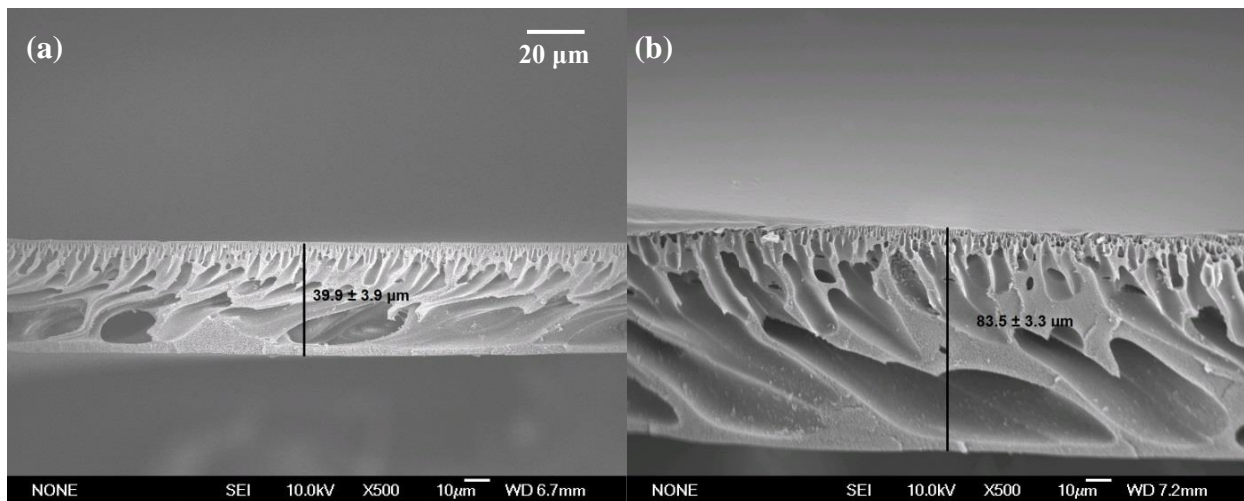


Figure 4.1. Cross-sectional SEM images of PANi membranes cast on glass using a) 102 μm b) 152 μm blade height

The FO performance of the membranes cast at different blade heights is presented in Figure 4.2, which shows that PANi-102 is significantly more permeable to water, but not to NaCl, compared to PANi-152. Since the SEM images in Figure 4.1 shows a similar cross-sectional morphology for the two membranes, the results indicate that the skin layer pores may be more important in determining the permeability of the membrane than the sublayer macrovoids. The difference in water permeability of the membranes may be attributed to the demixing conditions of the membrane, and the shorter diffusive path length of the thinner membrane. The thicker the polymer layer, the faster the solvent escapes the polymer solution, due to higher concentration of solvent in the coagulation bath, and the faster the nonsolvent penetrates into the polymer solution to induce precipitation. Thus, the thinner polymer layer had relatively slower demixing and formed a denser skin layer, which will be explored in subsequent sections.

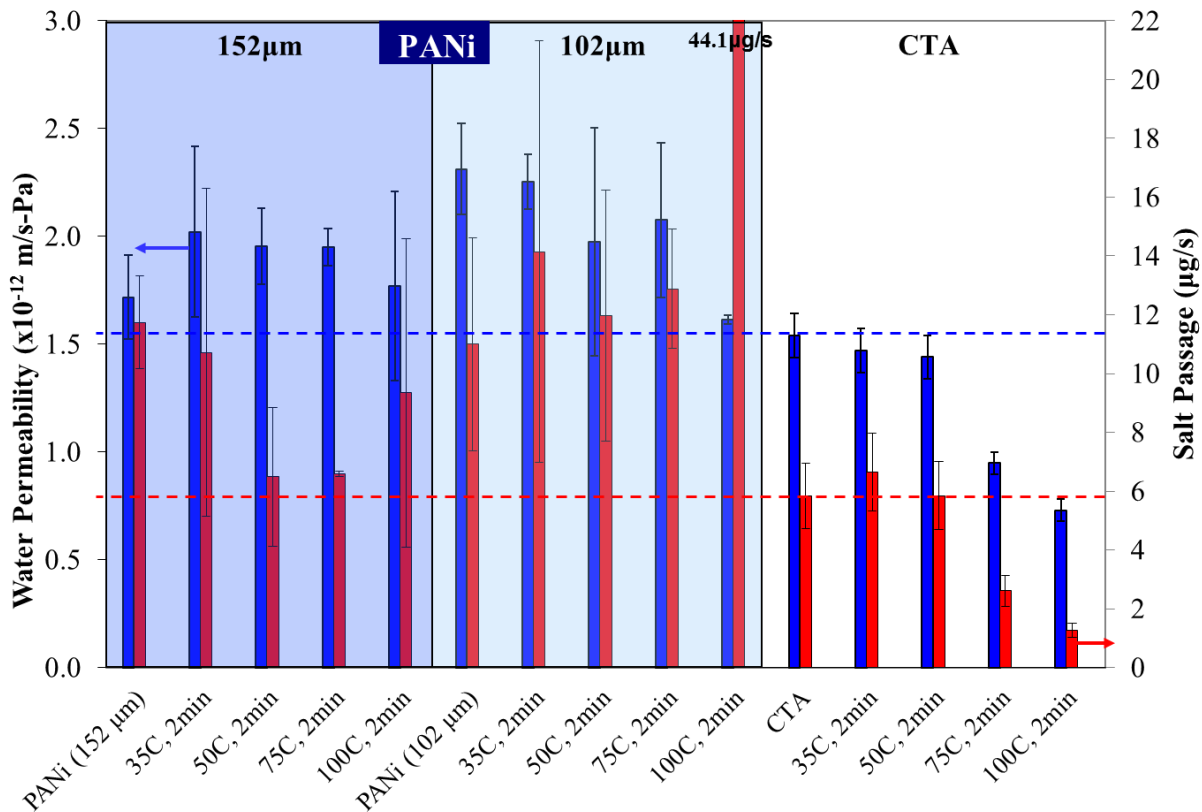


Figure 4.2. Wet-cured phase-inverted PANi and CTA membranes tested in FO-mode

4.2.2 Wet Curing PANi Membranes

After phase inversion, the already-casted PANi membranes were immersed into water baths of 35, 50, and 75°C and 100°C and tested in FO-mode. The same procedure was done with the commercial CTA membrane for comparison. From Figure 4.2, PANi-152 becomes more permeable but more selective than PANi-102 with increasing wet-curing temperature. As discussed previously, since PANi-152 may have faster demixing compared to PANi-102, it may have more skin layer pores. Therefore, the heat has a greater effect on annealing the polymer matrix and contracting the skin layer pores of PANi-152, increasing its selectivity, while not having significant effect on PANi-102. For PANi-152, wet curing at temperatures beyond 50°C

didn't increase the permeability or selectivity further, suggesting that it becomes impractical to use higher temperatures for lack of improving performance. As a comparison, the CTA membrane performance degrades rapidly with temperature beyond its optimal range of 20-35°C. The water permeability and salt passage of the CTA membrane decreases indicating that the membrane is becoming less porous with increasing curing temperature. When the CTA membrane was wet cured, the degree of hydrolysis was enhanced as discussed in Section 1.7, increasing the hydrogen bonding between polymer chains, which resulted in a tighter and less permeable membrane. These results show that the PANi membrane has better thermal stability than the CTA membrane when tested in FO-mode, as higher wet cure temperatures decreases the CTA membrane permeability significantly.

4.2.3 pH Stability of the Membranes

PANi-102 and PANi-152 along with the CTA membrane were post-treated with HCl at pH = 1 and NaOH solution at pH = 12 for 13 hours, gently rinsed with DI water and tested in FO-mode. As shown in Figure 4.3, post-treating the membranes with HCl, only caused the performance of the PANi-152 to improve, but did not cause significant changes in the performance of the PANi-102 and CTA. After the NaOH post-treatment, the performance of the PANi-152 remains relatively the same, while the performances of PANi-102 and the CTA were both degraded in terms of decreased water permeability and increased salt passage.

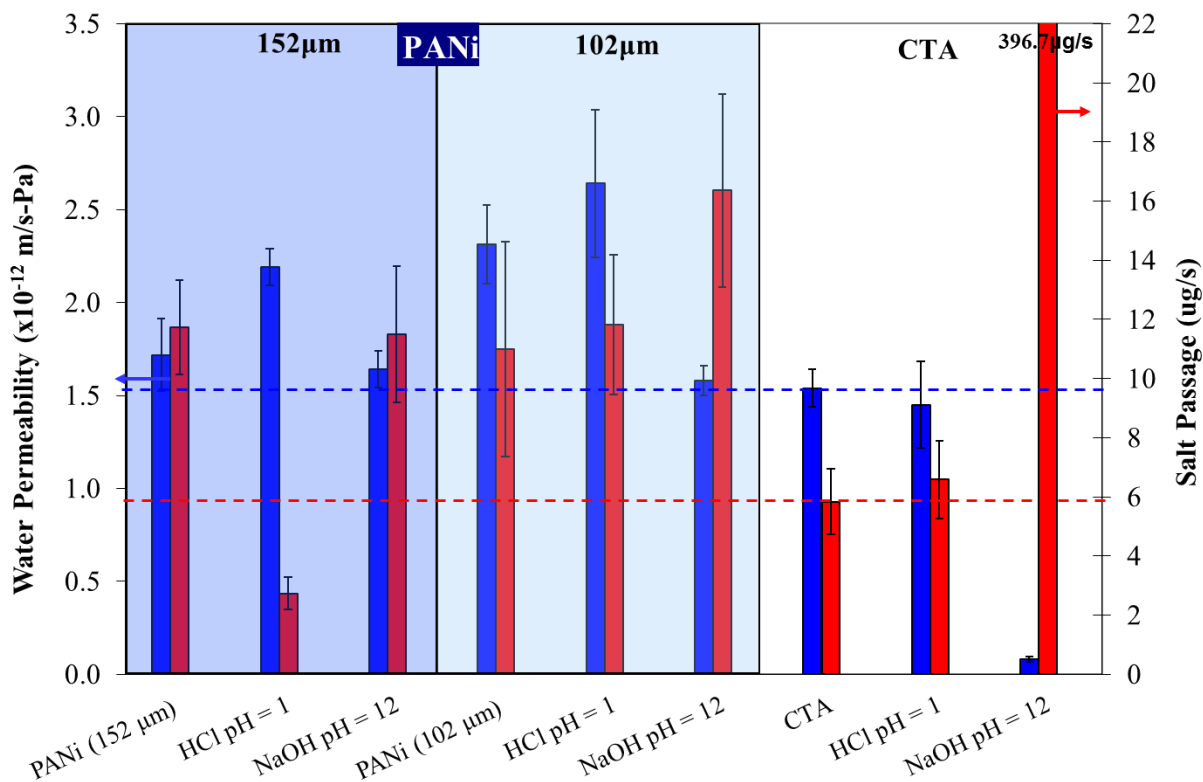


Figure 4.3. Water Permeability and Salt Passage of PANi and CTA after post-treatment with acid (HCl) at pH = 1 and base (NaOH) at pH = 12 for 13 hours

From previous studies of PANi membrane films formed for gas separations, a cycle of doping the films with strong acid (HCl), dedoping with strong base to remove the acid counterions, and redoping with a mild acid solution, caused the H_2/N_2 separation factor to increase ~15-fold [96]. The authors proposed that this cycle essentially increased the free volume in the polymer matrix and created channels through the polymer matrix, which strongly affected the diffusion of large gas molecules, thereby increasing the separation factor. Although the PANi membranes presented in this paper were prepared in a different method and for a different purpose, the doping and dedoping concepts may help in understanding the performance changes observed.

Using the same analogy for phase inverted PANi membranes, as shown in Figure 4.4, by acid doping the membrane (Fig 4.4b), the polymer was protonated, and halide counterions occupied spaces in the polymer matrix in-between pores. The membrane was then dedoped with water, indicated by a change in color of the membrane from green to blue or from emeraldine salt to emeraldine base form of PANi as discussed in Section 1.8. This doping/dedoping process increased the connectivity of the pores in the skin-layer or microporous layer of the membrane (Fig 4.4c), and thereby increasing the water permeability of the membrane (Fig 4.4c), and thereby increasing the water permeability of the membrane. Furthermore, the salt passage is significantly reduced as water permeation from the feed to the draw slows down the rate of salt diffusion from the draw to the feed solution, and the size of hydrated salt ions (diameter of Na^+ : $\sim 7\text{\AA}$) are much larger than water molecules (diameter: $\sim 2.54\text{\AA}$).

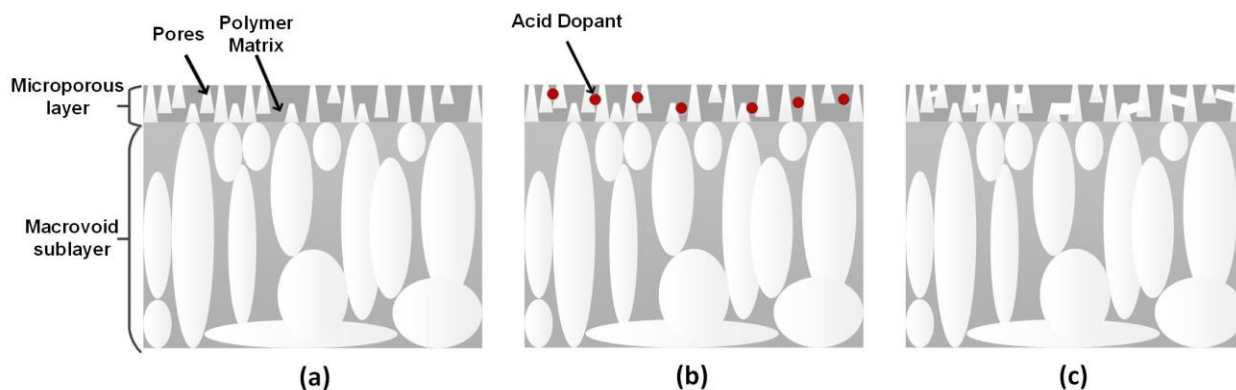
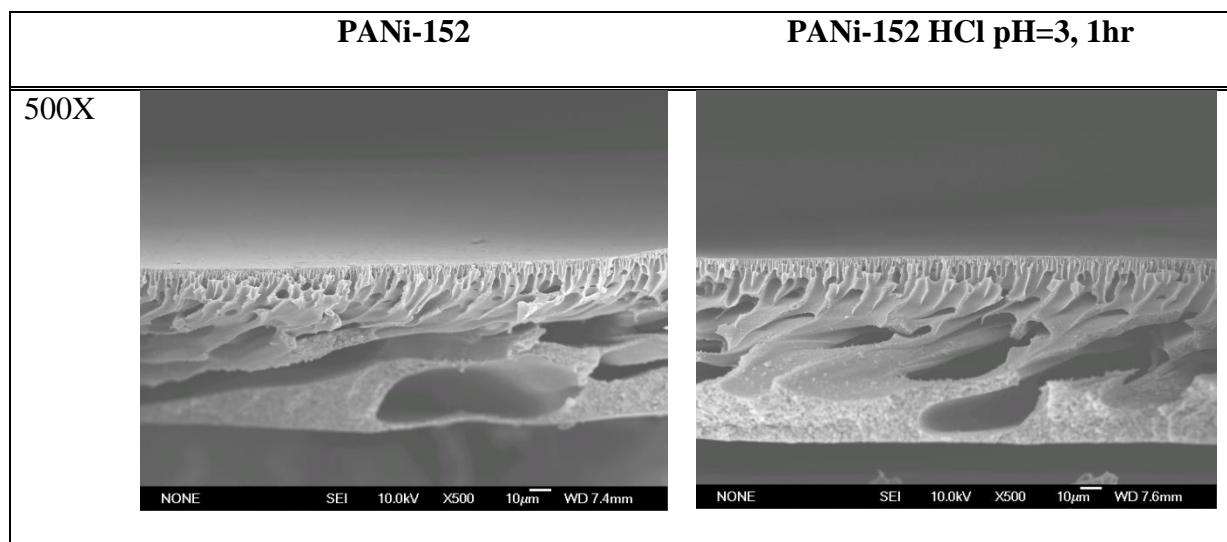


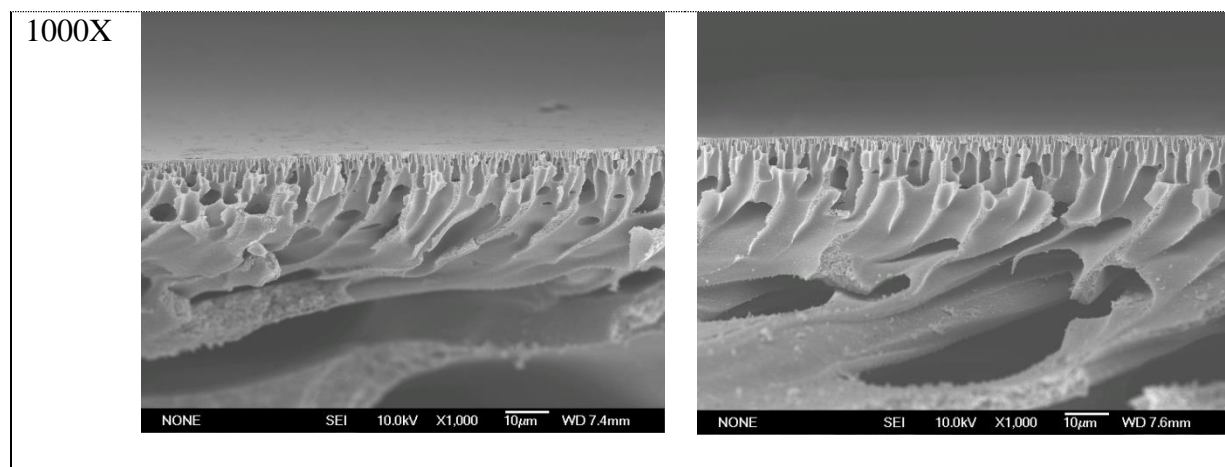
Figure 4.4. Schematic depicting the effect of acid doping on pore connectivity in the skin layer of a PANi membrane (a) as-cast, (b) with acid dopant and (c) dedoped with water [96]

This reasoning also explains why PANi-152 is more significantly enhanced while PANi-102 remains relatively unchanged by acid doping. Referring back to Figure 4.1, the cross-sectional SEM images show that PANi-152 has much more polymer in between pores, so any increase in connectivity between pores by dopant would significantly increase water permeability. To

further investigate the effect of HCl dopant on PANi-152, cross-sectional SEM images of the membrane cast on glass were taken to determine whether there were changes in the pore morphology before and after treatment shown in Table 4.1. From the images, there does not seem to be significant, observable changes in the pore size of the membrane after the HCl treatment that can be attributed to the improved performance of the membrane. Previous modeling efforts by Winokur et al. found that the crystal structure changed when comparing dried PANi powders with hydrated, doped or dedoped powders [84]. In their work, the researchers found that by dedoping the emeraldine PANi powders, additional crystalline phases appear, which may explain the observed decreased water permeability in the PANi-152 membranes due to the rigidity within the material. Furthermore, the doped emeraldine salt form of PANi highly adsorbed water molecules, increasing the ion channels in the structures, providing an explanation for the improved performance of HCl-doped PANi-152 membranes.

Table 4.1. Cross-sectional images of pre- and post- treated PANi-152 with 100mM HCl for 1hr





4.2.4 Acid Dependence

To determine whether it is the type of acid or pH that is improving the membrane water permeability and NaCl selectivity, PANi-152, PANi-102 and CTA were post-treated with 0.1 M CSA (pH ~1.3) and 0.1 M HCl (pH = 1) and 0.001 M HCl (pH = 3) for 1 hour and tested in FO-mode. From Figure 4.5, it is quite clear that the type of acid and the pH as a post-treatment affects the FO membrane performance to varying degrees. For PANi-152, the CSA post-treatment has no significant effect on the performance, whereas HCl post-treatment at pH = 3 causes the most enhanced performance compared to at pH = 1. For PANi-102, the opposite trend was observed, that is, the best post-treatment appears to be with 0.1 M followed by HCl at pH = 1 then at pH = 3, while CSA has enhances the performance most drastically. In comparison, the CTA membrane does not have significantly decreased performance after acidic post-treatments, mainly due to the stability of the acetate groups of CTA under mild acidic conditions, especially only after a duration of 1 hour.

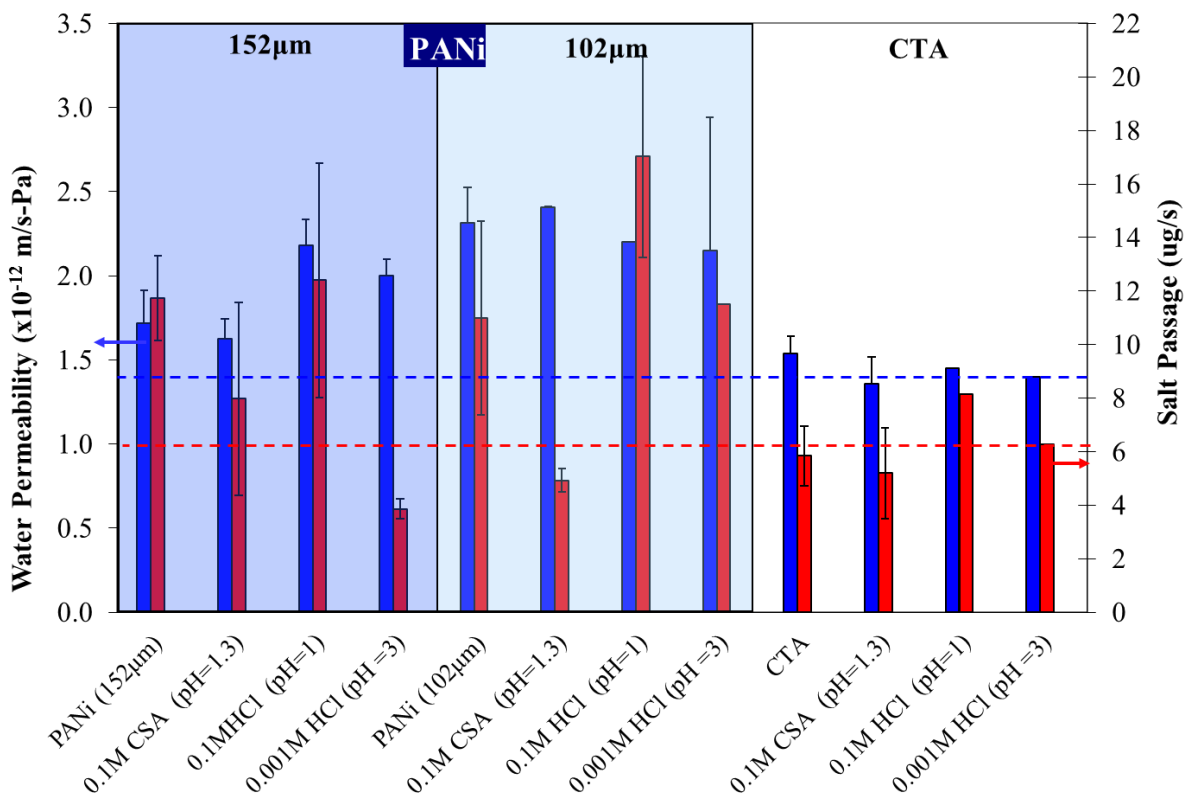


Figure 4.5. Phase-Inverted PANi membrane post treated with CSA and HCl in various pH for 1 hr

CSA was chosen to treat the membranes because previous studies suggested that it was able to remove the 4MP used as a cosolvent in the polymer solution, and increase the hydrophilicity of the membrane. However, based on Table 4.2, the contact angle of PANi-102 did not change significantly after CSA treatment, which means that perhaps the CSA is not removing the 4MP and has another effect on the PANi membrane that needs further investigation. The doping of the membrane may change the molecular conformation between the PANi chains due to intermolecular attractions which becomes permanent.

After post-treating the membrane with CSA, the membrane visibly becomes green from its original blue color indicative of the change from emeraldine base to emeraldine salt. After the duration of the experiment, the membrane returned back to its original blue color, probing the question of whether CSA leached out into solution, and whether performance returned back to the pre-treated state. To determine this, the performance of a PANi-102 was tested in FO-mode, then treated with 0.1M CSA treatment for 1 hour, and soaked in a beaker of DI water for 3 hours, and re-tested. The water permeability was, $A = 2.37 \times 10^{-12}$ m/s-Pa and salt passage = 4.77 $\mu\text{g/s}$, which indicates that the enhanced performance caused by CSA post-treatment did not degrade with cross-flow of water during experimentation or water immersion (post-treatment), and thus, some permanent morphological change has happened to the polymer matrix. Furthermore, a decrease in performance was not observed during the duration of the experiment, which indicates that the CSA post-treatment of the membrane is not reversible under the testing conditions used (feed solution: DI water, draw solution: 32g/L NaCl).

Table 4.2. Captive bubble water contact angle of PANi-152, PANi-102 and CTA before and after 100mM CSA and HCl post-treatments

Membrane	Post-Treatment	Contact Angle (°)
PANi-152	None	36.94 ± 6.25
	100mM CSA, 1hr	33.69 ± 0.71
	100mM HCl, 1hr	49.81 ± 5.39
PANi-102	None	38.75 ± 2.96
	100mM CSA, 1hr	41.82 ± 2.42

	100mM HCl, 1hr	42.15 ± 2.07
	None	53.67 ± 7.06
CTA	100mM CSA, 1hr	48.94 ± 3.44
	100mM HCl, 1hr	40.98 ± 1.63

Furthermore, from Table 4.2, the PANi membrane has significantly lower contact angle than the CTA membrane which suggests that PANi is more hydrophilic than CTA. This may be due to higher electron density concentrated in the benzene rings of the PANi chains compared to CTA that is attracting water molecules to the membrane.

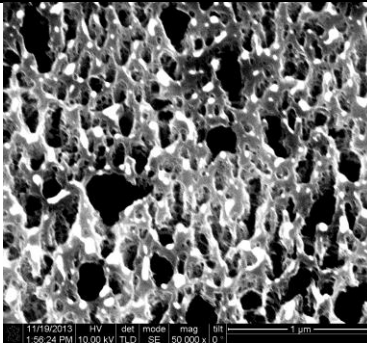
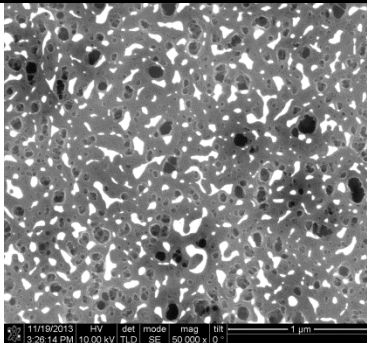
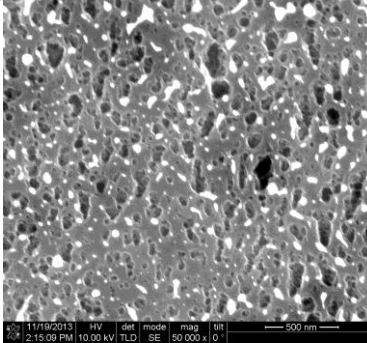
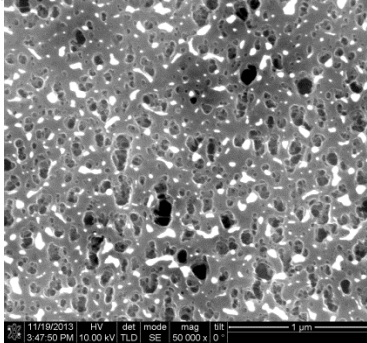
To summarize the results presented thus far, CSA post-treatment was observed to improve the FO performance of PANi-102, but not PANi-152, whereas wet-curing and HCl post-treatment improves PANi-152 and not PANi-102. This indicates that the smaller sized post-treatment “additives” has a much greater effect on the thicker PANi membrane and not the thinner. One reason for this is that for thicker membranes, the diffusion path length through the membrane may dictate the transport of the additives more than the solubility into the membrane. This means that HCl and H₂O molecules that are act to increase pore connectivity affect the diffusivity within PANi-152 greater than CSA that may be changing the polymer matrix properties in PANi-102.

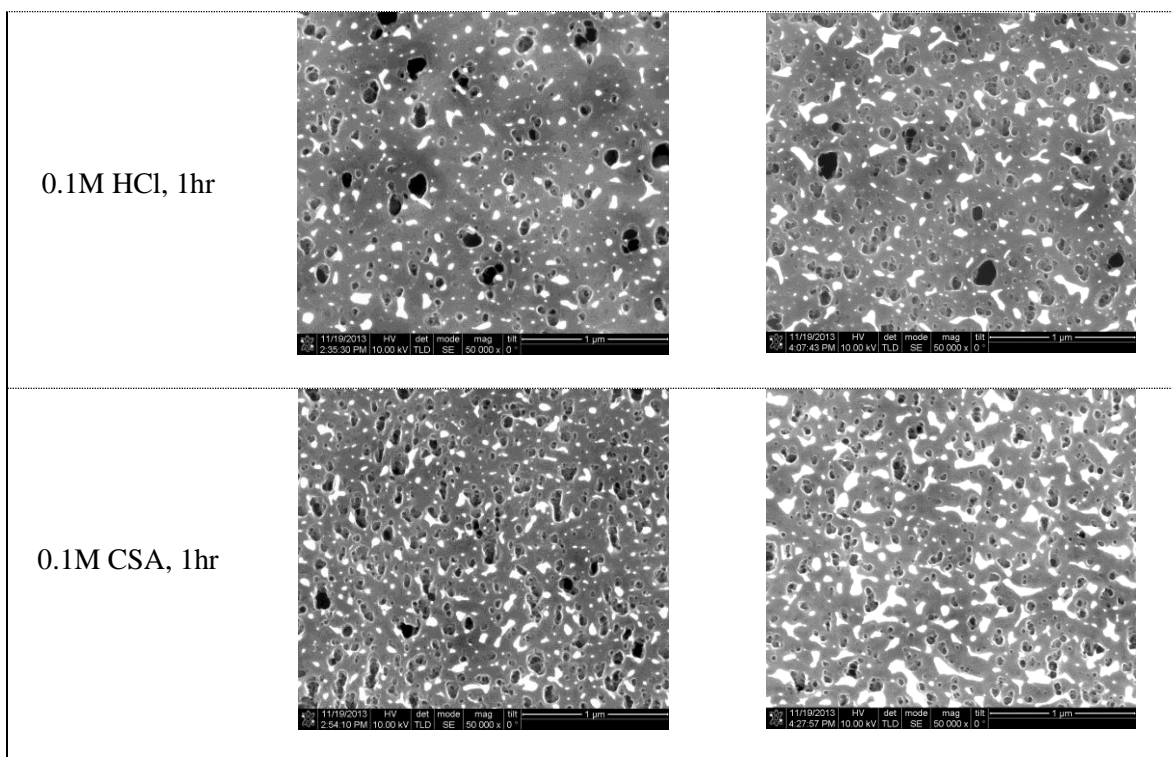
4.2.5 Membrane Skin-Layer Characterization

As discussed previously, a possible reason for the difference in performance between PANi-152 and PANi-102 and their membranes after post-treatment is the thickness of skin layers. From the previous sections, the resolution of SEM was not high enough to resolve minute

differences in the thickness or pore morphology of the skin layer. Here, scanning electron micrographs were taken while simultaneously exposing the membrane to a focused ion beam of gallium ions to systematically mill away membrane material for a specified amount of time. The resultant images are compared to see whether there are significant differences in the final morphology. If large, deep pores are present at the end of the FIB-SEM process, then the skin layer of the membrane was relatively thinner or less dense. Table 4.3 shows the resulting surface images of the membranes under the specified conditions after milled by the FIB for 15 min. The bright white spots on the image were the residual gold coatings that were not removed by the FIB.

Table 4.3. Surface FIB-SEM images of PANi-152 and PANi-102 pre- and post-treated

Condition	PANi-152	PANi-102
Un-treated		
Wet-cured at 50°C, 2min		



One significant difference is that after the same amount of milling, the PANi-152 membrane surface is more damaged than PANi-102, exposing large, deep sublayer pores. This may reveal that PANi-102 has a denser, but thinner skin layer than PANi-152, explaining the higher water permeability but comparable salt passage than PANi-152 (Fig 4.2). This may indicate that the casting height not only changes the thickness of the overall membrane, it also changes the phase inversion kinetics. As hypothesized, PANi-152 has faster demixing conditions than PANi-102, which created more porous, skin layer for PANi-152 but a denser, less porous skin layer for PANi-102. Once PANi-152 is wet cured at 50°C, the skin layer becomes tighter, exposing less large pores than the untreated membrane, which explains the improved performance. Not significant improvements can be seen with the HCl treatment, while the CSA seems to improve the skin layer drastically. As for PANi-102, only with the CSA post-treatment does the skin layer appear to be tighter with less larger pores, confirmed by the improved performance. These

images show that the skin layer of a phase-inverted membrane has significant impact on the performance.

4.2.6 Dopant Reversibility

As PANi-152 had the highest water permeability and lowest salt passage when post-treated with 100mM HCl (pH = 3) for 1 hr, this membrane was chosen to be studied further. First, the post-treated membrane was put into an extended experimental trial to determine whether the effect of HCl was temporary and if any leaching of the acid would occur to revert the performance of the membrane back to its original permeability. As shown in Table 4.4, the water permeability and salt passage of the short and extended trial of the post treated membrane was not significantly different, indicating that hydraulic cross flow across the membrane, and water permeation through the membrane does not reduce the enhancement effect by acid dopant on the PANi membrane.

Table 4.4. Comparison of Water Permeability and Salt Passage of Post-treated PANi-152 in Short and Extended FO test

Conditions	Water Permeability ($\times 10^{-12}$ m/s-Pa)	Salt Passage ($\mu\text{g/s}$)
PANi-152 untreated	1.72 ± 0.20	11.74 ± 1.59
Post-treated PANi-152 Short test	2.18 ± 0.16	3.87 ± 0.37
Post-treated PANi-152 Extended test	1.80	3.28

To better understand the effect of acid dopant on the PANi membrane, a dopant cycling procedure was done similar to one performed by Virji et al. for PANi nanofibers [82]. Four membranes were tested in FO for water permeability and salt passage: 1) PANi-152, 2) PANi-

152 post-treated with 0.1M HCl (pH = 3) for 1hr, 3) PANi-152 post-treated with 0.1M HCl (pH = 3) for 1hr and then with 0.1M of NaOH (pH = 11) for 1hr and 4) PANi-152 post-treated with 0.1M HCl (pH = 3) for 1hr and then with 0.1M of NaOH (pH = 3) for 1hr, and finally with 0.1M HCl (pH = 3) for 10 min. Figure 4.6 presents the FO water permeability and salt passage for the membranes after each of each post-treatments compared to the original PANi-152 membrane. After the membrane was doped with acid, the permeability and NaCl selectivity increased, as shown in previous sections. Then, after dedoping with 0.1M NaOH, the performance returned to the original untreated membrane, indicating some level of reversibility, although this has to be tested for the long term. After this dedoping step, the membrane was re-immersed into 0.1M HCl solution for 10 min to slightly re-dope the membrane. The dopant cycling proved that PANi membrane was able to recover its performance.

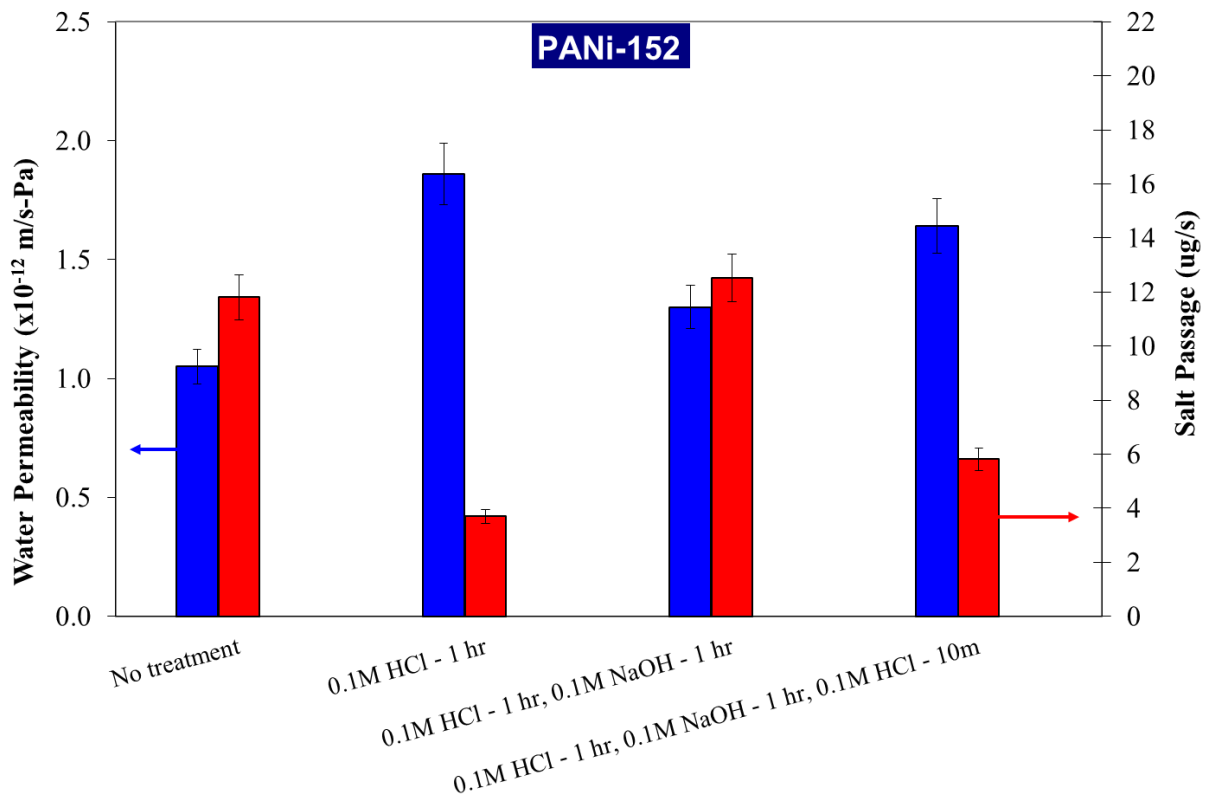


Figure 4.6. PANi-152 membrane FO water permeability and salt passage for a dopant cycle

To preliminarily determine whether chemical changes or morphological changes occurred to cause the observed changes in membrane performance, ATR-FTIR was done on PANi-152 membranes doped with HCl, dedoped with H₂O and with NaOH. As shown in Figure 4.7, no significant difference is observed between the spectra of each membrane, which confirms that no chemical change has been made on the PANi.

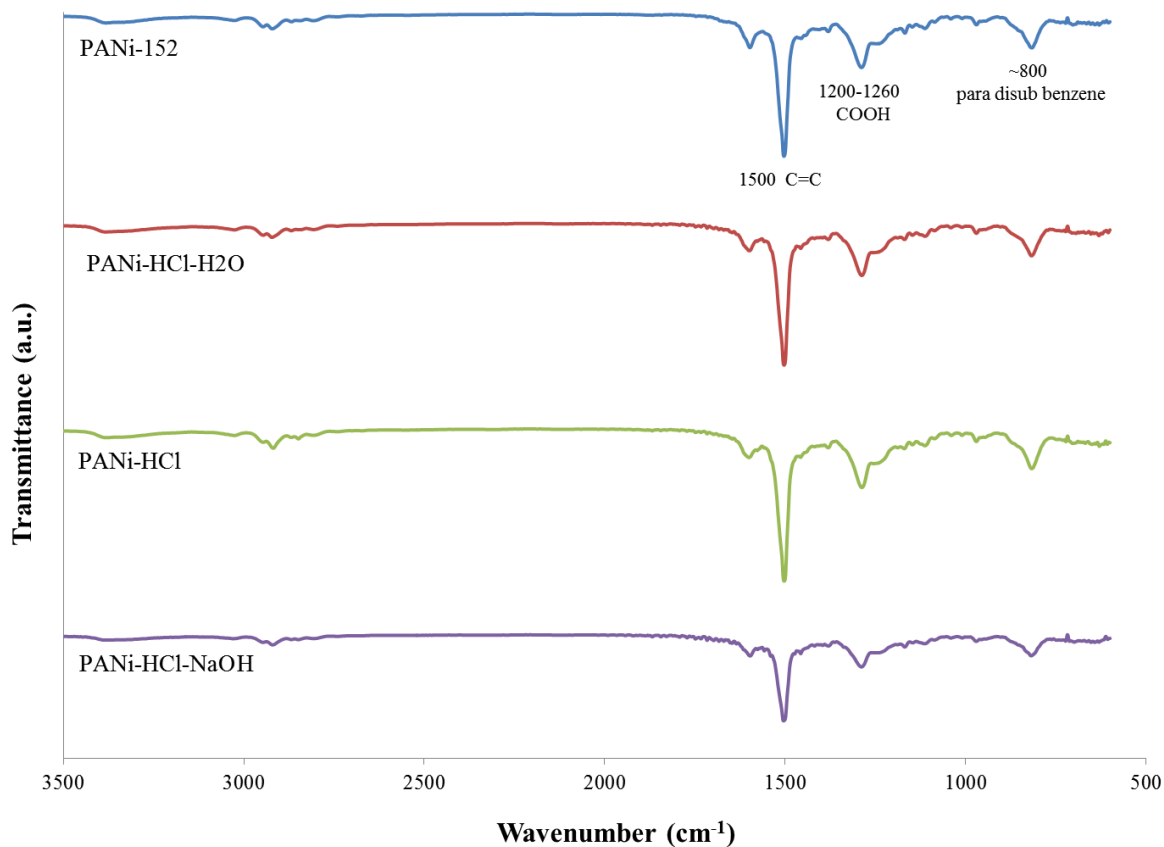


Figure 4.7. FTIR spectra for PANi-152 post-treated membranes in a dopant cycle

4.3. Summary

In this chapter we investigated the prospect of forming FO membranes by phase inversion of polyaniline. First, by simply changing the height of which the membrane was cast, the FO performance could be changed significantly. By post-treating the membranes with acid, heat and caustic the FO performance was varied and enhanced compared to the untreated membrane. The membrane (PANi-152) cast at a higher casting height had higher water permeability and lower salt passage than the commercial CTA membrane when post-treated with HCl, while the thinner membrane (PANi-102) achieved similar enhanced performance using an organic acid (CSA). The acid dopant is postulated to increase the free volume in the polymer matrix, but is difficult to confirm with the resolution of SEM images. The reasoning behind enhanced water permeability and selectivity will require further investigation. The PANi membranes in this chapter were all cast on the same fabric, however, recent research has shown that the structure of the fabric can significantly affect the performance of the composite membrane by dictating factors such as polymer seepage and demixing conditions during phase inversion, and resistance to diffusion in the porous substructure [97].

CHAPTER 5

Conclusions and Future Work

5. Conclusions and Future Work

The first chapter provided a brief overview of osmosis and its applications, motivating this research. This overview is followed by an in-depth discussion of osmotic membranes and materials, and its formation techniques, namely, phase inversion and interfacial polymerization. Both membrane formation techniques can be altered by changing the solvent system, using additives, or post-treating the membranes, to induce properties such as increased hydrophilicity, permeability or anti-fouling functionalities. Phase-inverted membranes are typically used to form microfiltration and ultrafiltration membranes, as well as substrates for thin film composite (TFC) membranes. To increase selectivity of phase-inverted membranes for osmotic applications, polymeric thin-films are formed on the surface via interfacial polymerization to form TFC membranes. Although commercial RO TFC membranes are able to reject up to 99.9% of NaCl, mass transfer limitations reduce the efficiency of the membranes. First, concentration polarization, or solute buildup on the surface of the membrane occurs, which decreases the driving force across the membrane, requiring higher hydraulic pressure for water permeation. In FO, the porous substructure creates an unstirred boundary layer, which decreases the effective driving force across the membrane, thereby causing yet another mass transfer limitation called internal concentration polarization. The support layer also interplays with the thin film by changing the flux distribution throughout the membrane, which creates hotspots or regions of higher fouling and scaling propensity. Current membrane materials for reverse osmosis has properties such as negative surface charge and high surface roughness that provide the ideal grounds to initiate biofilm formation, against which traditional methods of cleaning such as back washing and chemical cleanings are ineffective. Furthermore, chlorine, a common disinfectant, degrades polyamide reverse osmosis membranes, thereby requiring a pre-treatment process to

remove residual chlorine before the feed water is fed through the membrane modules. The only commercially available forward osmosis membrane material has limited chemical and thermal stability, limiting its use in extended applications such as low energy desalination. The research done in this thesis primarily focuses on using polyaniline to understand the relationship between membrane structure and performance. This is because previous research has shown that polyaniline is has potential to be a membrane material for filtration applications due to its hydrophilicity and tunable pore structure.

In the second chapter, the relationship between the support membrane and thin film was developed using computational fluid dynamics modeling. Based on previous modeling efforts, voids of higher diffusivity were introduced into the thin film, and the effect of non-uniform thin films on the permeability of composite membranes was explored. It was found that the permeability of the membrane will only decrease if the base film thickness is kept constant, regardless of the thin film morphology added on top, as the base film determines the upper bound of membrane performance. However, using the same amount of polymer, if the membrane is formed into an undulating film, higher permeability is achieved due to the creation of shorter diffusion path lengths. The most effective method in increasing the permeability of a membrane is to decrease the base film thickness, which indicates that the surface area of the thin film has limited effect on membrane performance. When the support membrane pores are not aligned with the valleys of the thin film roughness, the top film thickness changes the flux distribution, which has implications on “hotspots” for fouling in real world applications. Thus, by tuning the volume of the voids, the location of these hotspots can be tailored such that fouling can be localized to areas in which cleaning or surface modifications would be easier.

In the third chapter, TFC membranes were made using pure PANi and PANi/PSf blended support membranes. However, based on MPD absorption tests, it was observed that due to the hydrophilicity of PANi, more water is absorbed during the immersion step of interfacial polymerization compared to PSf. Thus, variations were made to alter the traditional recipe of thin film formation done on PSf substrates. It was found that increasing the immersion time in the aqueous MPD solution did not improve RO performance, while increasing MPD concentration did due to increased MPD partitioning into the reaction zone instead of water. Using less dense, lower vapor pressure hexane as the organic solvent instead of isopar, the RO permeability is drastically reduced, indicating the formation of a denser, less permeable thin film. However, when the TFC membranes were tested in FO-mode, the permeability was comparable regardless of the organic solvent used, and was lower compared to the commercial CTA membrane. Using the obtained RO and FO parameters, the structural parameter for the PANi/PSf TFC membranes were calculated using accepted theory, but was found to change with changes in the organic solvent used in the thin film formation. However, the structural parameter is used to describe the thickness, tortuosity, and porosity of the substructure underneath the thin film, which should not be affected by changes in organic solvent used in interfacial polymerization. These results reinforce the fact that the structural parameter should not be calculated using RO permeability parameters, as recent research has started to indicate, as the substructure behaves differently under compaction, thereby not reflecting the membrane under FO conditions. Furthermore, the structural parameter does not account for factors such as membrane chemistry, solution chemistry and wettability. Future research should move towards a model where these factors are accounted for in the structural parameter, and is dependent solely on parameters under similar experimental conditions. Also, hopefully as instruments become more advanced, physical

measurement methods (mercury porosimetry, FIB-SEM etc.) will become more accessible and economical so the structural parameter can be measured physically.

In the fourth chapter, FO membranes were formed by the phase inversion of pure polyaniline without the need of a thin film as the previous chapter showed its limitation on FO performance. In an attempt to increase water permeability and selectivity, post-treatments with acid, heat and caustic were applied to the untreated membrane. Wet-curing appeared to tighten the skin layer of the membrane cast at higher blade height (PANi-152), allowing for higher water permeability but higher selectivity as well, but had no significant effect on the membrane cast at a lower height (PANi-102). PANi-152 had higher water permeability and lower salt passage than the commercial CTA membrane when post-treated with HCl, while PANi-102 achieved similar enhanced performance using an organic acid (CSA). It is postulated that the acid dopants increased the free volume in the polymer matrix, but is difficult to confirm with the resolution of SEM images. The reasoning behind enhanced water permeability and selectivity will require further investigation. The PANi membranes in this chapter were all cast on the same fabric, however, recent research has shown that the structure of the fabric can significantly affect the performance of the composite membrane by dictating factors such as polymer seepage and demixing conditions during phase inversion, and resistance to diffusion in the porous substructure [97]. This factor of fabric variation is another factor to tune the performance of PANi-FO membranes.

This research has only exploited one main facet of PANi, namely its hydrophilicity, to form FO/RO membranes, and meanwhile study membrane structure. However, this diminishes the other major property of PANi, its induced conductivity when doped with acid, which may offer interesting effects on rejection performance. This has been studied for nanofiltration

membranes, for which research has found that water flux and salt passage were maximal at the pore isoelectric point due to decreased electrostatic repulsion and increased pore volume in the polymer matrix [98]. Furthermore, as demonstrated by Subramani and Hoek, surface functional groups contribute greatly in determining initial biofilm formation and the ease in cleaning afterwards. It was reported that monopolar electron-donor surfaces are generally more resistant to cell adhesion [99]. Thus, if a biofilm is formed on the surface of a PANi membrane, for example, it could be doped with acid, to switch the surface charge, and quickly dedoped, as a potential method to wash off the biofilm.

As this research has shown, PANi has high potential to be a membrane material for FO applications. Although the research presented in this dissertation focused on using PANi to understand membrane structure, future work includes exploring the viability of using PANi membranes for FO applications on a commercial scale. However, there are a many parameters that need to be studied in detail before scale up can take hold. This includes: the solvent system used in phase inversion, the molecular weight of PANi, and the fabric material. As discussed in section 1.4, the solvent system will dictate how quickly demixing occurs once the casting solution is immersed into the coagulation bath. Instantaneous demixing will most likely result in a porous membrane while delayed demixing results in a denser membrane [25]. The molecular weight of the polymer increases the viscosity of the casting solution, which delays demixing due to slower diffusive interchange between solvent and non-solvent [25]. Finally, as discussed previously, recent research determined that the type of fabric used to form phase inversion membranes can dramatically change the performance of the membrane. As the porosity and wettability of the fabrics determine the degree of polymer uptake into the fabric during casting, which in turn determines the macrovoid structure of the membrane [100].

6. REFERENCES

- [1] Provide access to clean water, in: Grand Challenges for Engineering, National Academy of Engineering, 2011.
- [2] M. Elimelech, The global challenge for adequate and safe water, *Journal of Water Supply: Research and Technology - AQUA*, 55 (2006) 3-10.
- [3] P. Gleick, *The World's Water*, Island Press, 2008.
- [4] M. Elimelech, W.A. Phillip, The Future of Seawater Desalination: Energy, Technology, and the Environment, *Science*, 333 (2011) 712-717.
- [5] M.B. Fabiola Alvarado-Revilla, Lorenzo Bosi, James Brooks,, I.E. Victoria David, Tse Han, Gabriela Gadêlha, Christopher Gasson, Clara González-Manchón, Adam Heffill, Hiroko Kasama, Heather Lang, Karin Maree, Rhys Owen, Tom Pankratz, Miriam Scruby and Richard Weyndling, *Desalination Markets*, in: G.W. Intel (Ed.), Oxford, UK, 2010.
- [6] J.C. Crittenden, R.R. Trussell, D.W. Hand, K.J. Howe, G. Tchobanoglous, *Water Treatment: Principles and Design*, 2 ed., John Wiley & Sons, Hoboken, New Jersey, 2005.
- [7] G.R. Guillen, T.P. Farrell, R.B. Kaner, E.M.V. Hoek, Pore-structure, hydrophilicity, and particle filtration characteristics of polyaniline-polysulfone ultrafiltration membranes, *Journal of Materials Chemistry*, 20 (2010) 4621-4628.
- [8] T.Y. Cath, A.E. Childress, M. Elimelech, Forward Osmosis: Principles, applications and recent developments, *Journal of Membrane Science*, 281 (2006) 70-87.
- [9] J.R. McCutcheon, R.L. McGinnis, M. Elimelech, Desalination by ammonia-carbon dioxide forward osmosis: Influence of draw and feed solution concentrations on process performance., *Journal of Membrane Science*, 278 (2006) 114-123.
- [10] Q. Ge, J. Su, T.-S. Chung, G. Amy, Hydrophilic Superparamagnetic Nanoparticles: Synthesis, Characterization, and Performance in Forward Osmosis Process, *Industrial & Engineering Chemistry Research* 50 (2011) 382-388.
- [11] A. Achilli, T.Y. Cath, A.E. Childress, Selection of inorganic-based draw solutions for forward osmosis applications. , *Journal of Membrane Science*, 364 (2010) 233-241.
- [12] R.L. McGinnis, J.R. McCutcheon, M. Elimelech, A novel ammonia-carbon dioxide osmotic heat engine for power generation, *Journal of Membrane Science*, 305 (2007) 13-19.
- [13] R.L. McGinnis, M. Elimelech, Global Challenges in Energy and Water Supply: The Promise of Engineered Osmosis, *Environ. Sci. Technol.*, 42 (2008) 8625-8629.

- [14] J.E. Miller, L.R. Evans, Forward Osmosis: A New Approach to Water Purification and Desalination, in, Sandia National Laboratories, Albuquerque, NM, 2006.
- [15] K.W. Hameed, Concentration of Orange Juice Using Forward Osmosis Membrane Process, Iraqi Journal of Chemical and Petroleum Engineering, 14 (2013) 71-79.
- [16] R.J. Salter, Forward Osmosis, Water Conditioning & Purification, (2006).
- [17] N. Widjojo, T.-S. Chung, M. Weber, C. Maletzko, V. Warzelhan, The role of sulphonated polymer and macrovoid-free structure in the support layer for thin-film composite (TFC) forward osmosis (FO) membranes, Journal of Membrane Science, 383 (2011) 214-223.
- [18] HTI OsMeM CTA-ES Membrane, in: H.T. Innovations (Ed.), Albany, OR, Received 2014, pp. 2.
- [19] N.-N. Bui, M.L. Lind, E.M.V. Hoek, J.R. McCutcheon, Electrospun nanofiber supported thin film composite membranes for engineered osmosis, Journal of Membrane Science, 385–386 (2011) 10-19.
- [20] K.P. Lee, T.C. Arnot, D. Mattia, A review of reverse osmosis membrane materials for desalination - Development to date and future potential, Journal of Membrane Science, (2011) 1-22.
- [21] J.R. McCutcheon, M. Elimelech, Influence of membrane support layer hydrophobicity on water flux in osmotically driven membrane processes, Journal of Membrane Science, 318 (2008) 458-466.
- [22] N. Misdan, W.J. Lau, A.F. Ismail, Seawater Reverse Osmosis (SWRO) desalination by thin-film composite membrane - Current development, challenges and future prospects, Desalination, (2011).
- [23] G.R. Guillen, Y. Pan, M. Li, E.M.V. Hoek, Preparation and Characterization of Membranes Formed by Nonsolvent Induced Phase Separation: A Review, Industrial & Engineering Chemistry Research, 50 (2011) 3798-3817.
- [24] A. Tiraferri, N.Y. Yip, W.A. Phillip, J.D. Schiffman, M. Elimelech, Relating performance of thin-film composite forward osmosis membranes to support layer formation and structure, Journal of Membrane Science, 367 (2011) 340-352.
- [25] M. Sadrzadeh, S. Bhattacharjee, Rational design of phase inversion membranes by tailoring thermodynamics and kinetics of casting solution using polymer additives Journal of Membrane Science, 441 (2013) 31-44.
- [26] S. Loeb, The Loeb-Sourirajan Membrane: How It Came About, in: Synthetic Membranes:, American Chemical Society, 1981, pp. 1-9.
- [27] M. Mulder, Basic Principles of Membrane Technology, Kluwer Academic Publishers, Dordrecht, Netherlands, 1997.

- [28] G.R. Guillen, G.Z. Ramon, H.P. Kavehpour, R.B. Kaner, E.M.V. Hoek, Direct microscopic observation of membrane formation by nonsolvent induced phase separation, *Journal of Membrane Science*, 431 (2013) 212-220.
- [29] R.J. Petersen, Composite reverse osmosis and nanofiltration membranes, *Journal of Membrane Science*, 83 (1993) 81-150.
- [30] T.A. Tweddle, O. Kutowy, W.L. Thayer, S. Sourirajan, Polysulfone ultrafiltration membranes, *Industrial & Engineering Chemistry Product Research and Development*, 22 (1983) 320-326.
- [31] M.L. Lind, A.K. Ghosh, A. Jawor, X. Huang, W. Hou, Y. Yang, E.M.V. Hoek, Influence of Zeolite Crystal Size on Zeolite-Polyamide Thin Film Nanocomposite Membranes, *Langmuir*, 25 (2009) 10139-10145.
- [32] A.K. Ghosh, B.H. Jeong, X.F. Huang, E.M.V. Hoek, Impacts of reaction and curing conditions on polyamide composite reverse osmosis membrane properties, *Journal of Membrane Science*, 311 (2008) 34-45.
- [33] C. Tang, Y. Kwon, J.O. Leckie, Effect of membrane chemistry and coating layer on physiochemical properties of thin film composite polyamide RO and NF membranes: I. FTIR and XPS characterization of polyamide and coating layer chemistry, *Desalination*, 242 (2009) 149-167.
- [34] I.J. Roh, A.R. Greenberg, V.P. Khare, Synthesis and characterization of interfacially polymerized polyamide thin films, *Desalination*, 191 (2006) 279-290.
- [35] B.H. Jeong, E.M.V. Hoek, Y.S. Yan, A. Subramani, X.F. Huang, G. Hurwitz, A.K. Ghosh, A. Jawor, Interfacial polymerization of thin film nanocomposites: A new concept for reverse osmosis membranes, *Journal of Membrane Science*, 294 (2007) 1-7.
- [36] A.K. Ghosh, E.M.V. Hoek, Impacts of support membrane structure and chemistry on polyamide-polysulfone interfacial composite membranes, *Journal of Membrane Science*, 336 (2009) 140-148.
- [37] M.L. Lind, D. Eumine Suk, T.-V. Nguyen, E.M.V. Hoek, Tailoring the Structure of Thin Film Nanocomposite Membranes to Achieve Seawater RO Membrane Performance, *Environ. Sci. Technol.*, 44 (2010) 8230-8235.
- [38] M.T.M. Pendergast, J.M. Nygaard, A.K. Ghosh, E.M.V. Hoek, Using nanocomposite materials technology to understand and control reverse osmosis membrane compaction, *Desalination*, 261 (2010) 255-263.
- [39] G.M. Geise, H.-S. Lee, D.J. Miller, B.D. Freeman, J.E. McGrath, D.R. Paul, Water purification by membranes: The role of polymer science, *Journal of Polymer Science Part B: Polymer Physics*, 48 (2010) 1685-1718.
- [40] D.W. Green, *Perry's Chemical Engineers' Handbook*, in, McGraw-Hill, New York, 1997.

- [41] P.J. Linstrom, W.G. Mallard, NIST Chemistry WebBook, in: NIST Standard Reference Database Number 69, The National Institute of Standards and Technology (NIST), 2005.
- [42] D.R. Lide, CRC Handbook of Chemistry and Physics, in, CRC Press, New York, 2003.
- [43] S.H. Kim, S.-Y. Kwak, T. Suzuki, Positron Annihilation Spectroscopic Evidence to Demonstrate the Flux-Enhancement Mechanism in Morphology-Controlled Thin-Film Composite (TFC) Membrane, *Environ. Sci. Technol.*, 39 (2005) 1764-1770.
- [44] W.J. Lau, A.F. Ismail, N. Misdan, M.A. Kassim, A recent progress in thin film composite membrane: A review, *Desalination*, 287 (2012) 190-199.
- [45] B.-H. Jeong, E.M.V. Hoek, Y. Yan, A. Subramani, X. Huang, X. Huang, A.K. Ghosh, A. Jawor, Interfacial polymerization of thin film nanocomposites: A new concept for reverse osmosis membranes, *Journal of Membrane Science*, 294 (2007).
- [46] H. Tomioka, K. Sugita, K. Oto, Composite semipermeable membrane, and production process thereof, in, Toray Industries, Inc, United States, 2007.
- [47] J.E. Cadotte, R.J. Petersen, R.E. Larson, E.E. Erickson, A new thin-film composite seawater reverse osmosis membrane, *Desalination*, 32 (1980) 25-31.
- [48] A. Subramani, X.F. Huang, E.M.V. Hoek, Direct observation of bacterial deposition onto clean and organic-fouled polyamide membranes, *J. Colloid Interface Sci.*, 336 (2009) 13-20.
- [49] C. Tang, Y. Kwon, J.O. Leckie, Effect of membrane chemistry and coating layer on physiochemical properties of thin film composite polyamide RO and NF membranes: II. Membrane physiochemical properties and their dependence on polyamide and coating layers. , *Desalination*, 242 (2009) 168-182.
- [50] S. Yu, M. Ma, J. Liu, J. Tao, M. Liu, C. Gao, Study on polyamide thin-film composite nanofiltration membrane by interfacial polymerization of polyvinylamine (PVAm) and isophthaloyl chloride (IPC), *Journal of Membrane Science*, (2011) 164-173.
- [51] R.W. Baker, Membrane Transport Theory, in: *Membrane Technology and Applications*, John Wiley & Sons Ltd., Menlo Park, CA, 2004, pp. 16-36.
- [52] J. Wang, D.S. Dlamini, A.K. Mishra, M.T.M. Pendergast, M.C.Y. Wong, B.B. Mamba, V. Freger, A.R.D. Verliefde, E.M.V. Hoek, A critical review of transport through osmotic membranes, *Journal of Membrane Science*, 454 (2014) 516-537.
- [53] S. Loeb, T. Leonid, E. Korngold, J. Freiman, Effect of porous support fabric on osmosis through a Loeb-Sourirajan type asymmetric membrane, *Journal of Membrane Science*, 129 (1997) 243-249.

- [54] J.C. Crittenden, R.R. Trussell, D.W. Hand, K.J. Howe, G. Tchobanoglous, Reverse Osmosis, in: Water Treatment: Principles and Design, John Wiley & Sons, Hoboken, New Jersey, 2005, pp. 1429-1506
- [55] FILMTEC Membranes - Basics of RO and NF: Membrane Performance, in: Tech Manual Exerpt, The Dow Chemical Company, pp. 2.
- [56] G. Shock, A. Miquel, Mass transfer and pressure loss in spiral wound modules, *Desalination*, 64 (1987) 339-352.
- [57] G. Guillen, E.M.V. Hoek, Modeling the impacts of feed spacer geometry on reverse osmosis and nanofiltration processes, *Chemical Engineering Journal*, 149 (2009) 221-231.
- [58] A. Achilli, T.Y. Cath, A.E. Childress, Power generation with pressure retarded osmosis: An experimental and theoretical investigation, *Journal of Membrane Science*, 343 (2009) 42-52.
- [59] M.C.Y. Wong, K. Martinez, G.Z. Ramon, E.M.V. Hoek, Impacts of operating conditions and solution chemistry on osmotic membrane structure and performance, *Desalination*, 287 (2012) 340-349.
- [60] K.L. Lee, R.W. Baker, H.K. Lonsdale, Membranes for Power Generation by Pressure-Retarded Osmosis, *Journal of Membrane Science*, 8 (1981) 141-171.
- [61] N.Y. Yip, A. Tiraferri, W.A. Phillip, J.D. Schiffman, L.A. Hoover, Y.C. Kim, M. Elimelech, Thin-Film Composite Pressure Retarded Osmosis Membranes for Sustainable Power Generation from Salinity Gradients, *Environ. Sci. Technol.*, 45 (2011) 4360-4369.
- [62] A. Tiraferri, N.Y. Yip, A.P. Straub, S. Romero-Vargas, Castrillon, M. Elimelech, A Method for the Simultaneous Determination of Transport and Structural Parameters of Forward Osmosis Membranes, *Journal of Membrane Science*, (2013).
- [63] G.Z. Ramon, M.C.Y. Wong, E.M.V. Hoek, Transport through composite membrane, part 1: Is there an optimal support membrane?, *Journal of Membrane Science*, 415-416 (2012) 298-305.
- [64] G.Z. Ramon, E.M.V. Hoek, Transport through composite membranes, part 2: Impacts of roughness on permeability and fouling, *Journal of Membrane Science*, 425-426 (2013) 141-148.
- [65] X. Jin, X. Huang, E.M.V. Hoek, Role of Specific Ion Interactions in Seawater RO Membrane Fouling by Alginic Acid, *Environmental Science and Technology*, 43 (2009) 3580-3587.
- [66] S. Avlonitis, W.T. Hanbury, T. Hodgkiess, Chlorine degradation of aromatic polyamides, *Desalination*, 85 (1992) 321-334.

[67] G.-D. Kang, C.-J. Gao, W.-D. Chen, X.-M. Jie, Y.-M. Cao, Q. Yuan, Study on hypochlorite degradation of aromatic polyamide reverse osmosis membrane, *Journal of Membrane Science*, 300 (2007) 165-171.

[68] Y.-N. Kwon, J.O. Leckie, Hypochlorite degradation of crosslinked polyamide membranes: I. Changes in chemical/morphological properties, *Journal of Membrane Science*, 283 (2006) 21-26.

[69] S.T. Mitrouli, A.J. Karabelas, N.P. Isaias, Polyamide active layers of low pressure RO membranes: Data on spatial performance non-uniformity and degradation by hypochlorite solutions, *Desalination*, 260 (2010) 91-100.

[70] G.-d. Kang, Y.-m. Cao, Development of antifouling reverse osmosis membranes for water treatment: A review, *Water Research*, 46 (2012) 584-600.

[71] L. Chen, H. Therien-Aubin, M.C.Y. Wong, E.M.V. Hoek, C.K. Ober, Improved antifouling properties of polymer membranes using a 'layer-by-layer' mediated method, *Journal of Materials Chemistry B*, 1 (2013) 5651-5658.

[72] G. Kang, M. Liu, B. Lin, Y. Cao, Q. Yuan, A novel method of surface modification on thin-film composite reverse osmosis membrane by grafting poly(ethylene glycol), *Polymer*, 48 (2007) 1165-1170.

[73] V. Freger, J. Gilron, S. Belfer, TFC Polyamide membranes modified by grafting of hydrophilic polymers: an FT-IR/AFM/TEM study, *Journal of Membrane Science*, 209 (2002) 283-292.

[74] B.T. McVerry, M.C.Y. Wong, K.L. Marsh, J.A. Temple, C. Marambio-Jones, E.M.V. Hoek, R.B. Kaner, Scalable Antifouling Reverse Osmosis Membranes Utilizing Perfluorophenyl Azide Photochemistry, *Macromolecules Rapid Communications*, (2014).

[75] S.-Y. Kwak, S.H. Kim, S.S. Kim, Hybrid Organic/Inorganic Reverse Osmosis (RO) Membrane for Bactericidal Anti-Fouling. 1. Preparation and Characterization of TiO₂ Nanoparticle Self-Assembled Aromatic Polyamide Thin-Film-Composite (TFC) Membrane, *Environ. Sci. Technol.*, 35 (2001) 2388-2394.

[76] E.M. Vrijenhoek, S. Hong, M. Elimelech, Influence of membrane surface properties on initial rate of colloidal fouling of reverse osmosis and nanofiltration membranes, *Journal of Membrane Science*, 188 (2001) 115-128.

[77] M. Edge, N.S. Allen, T.S. Jewitt, Fundamental Aspects of the Degradation of Cellulose Triacetate Base Cinematograph Film, *Polymer Degradation and Stability*, 25 (1989) 345-362.

[78] N.S. Allen, M. Edge, J.H. Appleyard, T.S. Jewitt, C.V. Horie, D. Francis, Degradation of Historic Cellulose Triacetate Cinematographic Film: The Vinegar Syndrome, *Polymer Degradation and Stability*, 19 (1987) 379-387.

- [79] A. Scotney, The Thermal Degradation of Cellulose Triacetate - III: The Degradation Mechanism, *European Polymer Journal*, 8 (1972) 185-193.
- [80] Y. Liao, C. Zhang, Y. Zhang, V. Strong, J. Tang, X.-G. Li, K. Kalantar-zadeh, E.M.V. Hoek, K.L. Wang, R.B. Kaner, Carbon Nanotube/Polyaniline Composite Nanofibers: Facile Synthesis and Chemosensors, *Nano Letters*, 11 (2011) 954-959.
- [81] J. Stejskal, P. Kratochvíl, A.D. Jenkins, The formation of polyaniline and the nature of its structures, *Polymer*, 37 (1996) 367-369.
- [82] S. Virji, J. Huang, R.B. Kaner, B.H. Weiller, Polyaniline Nanofiber Gas Sensors: Examination of Response Mechanisms, *Nano Letters*, 4 (2004) 491-496.
- [83] Z. Fana, Z. Wang, M. Duana, J. Wang, S. Wang, Preparation and characterization of polyaniline/polysulfone nanocomposite ultrafiltration membrane, *Journal of Membrane Science*, 310 (2008) 402-408.
- [84] M.J. Winokur, B.R. Mattes, Structural Studies of Halogen Acid Doped Polyaniline and the Role of Water Hydration, *Macromolecules*, 31 (1998) 8183-8191.
- [85] B.R. Mattes, M.R. Anderson, J.A. Conklin, H. Reiss, R.B. Kaner, Morphological modification of polyaniline films for the separation of gases, *Synthetic Metals*, 57 (1993) 3655-3660.
- [86] M. Elimelech, Z. Xiaohua, A.E. Childress, H. Seungkwan, Role of membrane surface morphology in colloidal fouling of cellulose acetate and composite aromatic polyamide reverse osmosis membranes, *Journal of Membrane Science*, 127 (1997) 101-109.
- [87] V. Freger, S. Srebnik, Mathematical Model of Charge and Density Distributions in Interfacial Polymerization of Thin Films, *Journal of Applied Polymer Science*, 88 (2003) 1162-1169.
- [88] B. Mi, O. Coronell, B. Marinas, F. Watanabe, D.G. Cahill, I. Petrov, Physico-chemical characterization of NF/RO membrane active layers by Rutherford backscattering spectrometry, *Journal of Membrane Science*, 282 (2006) 71-81.
- [89] O. Coronell, B. Marinas, D.G. Cahill, Depth heterogeneity of fully aromatic polyamide active layers in reverse osmosis and nanofiltration membranes, *Environ. Sci. Technol.*, 45 (2011) 4513-4520.
- [90] F.A. Pacheco, I. Pinnau, M. Reinhard, J.O. Leckie, Characterization of isolated polyamide thin films of RO and NF membranes using novel TEM techniques, *Journal of Membrane Science*, 358 (2010) 51-59.
- [91] T. Kato, M. Henmi, Self-Organized Liquid-Crystalline Nanostructured Membranes for Water Treatment: Selective Permeation of Ions, in: *Advances in Materials and Processes for Polymer Membrane Mediated Water Purification Asilomar Conference Grounds, Pacific Grove, CA, 2013.*

- [92] M. Kurihara, M. Hanakawa, Mega-ton Water System: Japanese national research and development project on seawater desalination and wastewater reclamation, *Desalination*, 308 (2013) 131-137.
- [93] D. Yang, G. Zuccarello, B.R. Mattes, Physical Stabilization or Chemical Degradation of Concentrated Solutions of Polyaniline Emeraldine Base Containing Secondary Amine Additives, *Macromolecules*, 35 (2002) 5304-5313.
- [94] M.L. Lind, B.H. Jeong, A. Subramani, X.F. Huang, E.M.V. Hoek, Effect of mobile cation on zeolite-polyamide thin film nanocomposite membranes, *Journal of Materials Research*, 24 (2009) 1624-1631.
- [95] P.K. Gallagher, Ultraviolet Absorption Spectra of o-, m-, and p- phenylenediamines and their mono- and dihydrochlorides in aqueous solution, *Journal of Physical Chemistry*, 67 (1963) 807-811.
- [96] M.R. Anderson, B.R. Mattes, H. Reiss, R.B. Kaner, Conjugated Polymer Films for Gas Separations, *Science*, 252 (1991) 1412-1415.
- [97] G.D. Vilakati, E.M.V. Hoek, B.B. Mamba, Investigating the structure and water permeation of membranes modified with natural and synthetic additives using tensile, porosity, and glass transition temperature studies, *Journal of Applied Polymer Science*, (2014).
- [98] A.E. Childress, M. Elimelech, Relating Nanofiltration Membrane Performance to Membrane Charge (Electrokinetic) Characteristics, *Environ. Sci. Technol.*, 34 (2000) 3710-3716.
- [99] A. Subramani, E.M.V. Hoek, Biofilm formation, cleaning, re-formation on polyamide composite membranes, *Desalination*, 257 (2010) 73-79.
- [100] G.D. Vilakati, M.C.Y. Wong, E.M.V. Hoek, B.B. Mamba, Relating thin film composite membrane performance to support membrane morphology Fabricated using lignin additive, *Journal of Membrane Science*, 469 (2014) 216-224.